THE CHEMICAL MECHANISMS OF FLAVIN-DEPENDENT AMINE OXIDASES AND THE PLASTICITY OF THE TWO-HIS-ONE-CARBOXYLATE FACIAL TRIAD IN TYROSINE HYDROXYLASE

A Dissertation

by

ERIK C. RALPH

Submitted to the Office of Graduate Studies of
Texas A&M University
in partial fulfillment of the requirements for the degree of

DOCTOR OF PHILOSOPHY

December 2006

Major Subject: Biochemistry

THE CHEMICAL MECHANISMS OF FLAVIN-DEPENDENT AMINE OXIDASES AND THE PLASTICITY OF THE TWO-HIS-ONE-CARBOXYLATE FACIAL TRIAD IN TYROSINE HYDROXYLASE

A Dissertation

by

ERIK C. RALPH

Submitted to the Office of Graduate Studies of
Texas A&M University
in partial fulfillment of the requirements for the degree of

DOCTOR OF PHILOSOPHY

Approved by:

Chair of Committee,	Paul F. Fitzpatrick
Committee Members,	Donald W. Pettigrew
	Michael Polymenis
	Frank M. Raushel
Head of Department,	Gregory D. Reinhart

December 2006

Major Subject: Biochemistry

ABSTRACT

The Chemical Mechanisms of Flavin-Dependent Amine Oxidases and the Plasticity of the Two-His-One-Carboxylate Facial Triad in Tyrosine Hydroxylase.

(December 2006)

Erik C. Ralph, B.S., Bucknell University

Chair of Advisory Committee: Dr. Paul F. Fitzpatrick

Despite a number of kinetic and spectroscopic studies, the chemical mechanisms of amine oxidation by flavoenzymes remain widely debated. The mechanisms of by *N*-methyltryptophan oxidase (MTOX) and tryptophan 2-monooxygenase (TMO) were probed using a combination of pH and primary deuterium, solvent, and ^{15}N kinetic isotope effects. Slow substrates were chosen for these studies; MTOX was characterized with *N*-methylglycine and TMO was characterized with L-alanine. Primary deuterium kinetic isotope effects of 7.2 and 5.3 were observed for sarcosine oxidation by MTOX and for alanine oxidation by TMO, respectively, independent of the substrate concentration and pH. Monitoring the reduction of flavin spectroscopically revealed no intermediate flavin species with both enzyme-substrate systems. Furthermore, the magnitudes of the ^{15}N kinetic isotope effects observed with both systems suggest that nitrogen rehybridization and C-H bond cleavage are concerted. These results are consistent with both enzymes utilizing a hydride transfer mechanism for amine oxidation.

The role of the iron ligands of tyrosine hydroxylase (TyrH) was also investigated.

TyrH contains one iron per monomer, which is held by three conserved amino acid residues, two histidines and a glutamate. As a probe of the plasticity of the metal binding site, each of the metal ligands in TyrH was substituted with glutamine, glutamate, or histidine. The resulting proteins were characterized for metal content, catalytic activity, and dopamine binding. The H336E and H336Q enzymes retain substantial catalytic activity. In contrast, the E376Q enzyme retains about 0.4% of the wild-type catalytic activity, and the E376H enzyme has no significant activity. The H331E enzyme oxidizes tetrahydropterin in a tyrosine-independent manner. The position of the charge-transfer absorbance band for the H336E and H336Q enzyme-inhibitor complexes is shifted relative to that of the wild-type enzyme, consistent with the change in the metal ligand. In contrast, the E376H and E376Q enzymes catalyze dopamine oxidation. These results provide a reference point for further structural studies of TyrH and the other aromatic amino acid hydroxylases, and for similar studies of other enzymes containing this iron-binding motif.

DEDICATION

This dissertation is dedicated to my parents for their continued love and support, and for their endless faith in my abilities.

ACKNOWLEDGMENTS

I would like to thank my advisor, Dr. Paul F. Fitzpatrick, for his enduring patience and his guidance. I would also like to thank all of the past and present Fitzpatrick lab members who have contributed a great deal through helpful discussions, and simply by providing an enjoyable working environment. I would like to thank my collaborators, Dr. Mark Anderson and Dr. W. Wallace Cleland at the University of Wisconsin and Jennifer Hirschi and Dr. Daniel Singleton at Texas A&M University. Finally and most importantly, I would like to thank my wife and my family, both here and abroad, without whose love and support I simply would not succeed.

ABBREVIATIONS

DAO	D-Amino acid oxidase
DOPA	1,2-Dihydroxyphenylalanine
FAD	Flavin adenine dinucleotide
FMN	Flavin mononucleotide
IRMS	Isotope ratio mass spectrometry
LB	Luria Bertani broth
MAO	Monoamine oxidase
MSOX	Monomeric sarcosine oxidase
MTOX	*N*-Methyltryptophan oxidase
PheH	Phenylalanine hydroxylase
TMO	Tryptophan 2-monooxygenase
TyrH	Tyrosine hydroxylase

TABLE OF CONTENTS

Page

CHAPTER Page

LIST OF FIGURES

LIST OF TABLES

CHAPTER I

INTRODUCTION

FLAVIN-DEPENDENT AMINE OXIDASES

Enzymes that utilize a flavin cofactor are ubiquitous in nature and are involved in a myriad of biological events, including prokaryotic and eukaryotic primary metabolic pathways, photosynthesis, DNA repair, and detoxification of soil pollutants, and have been implicated in regulation of cell death and in biological clocks (*1*). This diversity is due largely to the cofactor's ability to catalyze both one and two-electron oxidations or reductions and thereby couple two-electron reactions to one-electron systems such as metal complexes or molecular oxygen.

Figure 1.1 shows the three forms of flavin cofactors commonly found in flavoenzymes. Riboflavin, the simplest cofactor (Figure 1.1), was first isolated in 1879 by A. Wynter Blyth, and its structure was later determined independently by Richard Kuhn in Heidelberg and by Paul Karrer in Zurich (*1*). This form of the cofactor is comprised simply of an isoalloxazine ring system with a ribityl chain attached at N10, and serves as a precursor for the biosynthesis of the other two forms, flavin mononucleotide (FMN) and flavin adenine dinucleotide (FAD) (*2*).

This dissertation follows the style of *Biochemistry.*

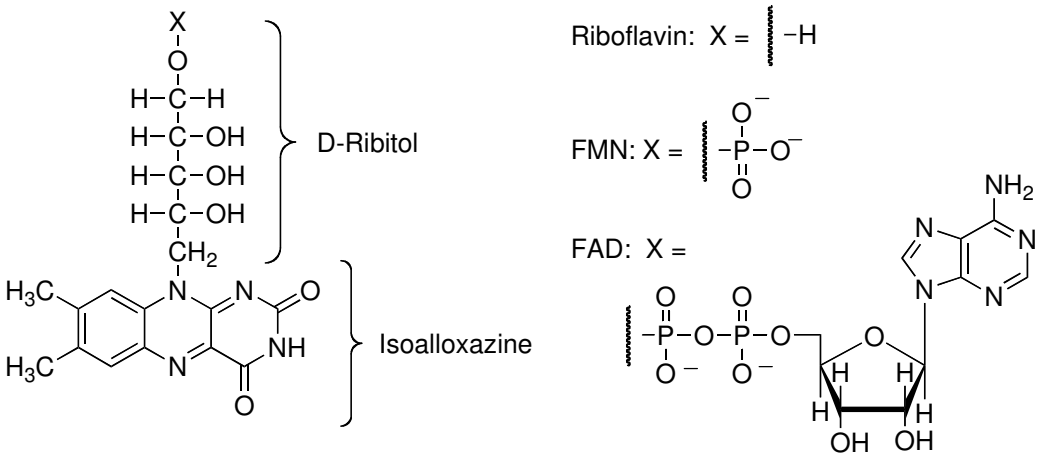

Figure 1.1. Structures of flavin cofactors.

It is the highly conjugated isoalloxazine ring system that gives flavin cofactors their chemical reactivity. The ring system has three different electronic states, and each oxidation state has its own unique visible absorbance spectrum as shown in Figure 1.2. Therefore, a great deal of information about the chemical mechanism of a flavoenzyme can be obtained simply by monitoring the enzyme's absorbance spectrum during the course of a reaction. The fully oxidized cofactor is characterized by a yellow color, with absorbance maxima around 370 and 450 nm (spectrum A in Figure 1.2), while the fully reduced cofactor (spectrum C) is colorless (*2*). The partially reduced flavin can exist in a neutral (not shown) or an anionic form (spectrum B); the pK_a for the proton exchange is approximately 8.5 in solution (*2*) although many proteins will stabilize one form over the other, drastically altering the observed pK_a value (*1*). Both forms of the partially reduced cofactor have an absorbance maximum around 490 nm, with reduced absorbance relative to the fully oxidized species. The anionic semiquinone is red in appearance and has an absorbance maximum around 390 nm with increased absorbance relative to the fully oxidized species (spectrum B) (*3*). Alternatively, the neutral semiquinone (spectrum not shown) is blue in appearance. It has reduced absorbance between 300 and 500 nm compared to the fully oxidized species, and has a broad absorbance band from around 500 to 650 nm (*3*).

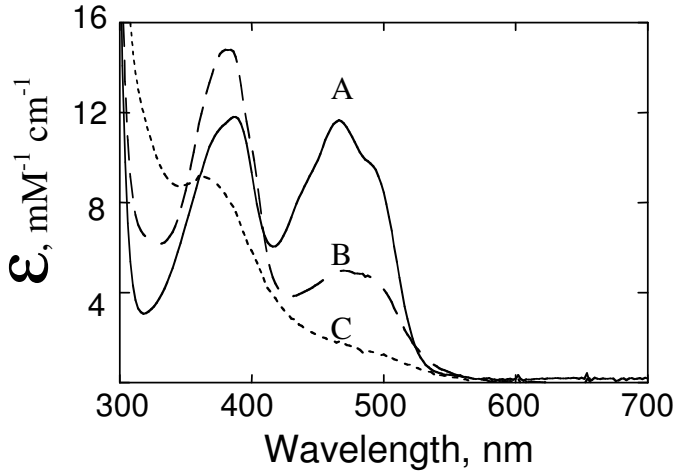

Figure 1.2. Absorbance spectra of different flavin oxidation states. The flavin cofactor can exist in three separate electronic states: the fully oxidized state (A, solid line), the one-electron reduced state (B, broken line), and the two-electron reduced state (C, dashed line). The one-electron reduced cofactor can exist in two protonation states; only the spectrum for the anionic state is shown.

Among the many classes of flavoenzymes, the flavin-dependent amine oxidases and dehydrogenases comprise one of the most commonly studied groups. These enzymes catalyze the oxidative deamination of primary amines and the oxidative dealkylation of secondary or tertiary amines in a myriad of biological activities.For example, glycine oxidase is involved in thiamin biosynthesis in microorganisms (*4*), while the recently discovered lysine-specific histone demethylase is involved in regulation of transcription in humans (*5*). D-Amino acid oxidase (DAO) metabolizes D-amino acids in yeast and has been linked to human neurodegenerative diseases such as schizophrenia through the oxidation of D-serine in the brain (*6*).

Flavin-dependent amine oxidases have been the subject of a number of kinetic, spectroscopic, and structural studies (reviewed in (*7-9*)). However, only in the case of DAO have these studies led to a consensus that the reaction utilizes a hydride transfer. DAO was first discover by Krebs in 1932 (*10*), and quickly became one of the most heavily studied flavoenzymes. In the early 1970's, Walsh and coworkers described the ability of DAO to catalyze the elimination of HCl from β-Cl-substituted D-amino acids to form the respective keto-acids (*8*). The oxygen dependence of this elimination and kinetic isotope effects on the rate of elimination were interpreted as evidence for the initial removal of the substrate α-proton to form a carbanion intermediate, which can then undergo either oxidation or HCl elimination (Scheme 1.1) (*8*).

Scheme 1.1

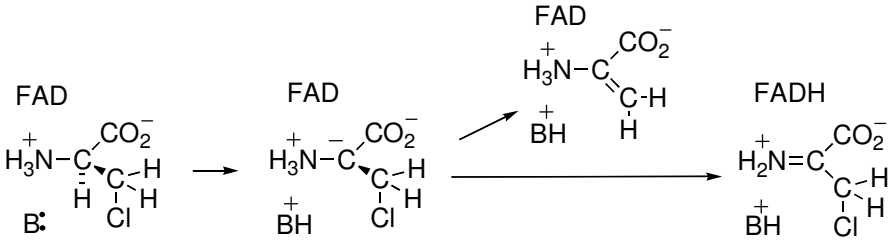

The mechanism of Scheme 1.1 was generally accepted as the mechanism of catalysis for DAO up through the mid-1990's. Then in 1996, the three dimensional crystal structure of pig kidney DAO was solved by two independent groups (*11, 12*). These structures had important mechanistic implications, as they showed the clear absence of the active site base required by the carbanion mechanism. Furthermore, the carbon corresponding to the α-carbon is about 3.4 Å from the flavin N5, a distance well suited for a hydride transfer mechanism.

Strong evidence for a hydride transfer mechanism (Scheme 1.2) came in 2000 from the ^{15}N kinetic isotope effects on D-serine oxidation by DAO (*13*). ^{15}N Kinetic isotope effects report on changes in the substrate nitrogen's bonding order that occur prior to or during the first irreversible step in oxidation. The observed deuterium kinetic isotope effects for D-serine oxidation by DAO are consistent with an irreversible C-H bond cleavage (*14*). Therefore, the ^{15}N kinetic isotope effects also report on the relative timing of changes in the nitrogen bond order and C-H bond cleavage. After correcting for the protonation state of the substrate, an inverse ^{15}N kinetic isotope effect of 0.996 was observed (*13*). This value agrees with the expected value for conversion of an sp^3

nitrogen to sp^2 (*15*), consistent with C-H bond cleavage and nitrogen rehybridization occurring in the same step, as predicted by a hydride transfer mechanism.

Scheme 1.2

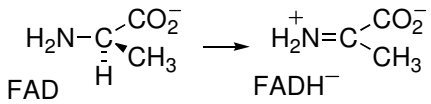

Although the hydride transfer mechanism shown in Scheme 1.2 accounts for the data observed with normal amino acids substrates, it does not make any obvious explanation for the well documented β-elimination reactions. As reviewed by Fitzpatrick (*7*), the data are most consistent with a nucleophilic attack of the reduced flavin on the β-labeled keto-acid. The initial flavin reduction by hydride transfer accounts for the observed kinetic isotope effects on β-elimination as well as the oxygen dependence of the partitioning between the Cl-labeled and nonlabeled products. The difference between the elimination and oxidation reactions, and the history of how they affected the mechanistic studies of DAO serves as a well documented example of how mechanistic studies with activated substrate analogues may not reflect the mechanism of non-activated substrates.

Although a hydride transfer mechanism is now generally accepted for DAO, the chemical mechanism for other flavin-dependent oxidases is still debated. In addition to the carbanion and hydride transfer mechanisms, commonly proposed mechanisms of amine oxidation involve the formation of a substrate-radical pair or the formation of a

substrate-flavin adduct. The various pieces of evidence for or against these mechanisms is perhaps best discussed in the literature regarding monoamine oxidase (MAO) (*9*).

Evidence for a radical mechanism for amine oxidases has come from studies with cyclopropyl or cyclobutyl substrate analogues, with the best studied example being the inactivation of MAO. As reviewed by Silverman (*16*), a number of cyclopropyl-amine containing compounds have been shown to inactivate this enzyme. The inactivation is attributed to formation of an aminium radical followed by a rapid ring-opening reaction, the product of which inactivates the enzyme (Scheme 1.3) (*16*). Some of these inhibitors label the flavin cofactor exclusively, while others label either the flavin or various amino acid residues, and a third set label amino acid residues only (*16*). Subsequent elucidation of the three-dimensional structure of MAO B shows that the cysteine that is labeled by many of these inhibitors is well outside the active site (*17*), suggesting that inactivation and normal catalysis utilize different mechanisms. Similarly, methanol oxidase (*18*) and cholesterol oxidase (*19*), two members of a family of homologous flavoprotein alcohol oxidases (*20*), are both inactivated by cyclopropyl compounds; in this case the available evidence is most consistent with a hydride transfer mechanism for these enzymes (*21, 22*).

Scheme 1.3

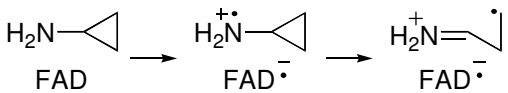

A final type of mechanism commonly proposed for flavin-dependent oxidases utilizes a substrate-flavin adduct, as shown in Scheme 1.4 with D-alanine. First proposed by Hamilton in 1970 (*23*), this mechanism was later supported by Mariano and coworkers using model studies of amines with lumiflavins (*24-26*). For MAO A, quantitative structure-activity relationship studies are consistent with the formation of an electron rich intermediate, and have been interpreted as evidence for a Hamilton-type mechanism (*27*). However, these studies do not address some of the previously raised concerns regarding this mechanism for MAO (*16*), including the ability of MAO to oxidize secondary and tertiary amines, some of which are very sterically-hindered, and in some cases with higher turnover rates than that of primary amines.

Scheme 1.4

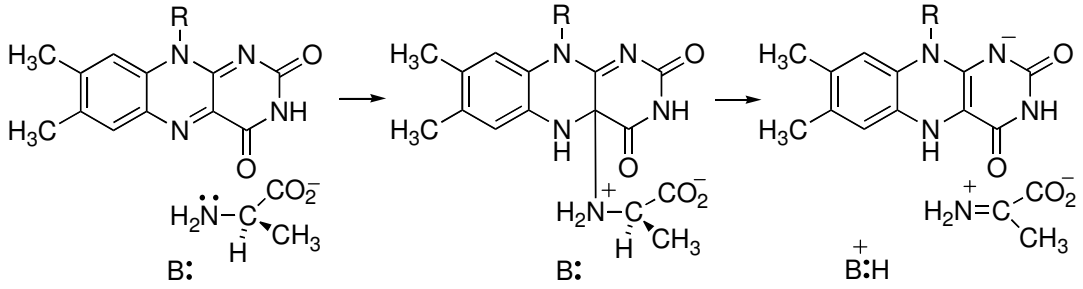

To date, flavoenzymes that catalyze amine oxidations have fallen into two structural families, exemplified by the above mentioned enzymes, DAO and MAO. The DAO family includes DAO (*11, 12*), monomeric sarcosine oxidase (*28*) and glycine oxidase (*4*), while the MAO family includes MAO (*17*), polyamine oxidase (*29*), and L-amino acid oxidase (*30*). Despite differences in the overall protein structure, both

families share properties that are common among most flavin-dependent dehydrogenases. Specifically, the crystal structures of enzyme-substrate analogue complexes suggest the reactive substrate carbon binds in front of the flavin within approximately 3.5 Å of the flavin N5, with a highly conserved angle of orientation with regards to the flavin cofactor (*31*). As these enzymes all catalyze essentially identical reactions (i.e., the oxidation of a C-N bond) using similar active-site orientations, it seems reasonable that all flavin-dependent amine oxidases may utilize a similar chemical mechanism.

N-Methyltryptophan oxidase (MTOX) catalyzes the oxidative demethylation of *N*-methyl amino acids (Scheme 1.5). MTOX is commonly found in both prokaryotes and eukaryotes, including humans (*32-36*), and was rediscovered in *Escherichia coli* in 1996 due to its 43% amino acid identity to the more thoroughly studied monomeric sarcosine oxidase (*37*). Initial characterizations have shown that although MTOX will demethylate sarcosine (*N*-methylglycine) and *N*-methylalanine, it has a preference for bulkier hydrophobic substrates, with the fastest known substrate being L-abrine (*N*-methyl-L-tryptophan) (*37*). The metabolic roles and physiological substrate for MTOX in *E. coli* are unknown (*38*).

Scheme 1.5

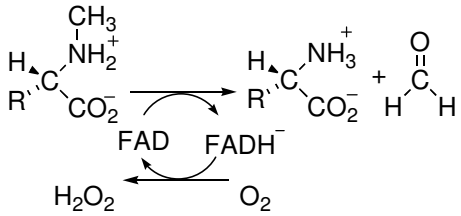

The flavoenzyme tryptophan 2-monooxygenase (TMO) from *Pseudomonas savastoni* catalyzes the oxidative decarboxylation of L-tryptophan (Scheme 1.6) in the first step of a two-step biosynthetic pathway for the plant hormone indoleacetic acid (*39-41*). The kinetic mechanism of TMO has been determined with its fastest substrate L-tryptophan (*42*), and can be divided into two half-reactions (Scheme 1.7). The reductive half-reaction involves cleavage of the α-C-H bond of the amino acid (AA) and transfer of a hydride equivalent to the FAD. In the oxidative half-reaction, the reduced cofactor reacts with oxygen to produce hydrogen peroxide (*43*). Decarboxylation of the imino acid is thought to occur through the reaction of hydrogen peroxide with the imino acid (pathway a), analogously to the mechanism proposed by Lockridge et al. (*44*) for the decarboxylation of pyruvate by lactate oxidase. Although indoleacetamide is the only product of tryptophan turnover by wild-type TMO, amine oxidation can be uncoupled from decarboxylation (pathway b) to yield a keto-acid by using anaerobic conditions (*42*) or variant enzymes (*45, 46*). Therefore, TMO can function not only as a monooxygenase, but also as a flavin-dependent amine oxidase.

Scheme 1.6

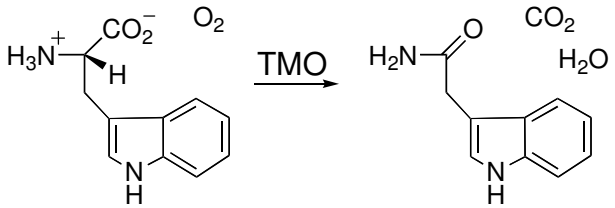

Scheme 1.7

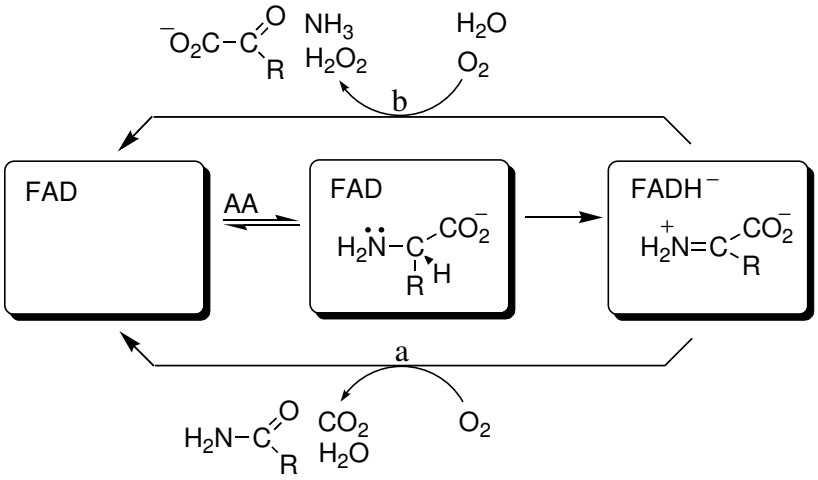

MTOX and TMO represent the two separate structural families of flavin-dependent amine oxidases. Although no structural information is available for either enzyme, the high percent amino acid identity as well as other characteristics shared with monomeric sarcosine oxidase (*38*) suggests that both monomeric sarosine oxidase and MTOX belong to the DAO structural family. Alternatively, TMO was proposed by Sobrado and Fitzpatrick (*47*) to be in the second family of enzymes with MAO and L-amino acid oxidase. Subsequent studies have supported this assignment (*45, 46*).

While MTOX catalyzes oxidative demethylation and TMO catalyzes oxidative decarboxylation, both enzymes catalyze the oxidation of a substrate C-N bond yielding the corresponding Schiff base (*38, 42*). Therefore, similar mechanisms, including each of the mechanistic possibilities presented above (i.e., the utilization of a substrate carbanion, single-electron transfers, a covalent substrate-flavin adduct, or a simple hydride transfer) can be proposed for both enzymes. Further mechanistic studies are

necessary to address each of these possibilities. These studies would give a great deal of insight into a very important and functionally diverse class of enzymes.

2-HIS 1-CARBOXYLATE FACIAL TRIAD IN TYROSINE HYDROXYLASE

Tyrosine hydroxylase, phenylalanine hydroxylase, and tryptrophan hydroxylase comprise a small class of enzymes referred to as the aromatic amino acid hydroxylases. These enzymes catalyze the iron-dependent hydroxylation of their respective amino acid substrates utilizing the additional substrates, molecular oxygen and tetrahydropterin (Scheme 1.8) (*48*). Tyrosine hydroxylase (TyrH) catalyzed formation of 2,3-dihydroxy-phenylalanine is the first step in the formation of neurotransmitters dopamine, epinephrine, and norepinephrine, while phenylalanine hydroxylase (PheH) and tryptophan hydroxylase (TrpH) are involved in tyrosine biosynthesis and serotonin biosynthesis, respectively (*48*).

Scheme 1.8

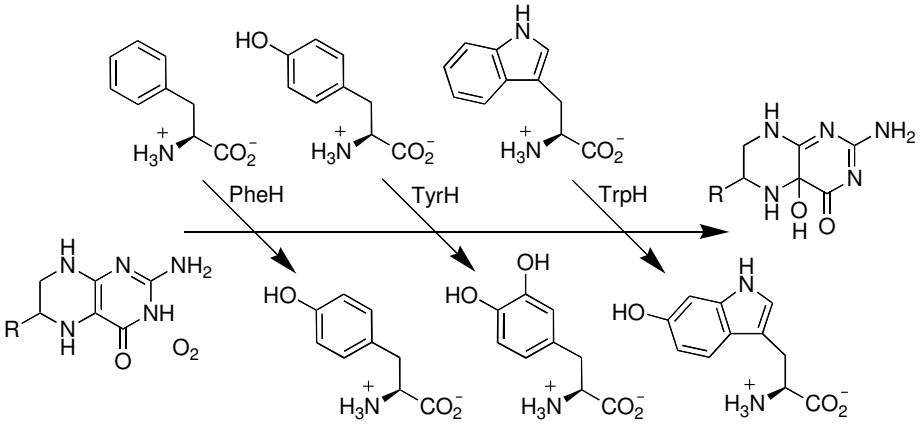

The importance of the reactions catalyzed by this class of enzymes has prompted many studies on the enzymes' chemical and regulatory mechanisms, including three-dimensional structural determinations. All three enzymes share significant structural similarities. They all exist as homotetramers (although phenylalanine hydroxylase exists in an equilibrium between the homodimeric and homotetrameric forms) and the monomeric units are comprised of an N-terminal regulatory domain, a C-terminal tetramerization domain, and a catalytic domain of approximately 290 amino acids (*48*). The structures of the catalytic domains of all three eukaryotic enzymes have recently been determined (*49-51*), revealing superimposable catalytic domains. Importantly, the enzymes contain one iron per subunit located in an active site cleft approximately 10 Å below the protein surface. The iron is held in a distorted octahedral orientation, ligated by two histidines and a glutamate on one face and three water molecules on the opposing face.

The structural similarities in this small family of enzymes are suggestive of a common chemical mechanism of hydroxylation. This interpretation is strongly supported by a more recent study that showed nearly identical intrinsic deuterium kinetic isotope effects and temperature dependencies for all three enzymes for their enzymatic hydroxylation of methylated amino acids (*52*). The accepted chemical mechanism of hydroxylation is shown in Scheme 1.9. As reviewed by Fitzpatrick (*48*), all three substrates bind to the enzyme before any chemistry occurs. The oxygen and pterin then undergo a one-electron exchange; the resultant radical pair rapidly collapses to a peroxypterin bridge that may ligate to the active site iron. Heterolytic cleavage of the

oxygen-oxygen bond leads to formation of a ferryl oxygen species, which is the hydroxylating intermediate. Electrophilic attack of this species on the aromatic ring forms a cationic amino acid, which is resolved through proton abstraction and rearomatization.

Scheme 1.9

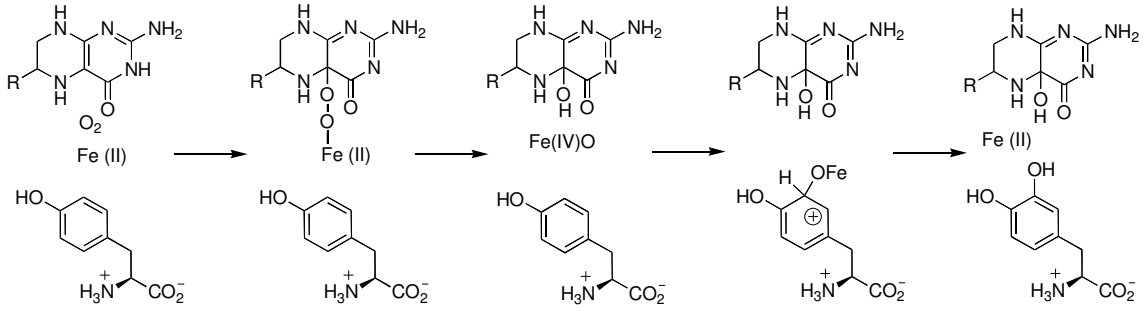

Although the aromatic amino acid hydroxylases often purify with bound ferric iron, the enzymes require ferrous iron for catalytic activity (*48*). As shown in Scheme 1.9, the ferrous iron is oxidized to higher oxidation states during catalysis, but is returned to the ferrous form by the end of the catalytic cycle. The ferric form of the enzymes results from a non-catalytic side reaction with oxygen. In vivo, the ferric enzymes can be reduced back into the ferrous form by tetrahydrobiopterin (*53*). Alternatively, the ferrous form of the enzymes has a high affinity for catecholamines, the binding of which effectively traps the enzyme in an inactive complex (*54*). As tyrosine hydroxylase catalyzes the first step in the catecholamine biosynthetic pathway, trapping the inactive ferrous enzyme via catecholamine binding is an important method for regulating

enzymatic activity. Although dissociation of catecholamines is extremely slow with the unphosphorylated enzyme (*54*), phosphorylation of tyrosine hydroxylase Ser40 increases the rate by 3 orders of magnitude, thereby allowing for the enzyme to be reduced back to the active ferric form (*55, 56*).

As mentioned, the active-site iron in the aromatic amino acid hydroxylases is ligated by two histidines and a glutamate. A similar arrangement of amino acid ligands is found in a number of other non-heme iron-dependent enzymes, and has been termed a 2-His-1-carboxylate facial triad by Que (*57*). Other enzymes that utilize this motif include several enzymes involved in β-lactam biosynthesis, α-ketoglutarate-dependent diooxygenases, the extradiol cleaving catechol dioxygenases, and the aromatic dioxygenases (*57*). The presence of this iron-binding motif in such structurally and functionally diverse enzymes suggests that this motif may provide some unique catalytic advantages.

In all cases that have been described to date, substitution of one of the ligating residues with alanine results in inactive enzyme (*58-64*). To our knowledge, the only previous report of residual activity upon substitution of any of the residues is the report by Khaleei et al. (*59*) that the H145Q and H280Q variants of clavaminate synthase have low (<3%) residual activity. Further characterization of amino acid substitutions for the metal ligands of tyrosine hydroxylase would increase the understanding of the specific properties of this metal binding motif. The results would then not only provide insight into tyrosine hydroxylase and the other aromatic amino acid hydroxylases, but serve as a reference point for similar studies on other enzymes in which this motif is found.

CHAPTER II

pH AND DEUTERIUM KINETIC ISOTOPE EFFECTS ON SARCOSINE OXIDATION BY *N*-METHYLTRYPTOPHAN OXIDASE*

N-Methyltryptophan oxidase (MTOX) catalyzes the oxidative demethylation of *N*-methyl amino acids (Scheme 2.1). The earliest studies of the enzyme, dating back to the 1940's, showed that MTOX is commonly found in both prokaryotes and eukaryotes, including humans (*32-36*). It was rediscovered in *Escherichia coli* in 1996 due to its 43% amino acid identity to the more thoroughly studied monomeric sarcosine oxidase (MSOX) (*37*). Like MSOX, MTOX is a monomeric enzyme with a covalently attached flavin cofactor (*38*). Although MTOX can demethylate sarcosine (*N*-methylglycine), it has a preference for bulky hydrophobic substrates, such as *N*-methyl-L-tryptophan (*37*).

Scheme 2.1

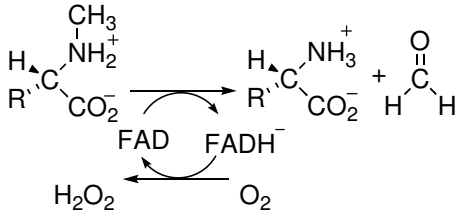

*Reproduced with permission from Ralph, E.C., and Fitzpatrick, P.F. (2005) *Biochemistry 44*, 3074-3081 (*65*). Copyright 2005 American Chemical Society.

The flavoproteins that catalyze amine oxidations have thus far fallen into two structural groups. D-Amino acid oxidase (*12*), MSOX (*28*) and glycine oxidase (*4*) all have a similar overall fold, although the relative orientation of the substrate and flavin differs in MSOX from that in the other two. Sarcosine is a substrate for D-amino acid oxidase (*66*), although the products are glycolate and methylamine instead of glycine and formaldehyde, the products with MSOX and MTOX. Monoamine oxidase B (*17*), polyamine oxidase (*29*), and L-amino acid oxidase (*30*) form a separate structural family. While a number of these enzymes have been the subject of kinetic, spectroscopic, and structural studies, only in the case of D-amino acid oxidase have mechanistic (*13*) and structural (*12*) studies led to a consensus that the reaction involves hydride transfer. In contrast, the chemical mechanism of amine oxidation by the remaining amine oxidases is still debated.

A variety of mechanisms has been proposed for amino acid oxidation by sarcosine oxidase and MTOX (*38, 67-70*). The mechanism shown in Scheme 2.2 involves two separate single electron transfers. The initial transfer of an electron from the substrate nitrogen to the flavin cofactor yields a flavin semiquinone, which is then further reduced either through sequential proton and electron transfers as shown, or through a hydrogen atom transfer. The mechanism shown in Scheme 2.3 involves a concerted electron and proton transfer in the form of a hydride transfer from the substrate methyl group. In the mechanism of Scheme 2.4, the substrate nitrogen attacks the flavin cofactor, forming a covalent substrate-flavin adduct. This is followed by loss of a proton from the substrate methyl carbon and electron rearrangement to give the final products.

Scheme 2.2

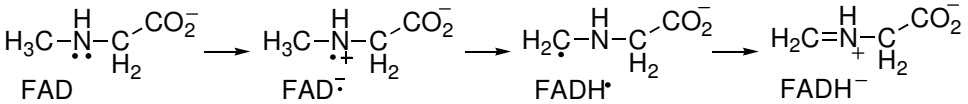

Scheme 2.3

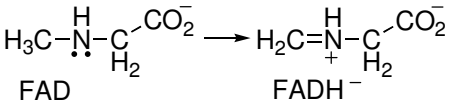

Scheme 2.4

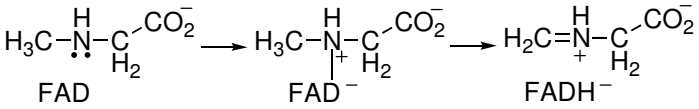

Whereas the hydride transfer mechanism (Scheme 2.3) involves no intermediates between fully oxidized and fully reduced flavin, the mechanisms of Scheme 2.2 and Scheme 2.4 involve a third, intermediate flavin species. The absorbance changes associated with the reduction of the flavin in MSOX or MTOX by a number of substrates have previously been monitored at 25 and 4 ºC (*70-72*). In all cases, flavin reduction could be described as an isosbestic conversion from fully oxidized flavin to fully reduced flavin with no detectable intermediates. Although these observations are consistent with a hydride transfer mechanism, they are insufficient to conclusively assign this mechanism as the mechanism of amine oxidation. As previously noted (*68,*

71) formation of the postulated intermediates may occur during a rate-limiting step. In such a scenario, the rate of decay of the flavin intermediate would be greater than the rate of its formation, thereby preventing any detectable concentration of the intermediate species. In the present study, we utilize pH and deuterium kinetic isotope effects to identify the rate-limiting step of sarcosine turnover by MTOX and to probe for intermediates prior to C-H bond cleavage.

EXPERIMENTAL PROCEDURES

Materials. L-abrine (*N*-Methyl-(L)-tryptophan) was purchased from Aldrich Chemical Company (Milwaukee, WI). Sarcosine (*N*-methylglycine) was purchased from Sigma Chemical Company (St. Louis, MO). *N*-Methyl-$^2H_3$-glycine was purchased from CDN Isotopes (Quebec, Canada). DNA vectors and *E. coli* cells were from Novagen (Madison, WI). The HiTrap Chelating HP column was from Amersham-Pharmacia Biotech (Uppsala, Sweden).

DNA Manipulation. Genomic DNA was prepared from BL21DE3* *E. coli* cells using the Qiagen genomic DNA purification kit. The MTOX gene was amplified by PCR using oligonucleotides 1 and 2 (Table 2.1) and ligated into pUC18 between the EcoRI and XbaI sites. The gene was later amplified with oligonucleotides 1 and 3 and subcloned into pET23d between the EcoRI and XhoI sites in frame with the C-terminal His_6 tag to form the plasmid pETMTOX. The resulting recombinant protein sequence is lengthened by a leucine, a glutamate, and the His_6 tag.

Table 2.1. Oligonucleotides used for PCR amplification and subcloning of the gene encoding for *N*-methyltryptophan oxidase.

Oligonucleotide 1	5'-CCATGAGAGCAGAGAGAATTCAATGAAATACGATCT
Oligonucleotide 2	5'-AAAACTTTCTCATTCTAGAGGCCGTAATGATGATTATTG
Oligonucleotide 3	5'-AGAGGACGAAATGACTCGAGTTGGAAGCGGG

Protein Expression and Purification. A culture of Luria Bertani broth (LB) containing 100 μg ml^{-1} ampicillin was inoculated from a single colony of BL21(DE3)* *E. coli* containing pETMTOX and grown overnight at 37 ˚C. Six liters of LB containing 100 μg mL^{-1} ampicillin were inoculated from the overnight culture using 10 mL culture per liter. The cells were grown at 37 °C to an absorbance at 600 nm of 0.6 to 0.8 and induced with 120 mg IPTG per liter. After an additional 5 hours, the cells were harvested by centrifugation at 5000 x g for 30 minutes at 4 ˚C. The cell pellets (approximately 20 g) were resuspended in 100 mL of 10 mM sodium pyrophosphate, 100 μg mL^{-1} phenylmethylsulfonyl fluoride, 1 μM leupeptin, and 1 μM pepstatin, pH 8.0. Cells were lysed using a French Press, and the cell debris was removed by centrifugation at 29000 x g for 20 minutes at 4 ˚C. The clarified lysate was filtered through a 0.45 μm filter and loaded onto a 5 mL HiTrap Chelating HP column charged with nickel sulfate. Using an Amersham-Pharmacia Biotech AKTA FPLC, the column was washed first with 15 mL of loading buffer, then with a 10 mL gradient of 0 to 6 mM imidazole in 10 mM pyrophosphate, pH 8.0. The protein was eluted with a 25 mL linear gradient of 6 to 120 mM imidazole. Fractions which had A_{280}/A_{460} values less than 15 were pooled and precipitated with 75% saturated ammonium sulfate. The protein was resuspended in a minimal volume and dialyzed against 10 mM sodium pyrophosphate, 10% glycerol, pH 8.0. The resulting protein exhibited a single band in polyacrylamide gel electrophoresis in the presence of sodium dodecyl sulfate. Approximately 130 mg of holoenzyme could be purified from a 6 L cell growth. Enzyme samples were stored at -80 ˚C at a

concentration of 250-300 μM. The flavin content of purified enzyme samples was determined as described by Wagner et al. (*38*).

Enzyme Assays. The rate of oxygen consumption was measured using a Hansatech oxygen monitoring system (Norfolk, UK) with a computer interfaced graphical mode or a Yellow Springs Instrument model 5300 oxygen electrode (Yellow Springs, OH). Steady state kinetic parameters were determined in air saturated 0.1 M ACES, 52 mM Tris, 52 mM ethanolamine-HCl, 1 M potassium chloride at 25 ºC, unless stated otherwise, to provide a constant ionic strength (not accounting for the substrate concentration) over the measured pH range (*73*). The rate of flavin reduction was determined by anaerobic stopped-flow spectroscopy using an Applied Photophysics SX.18MV stopped-flow spectro-photometer. Buffers used for anaerobic experiments included 5 mM glucose and were cycled 10 times between vacuum and argon prior to the addition of glucose oxidase (10 μg mL^{-1}). The active enzyme concentration was calculated from the absorbance at 456 nm using an extinction coefficient of 13.3 mM^{-1} cm^{-1} (*38*).

Data Analysis. The kinetic data were analyzed using the programs KaleidaGraph (Synergy Software, Reading, PA), Igor (Wavemetrics, Lake Oswego, OR), and SPECFIT (Spectrum Software Associates, Marlborough, MA). When the concentration of only one substrate was varied, initial rate data were fit to either the Michaelis-Menten equation or to a straight line. When the concentrations of both substrates were varied, initial rate data (v) were fit to different models described by equations 2.1-2.3; equation 2.1 describes a sequential reaction, equation 2.2 describes a ping-pong reaction, and

equation 2.3 describes an ordered rapid-equilibrium reaction. The k_{cat}/K_m pH profile was fit to equation 2.4, where C_1 is the pH-independent rate constant, L is the concentration of the lyonium ion, and K_1 and K_2 are the dissociation constants for the ionizable groups. Deuterium kinetic isotope effect values were obtained from fits of the data to equation 2.5. This equation describes equal isotope effects on k_{cat} and k_{cat}/K_{sarc}; v is the initial change in oxygen concentration per enzyme concentration per minute, F_i is the fraction of the heavy atom, and E is the observed isotope effect. Stopped-flow traces were fit to equation 2.6, which describes a monophasic exponential decay; k is the first order rate constant, A_t is the absorbance at time t, and A_∞ is the final absorbance. The rate constants for flavin reduction at different concentrations of sarcosine were analyzed using equation 2.7; k_{red} is the rate constant for flavin reduction at saturating sarcosine concentrations, and K_d is the apparent dissociation constant.

$$v = \frac{k_{cat}AB}{K_{ia}K_b + K_aB + K_bA + AB} \tag{2.1}$$

$$v = \frac{k_{cat}AB}{K_aB + K_bA + AB} \tag{2.2}$$

$$v = \frac{k_{cat}AB}{K_{ia}K_b + K_bA + AB} \tag{2.3}$$

$$\log\left(\frac{k_{cat}}{K_m}\right) = \log\left(\frac{C_1}{1 + L/K_1 + K_2/L}\right) \tag{2.4}$$

$$v = \frac{k_{cat} * A}{(K_m + A)(1 + F_i * (E - 1))} \tag{2.5}$$

$$A_{\text{total}} = A_t e^{-kt} + A_\infty \tag{2.6}$$

$$k_{obs} = \frac{k_{red} * A}{(K_d + A)} \tag{2.7}$$

RESULTS

Steady State Kinetics. The C terminus of the recombinant protein encoded by the pETMTOX vector has two extra amino acids followed by a His_6 tag. Analysis of the percent flavin content of purified enzyme indicated approximately 35% of the enzyme contained FAD. The concentration of the holoenzyme determined from the flavin spectrum was used in all calculations of kinetic parameters. The steady state kinetic parameters for this form of MTOX were determined in air saturated 0.1 M potassium pyrophosphate and 1 mM EDTA at pH 8.0 with both *N*-methyltryptophan and sarcosine as substrates and are in good agreement with previously published values (*70*) (Table 2.2). Thus, the His_6 tag does not affect the enzymatic activity of this enzyme.

Slow substrates, such as sarcosine in the case of MTOX, are of great utility in the study of enzyme mechanisms, in that chemical steps are typically rate-limiting in such

cases, allowing intrinsic rate constants, isotope effects, and pK_a values to be measured using steady state kinetics (*74*). Consequently, sarcosine was characterized as a substrate for MTOX to probe the chemical mechanism. To determine the oxygen dependence of sarcosine turnover, initial rates of oxygen consumption were measured in a constant ionic strength buffer at pH 9.4, 25 ºC, while varying both oxygen and sarcosine concentrations (Figure 2.1). The resulting data were fit to equations 2.1-2.3, which describe a sequential mechanism, a ping-pong mechanism, and an ordered rapid equilibrium mechanism, respectively; fitting the data to equation 2.3 required assignment of oxygen as the first substrate. The resulting kinetic parameters are shown in Table 2.3. While the fit to equation 2.1 is statistically better than the fit to equation 2.2, the $K_{i,sarc}$ is not significantly different from zero, consistent with a ping-pong mechanism. Importantly, both fits yield sufficiently low K_{O2} values to allow the determination of intrinsic k_{cat} and k_{cat}/K_{sarc} values under ambient oxygen concentrations.

pH Effects. The k_{cat}/K_{sarc} pH profiles were determined using a constant ionic strength buffer over the pH range 7.5 to 10.2. The presence of 1 M potassium chloride increased enzymatic activity, but did not change the observed pK_a values (data not shown). The k_{cat}/K_{sarc} data (Figure 2.2) were fit by a bell-shaped profile as described by equation 2.4, with a pK_a value of 8.8 ± 0.1 and a less well defined pK_a value around 10.

Table 2.2. Apparent steady state kinetic parameters for His_6 tagged *N*-methyltryptophan oxidase at pH 8.0[a]

	N-Methyltryptophan	Sarcosine
k_{cat} (min^{-1})	1190 ± 50	23 ± 7
K_m (mM)	0.25 ± 0.02	44 ± 5
k_{cat}/K_{sarc} (mM^{-1} min^{-1})	4700 ± 200	0.51 ± 0.04

[a]air saturated 0.1 M potassium phosphate, 1 mM EDTA, pH 8.0, 25 ºC.

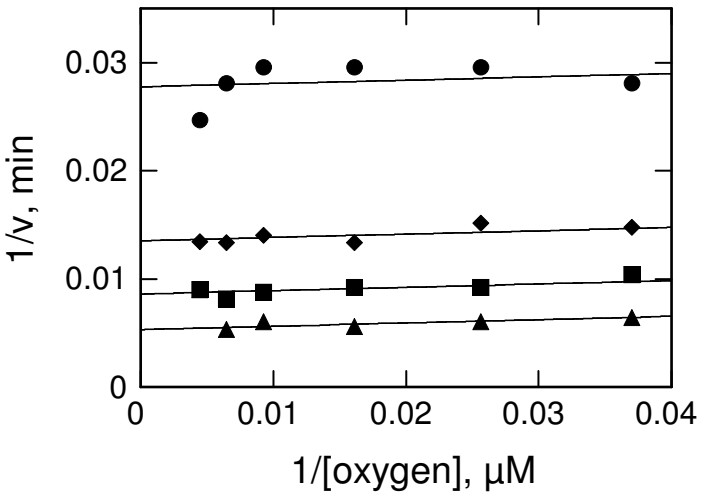

Figure 2.1. Initial rates of oxygen consumption by MTOX measured at various oxygen and sarcosine concentrations. Oxygen concentrations were varied in solutions containing 0.1 M ACES, 52 mM Tris, 52 mM ethanolamine-HCl, 1 M potassium chloride, and 18 (circles), 45 (diamonds), 90 (squares), or 280 (triangles) mM sarcosine at 25 °C, pH 9.4.

Table 2.3. Kinetic parameters for sarcosine oxidation by *N*-methyltryptophan oxidase at pH 9.4[a]

Model (equation)	k_{cat} (min^{-1})	K_{O2} (μM)	k_{cat}/K_{O2} (min^{-1} μM^{-1})	K_{sarc} (mM)	k_{cat}/K_{sarc} (min^{-1} μM^{-1})	$K_{i,\ sarc}$ (M)	$K_{i,\ O2}$ (μM)	χ^2
sequential (2.1)	251 ± 13	5 ± 3	50 ± 30	100 ± 14	2.5 ± 0.4	0.13 ± 0.16	NA	1724
ping-pong (2.2)	262 ± 12	8 ± 2	33 ± 8	114 ± 10	2.3 ± 0.2	NA	NA	1839
rapid eq. (2.3)	233 ± 8	NA	NA	83 ± 9	2.8 ± 0.8	NA	16 ± 5	1964

[a]0.1 M ACES, 52 mM Tris, 52 mM ethanolamine-HCl, 1 M potassium chloride, 25 °C pH 9.4.

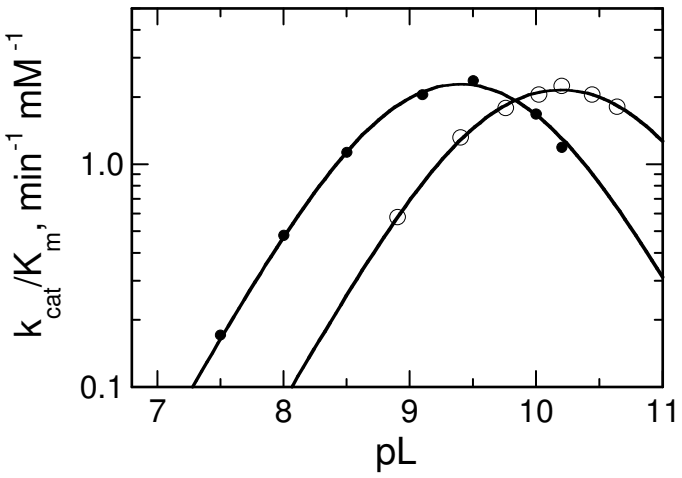

Figure 2.2. k_{cat}/K_{sarc} pH (closed circles) and pD (open circles) profiles for MTOX oxidation of sarcosine. The lines are from fits of the data to equation 2.4. The average error is indicated by the size of the circles. Assays were run in 0.1 M ACES, 52 mM Tris, 52 mM ethanolamine-HCl, 1 M potassium chloride, 25 °C.

Isotope Effects. k_{cat}/K_{sarc} values were also determined in D_2O over the pD range 8.9 to 10.6 (Figure 2.2). The k_{cat}/K_{sarc} values again fit to a bell-shaped profile (equation 2.4) with the pK_a values shifted to 9.5 ± 0.1 and approximately 10.9. Comparison of the pH-independent k_{cat}/K_{sarc} values calculated from the complete pL profiles using equation 2.4 gives a solvent isotope effect of 1.14 ± 0.10. Direct comparison of k_{cat}/K_{sarc} values measured at the pH and pD optima (9.4 and 10.2, respectively) gave a solvent isotope effect of 1.04 ± 0.03.

Deuterium kinetic isotope effects on steady state kinetic parameters were obtained using methyl-deuterated sarcosine (*N*-methyl-$^2H_3$-glycine). The isotope effect was measured at, above, and below the pH optimum of 9.4. In each case, the data fit best to equation 2.5, consistent with an equal isotope effect on k_{cat} and k_{cat}/K_{sarc}. The magnitude of the isotope effect is pH-independent, with an average value of 6.9 ± 0.8 (Table 2.4).

Rapid Reaction Kinetics. The reduction of the MTOX flavin by sarcosine under anaerobic conditions was monitored using single wavelength stopped-flow spectroscopy at various sarcosine concentrations. In all cases, the absorbance change upon flavin reduction could be described by a single exponential decay (equation 2.6) (Figure 2.3). The observed pseudo first order rate constants were fit to equation 2.7 to give k_{red} and K_d values of 220 ± 17 min^{-1} and 160 ± 40 mM, respectively, for the protiated substrate at pH 9.4. These values are in good agreement with the steady state k_{cat} and K_{sarc} values, consistent with the reductive half-reaction being rate-limiting under steady state conditions.

Table 2.4. Deuterium kinetic isotope effects on sarcosine oxidation by *N*-methyltryptophan oxidase

pH	Kinetic Isotope Effect
8.0[a,b]	6.8 ± 0.6
9.4[a,c]	6.6 ± 0.4
10.0[a,c]	7.4 ± 0.4
8.0[d,e]	7.4 ± 0.5
9.4[c,d]	7.7 ± 0.3

[a]From steady state kinetic analyses. [b]0.25 M potassium phosphate. [c]0.1 M ACES, 52 mM Tris, 52 mM ethanolamine-HCl, 1 M potassium chloride. [d]From anaerobic stopped-flow analyses with 250 mM sarcosine. [e]0.1 M Tris, 0.5 M potassium chloride.

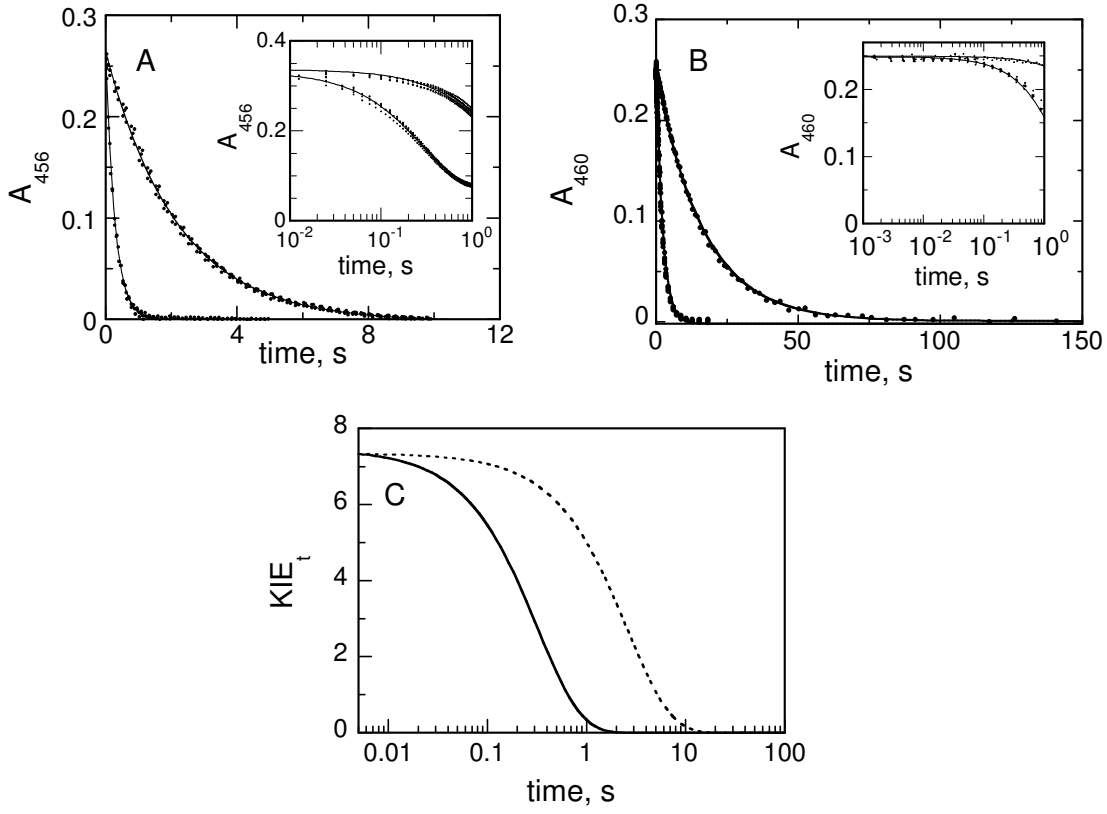

Figure 2.3. Representative time courses of flavin reduction by protiated and deuterated sarcosine at pH 9.4 (A) and 8.0 (B). Reactions contained 250 mM sarcosine (bottom curve in each panel) or deuterated sarcosine (top curve in each panel). The inset shows the first second on a logarithmic time scale. The lines are from the fits of the data to equation 2.6. Reaction conditions are described in Table 2.4. Panel C shows the transient isotope effect for flavin reduction at pH 9.4 (dotted line) and 8.0 (solid line).

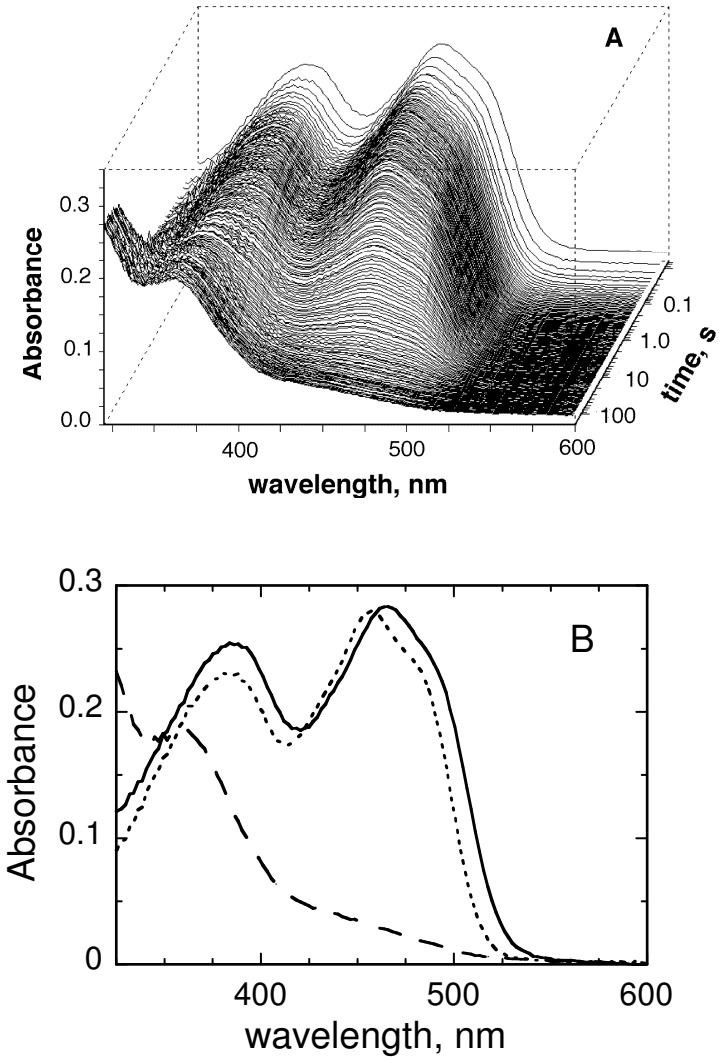

Figure 2.4. Flavin spectral changes during anaerobic reduction of MTOX by deuterated sarcosine (A) at pH 8.0. The conditions were as described in Figure 2.3. The data were fit to a single-step kinetic model. The extrapolated starting and final spectra (solid line and dashed line, respectively) and the spectrum of free enzyme (dotted line) are shown in B.

The equal values for $^{D}k_{cat}$ and $^{D}(k_{cat}/K_{sarc})$ establish that the observed deuterium kinetic isotope effect is independent of the sarcosine concentration and therefore allows for the determination of deuterium kintic isotope effects on the rate of flavin reduction ($^{D}k_{red}$) using a single sarcosine concentration. The $^{D}k_{red}$ value was determined with 250 mM sarcosine at pH 8.0 and 9.4. Direct comparison of the rate constants for flavin reduction yields isotope effects of 7.4 ± 0.5 and 7.7 ± 0.3, at pH 8.0 and 9.4, respectively. These values agree well with the kinetic isotope effects determined under steady state conditions. Analysis of the transient isotope effects as described by Fisher (*75, 76*) is shown in Figure 2.3C. In both cases, the transient isotope effect starts at a value equal to the observed isotope effect and decreases exponentially over time. This is consistent with a single isotope-sensitive step.

Reduction of the enzyme by deuterated sarcosine was also followed with a photodiode array detector, allowing the entire flavin spectrum to be monitored simultaneously. No intermediates were seen between the spectra of the oxidized and the fully reduced enzyme, either at the pH optimum (data not shown) or at pH 8.0 (Figure 2.4A). The complete spectral changes could be modeled with a single exponential decay with rate constants of 0.068 ± 0.001 and 0.43 ± 0.02 s^{-1} at pH 8.0 and 9.4, respectively. These numbers are in good agreement with the single wavelength data obtained under the same conditions (0.061 and 0.46 s^{-1}). Figure 2.4B shows the spectra at zero and infinite time, which were extrapolated from the global analysis of flavin reduction at pH 8.0. Similar results were obtained at pH 9.4 (data not shown). The spectrum of free enzyme is shown for comparison. The extrapolated spectra are those expected for fully

oxidized and fully reduced flavins, consistent with a single step, two-electron flavin reduction. The starting spectrum obtained from the global analysis is clearly different from that of the free enzyme. Differences in the spectra of the free enzyme and the extrapolated oxidized flavin spectra can be attributed to rapid substrate binding during the dead time of the stopped-flow instrument. The increase in absorbance intensity in the 350 nm region is not seen in fresh enzyme samples and is therefore attributed to slight enzyme denaturation after several hours at 25 °C The observed spectrum of the enzyme substrate complex is similar to that seen upon binding D-α-aminobutyrate to D-amino acid oxidase at cryogenic temperatures (*77*) and to the spectrum of MTOX with *N,N*-dimethylglycine bound (*78*).

DISCUSSION

The mechanism of substrate oxidation by flavin-dependent amine oxidases is still widely debated. The chemical mechanisms proposed for *N*-methyltryptophan oxidase or the highly similar sarcosine oxidase are shown in Schemes 2.2-2.4. Although the mechanisms shown in Schemes 2.2 and 2.4 involve the formation of a flavin intermediate between the fully oxidized and fully reduced flavin species, no spectroscopic evidence of such intermediates has been reported. To account for the lack of such evidence, it has been proposed that formation of the postulated intermediates may occur during a rate-limiting step, thereby preventing the accumulation of detectable intermediate concentrations. The slow substrate sarcosine was chosen for this study with the expectation that chemical steps rather than substrate binding or product release

would be rate-limiting, allowing intrinsic isotope effects and pK_a values to be determined. All of the kinetic data presented here are consistent with cleavage of the sarcosine C-H bond being rate-limiting, in line with this prediction.

With virtually all flavoprotein oxidases studied to date, the steady state kinetic mechanism can be described by a variation of the mechanism of Scheme 2.5 (*79*). Here, the enzyme containing oxidized flavin (EFl_{ox}) binds and oxidizes the substrate (S), producing the reduced enzyme-product complex ($EFl_{red}P$). This can then react with molecular oxygen or an alternative electron acceptor in the case of the related dehydrogenases. Whether the oxidized product (P) dissociates before or after reoxidation of the flavin varies with the specific enzyme and the substrate. This mechanism results in steady state kinetic patterns which fit to the equations developed for ping-pong or sequential mechanisms; the reversibility of the flavin reduction determines whether the rate equation contains the extra term in K_{ia} which distinguishes ping-pong and sequential mechanisms (*80*). Khanna and Jorns (*70*) previously reported that the initial rate data for *N*-methyltryptophan turnover by MTOX are consistent with the upper loop of Scheme 2.5. In contrast, the data with sarcosine as substrate were fit to a rapid equilibrium kinetic model with oxygen binding as the first substrate. This was the first report of oxygen binding by an oxidized flavoprotein, although MSOX variant H270Q[1] was

---

[1]H270 was previously described as H269 (*69, 72*) based on the crystal structure of MSOX ((*28*), which is missing the initial methionine residue.

subsequently reported to have a similar kinetic pattern, in contrast to the wild-type enzyme (*72*). However, MTOX is readily reduced by sarcosine in the absence of oxygen, and the kinetic parameters for that reduction establish the free oxidized enzyme as kinetically competent for reduction; this rules out any mechanism in which oxygen must bind before sarcosine. The reason for the discrepancy with the earlier data is not clear. The initial rate data described here for sarcosine turnover are fit well by the equation for ping-pong kinetics, in line with the common kinetic mechanism for flavoprotein oxidases of Scheme 2.5. The assignment of this kinetic mechanism over a sequential mechanism is further supported by the rapid reaction kinetics, which are most consistent with an effectively irreversible flavin reduction, and by the deuterium kinetic isotope effects, which are consistent with an effectively irreversible C-H bond cleavage. Most critically for the present work, whether the data are fit to equation 2.1 or equation 2.2, the K_{O2} value is sufficiently low that k_{cat} and k_{cat}/K_{sarc} values can be treated as independent of the oxygen concentrations under atmospheric oxygen conditions.

Scheme 2.5

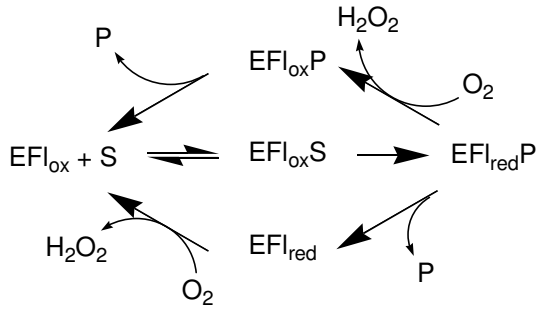

With sarcosine as substrate, the reductive half-reaction is clearly rate-limiting. The rate constant for flavin reduction at saturating sarcosine concentrations and the Kd value for sarcosine determined from the analysis of the reduction kinetics match the kcat and Ksarc values from steady-state kinetics. The agreement between the K_d value and the K_m value for sarcosine is also consistent with a lack of an external forward commitment to catalysis for this substrate. This conclusion is supported by the pH independence of the deuterium isotope effect on the k_{cat}/K_{sarc} value (*81*). The identity of $^{D}k_{cat}/K_{sarc}$, $^{D}k_{cat}$, and $^{D}k_{red}$ is consistent with a lack of any significant internal or reverse commitment, so that the average isotope effect of 7.2 obtained from both steady state and rapid reaction analyses is likely to be the intrinsic deuterium isotope effect. The magnitude of this value is consistent with the expectation for the intrinsic isotope effect upon cleavage of a C-H bond in a trideuterated methyl group. The value of 7.2 agrees well with the deuterium isotope effect of 7.3 for the heterotetrameric sarcosine oxidase from *Arthrobacter sp.* (*69*), suggesting that the extent of C-H bond cleavage in the transition state is similar for the two enzymes, even though sarcosine is a slow substrate for MTOX.

The bell-shaped k_{cat}/K_{sarc} pH profile is consistent with two groups in the free enzyme or substrate whose protonation state is critical for catalysis, with pK_a values of 8.8 ± 0.1 and approximately 10. While the inability to measure initial rates at high pH due to enzyme instability greatly limits the precision of the upper pK_a value, a pK_a value of 10 would match the pK_a value of substrate amino group (*82*), suggesting that the

zwitterionic form of the substrate is preferred and that the lower pK_a is due to a group on the enzyme which must be unprotonated.

Oxidation of the carbon-nitrogen bond in sarcosine by MTOX necessarily requires the loss of a hydrogen from the substrate nitrogen. The lack of a solvent isotope effect on the k_{cat}/K_{sarc} value limits the possibilities for the timing of the cleavage of this nitrogen-hydrogen bond. Deprotonation of enzyme-bound sarcosine must occur in a rapid and reversible step which precedes C-H bond cleavage. A similar order of events is seen with MSOX, where binding of zwitterionic proline is followed by the formation of a pH-dependent absorbance attributed to a charge transfer interaction between the oxidized flavin and electron rich anionic proline prior to C-H bond cleavage (*67*).

The changes in the flavin spectrum which occur upon reduction of MTOX by sarcosine are fully consistent with a minimal kinetic model in which binding of the amino acid is very rapid and is followed by a single step in which a hydride equivalent is transferred to the flavin. While these results do not rule out additional intermediates, they place limits on the extent to which they accumulate and thus on their energetics. The kinetic isotope effects establish that C-H bond cleavage occurs in the rate-limiting transition state for flavin reduction. This rules out rate-limiting formation of an intermediate in which the C-H bond is intact. Furthermore, for an intermediate between the oxidized enzyme-substrate complex and the reduced enzyme, the rate constant for productive decay necessarily equals the rate constant for flavin reduction. In the case of deuterated sarcosine, in which cleavage of the C-H bond has been slowed by seven-fold, the large decrease in the rate constant for reduction should result in a comparable

increase in the accumulation of any such intermediate. If one assumes that any intermediate that accumulates to 35% would be detected, the lack of such a detectable intermediate with the deuterated substrate places an upper limit of 5% on the maximum amount of the intermediate which builds up prior to C-H bond cleavage. The present data do not rule out a mechanism in which an intermediate is formed at lower concentrations than this due to its being at a free energy well above that of the enzyme-substrate complex. Still, the lack of detectable intermediates is most simply explained by a lack of intermediates, as is the case for a hydride transfer mechanism.

This conclusion is supported by structural data. Although structural information is not available for MTOX, a crystal structure is available for MSOX (*83*). In several crystal structures with product analogues bound, the carbon corresponding to the reactive carbon of the substrate is within 4 Å of the flavin N5, an arrangement which is common in flavoproteins catalyzing dehydrogenation reactions (*31*). This distance is compatible with a hydride transfer mechanism.

The anionic flavin semiquinone and flavin adducts proposed as intermediates in Scheme 2.2 and Scheme 2.4, respectively, should be readily detectable if they accumulate significantly. The spectrum of the anionic flavin semiquinone in MTOX has a visible absorbance maximum at 393 nm with an ε_{393} of 28,8000 $M^{-1}cm^{-1}$ (*78*), compared to the maximum of the free oxidized enzyme at 456 nm of 13,3000 $M^{-1}cm^{-1}$ (Figure 2.4) (*38*), and would be readily distinguished. Flavin N5 and C4a adducts have spectra which resemble that of fully reduced flavin, with an additional shoulder or peak at 300-400 nm (*84*). While such an intermediate might be difficult to distinguish from a

reduced enzyme-product complex in an analysis such as that shown in Figure 2.4, its presence would result in a decrease in the apparent absorbance of the enzyme substrate complex; this is ruled out by comparison of the spectra of the free oxidized enzyme and of the intermediate formed upon binding of sarcosine (Figure 2.4).

As an alternative to the anionic flavin semiquinone, the neutral flavin semiquinone is characterized by a reduced absorbance around 460 nm compared to fully oxidized flavin, and broad absorbance bands from around 500 to 650 nm with extinction coefficients of 3,000 to 10,000 M^{-1} cm^{-1} (*3*). This species is unlikely to form however, due to the low pK_a value for conversion into the anionic form. This pK_a value has been estimated as below pH 6.0 in MSOX (*83*); a similar value is expected for MTOX given the high percent identity between the two enzymes. The pH optimum for both enzymes is above pH 9 (*83*).

Some evidence for a radical mechanism for MTOX and related enzymes has come from studies of MSOX with substrate analogues. *N*-Cyclopropylglycine will slowly inactivate MSOX; the reaction simultaneously forms a species with a partially bleached visible absorbance spectrum that very slowly decomposes to fully reduced enzyme (*68*). In subsequent studies, the inactivated intermediate was trapped using sodium borohydride. The resulting enzyme is covalently labeled on the flavin cofactor (*85*). The inactivation was attributed to one-electron oxidation of the inhibitor to the cyclopropyl radical, which then reacted with the flavin semiquinone. However, cyclopropyl compounds have been found to inactivate other flavoprotein oxidases by mechanisms that are not analogous to the oxidation of more normal substrates. Thus, a

number of inhibitors that would be expected to utilize radical intermediates for inactivation have been described for monoamine oxidase (*16*). Recent elucidation of the three-dimensional structure of monoamine oxidase B shows that the amino acid residue which is labeled by some of these inhibitors is well outside the active site (*17*), suggesting that inactivation and normal catalysis utilize different mechanisms. Methanol oxidase (*18*) and cholesterol oxidase (*19*), two members of a family of homologous flavoprotein alcohol oxidases (*20*), are both inactivated by cyclopropyl compounds; in this case the available evidence is most consistent with hydride transfer mechanisms for these enzymes (*21, 22*).

In summary, the present results are most consistent with a hydride transfer mechanism for MTOX, in that no intermediates are detected prior to rate-limiting C-H bond cleavage. The structural similarities among the other known and predicted members of the MTOX/MSOX family suggest that these enzymes also utilize a similar mechanism.

CHAPTER III

^{15}N KINETIC ISOTOPE EFFECTS ON SARCOSINE OXIDATION BY *N*-METHYLTRYPTOPHAN OXIDASE

Flavin-dependent amine oxidases and dehydrogenases catalyze the oxidative deamination of primary amines and the oxidative dealkylation of secondary amines. These enzymes are ubiquitous in nature and are involved in a myriad of biological activities. For example, glycine oxidase is involved in thiamin biosynthesis in microorganisms (*4*), while the recently discovered lysine specific histone demethylase is involved in regulation of transcription in humans (*5*). The ubiquity and functional diversity of this family of enzymes underlies its importance and has prompted many structural and biochemical studies.

To date, flavoenzymes that catalyze amine oxidations have fallen into two structural groups. One class includes D-amino acid oxidase (*12*), monomeric sarcosine oxidase (*28*) and glycine oxidase (*4*), while monoamine oxidase B (*17*), polyamine oxidase (*29*), and L-amino acid oxidase (*30*) form a separate structural family. While a number of these enzymes have been the subject of kinetic, spectroscopic, and structural studies, only in the case of D-amino acid oxidase have mechanistic (*13*) and structural studies (*12*) led to a consensus that the reaction utilizes a hydride transfer. In contrast, the chemical mechanism of the remaining amine oxidases is still debated.

N-Methyltryptophan oxidase (MTOX) catalyzes the oxidative demethylation of *N*-methyl amino acids (Scheme 3.1), with a preference for bulky hydrophobic substrates

such as *N*-methyl-L-tryptophan (*37*). Although the three dimensional structure of MTOX is unavailable, it shares 41% sequence identity with monomeric sarcosine oxidase, suggesting it can be assigned to the same structural family. As shown in Schemes 3.2-3.4, a variety of mechanisms have been proposed for substrate oxidation by MTOX (*70*). Similar mechanisms have been proposed for other flavin-dependent amine demethylases (*67-69, 86*) and for flavin-dependent amine oxidation in general (for recent reviews, see references (*9*) and (*8*)). Therefore, investigation of the chemical mechanism of substrate oxidation by MTOX should aid in understanding a number of important flavoenzymes.

Scheme 3.1

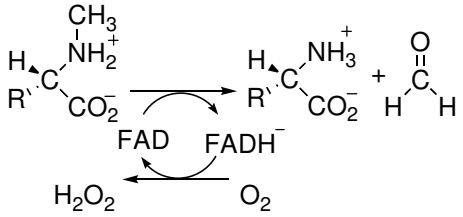

Schemes 3.2-3.4 are representative of the types of mechanisms commonly proposed for flavin-dependent amine oxidations. The simplest mechanism, shown in Scheme 3.2, involves a hydride transfer from the anionic substrate to the flavin without the formation of an intermediate species. In the mechanism of Scheme 3.3, the substrate nitrogen attacks the flavin cofactor to form a covalent substrate-flavin adduct. The subsequent relocalization of electrons results in decay of the adduct to yield the Schiff-base product. The mechanism of Scheme 3.4 involves the one electron oxidation of the

substrate, yielding an aminium radical and a flavin semiquinone. These intermediate species are then resolved either through sequential electron and proton transfers as shown, or through abstraction of a hydrogen atom. In all cases, dealkylation occurs via the non-enzymatic hydrolysis of the Schiff-base product.

Scheme 3.2

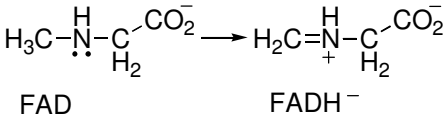

Scheme 3.3

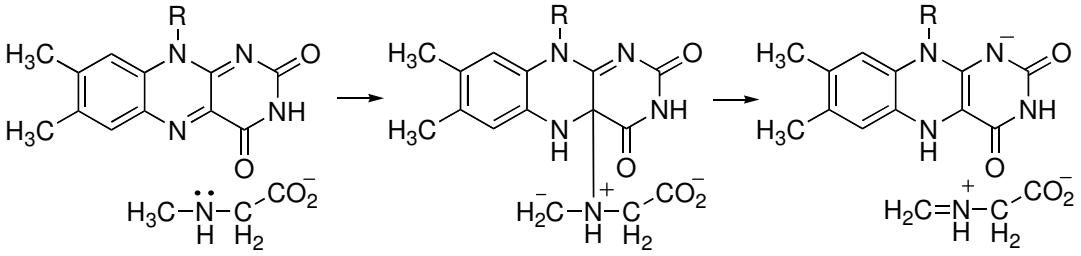

Scheme 3.4

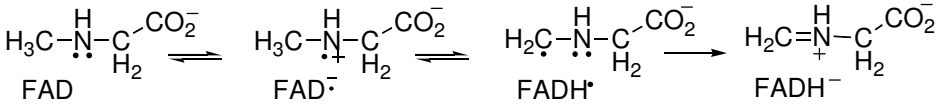

In the present study, ^{15}N isotope effects are utilized to probe the mechanism of sarcosine oxidation by MTOX. ^{15}N kinetic isotope effects on k_{cat}/K_m report on changes in the sarcosine nitrogen's bonding order that occur prior to or during the first irreversible step in oxidation. The previously determined primary deuterium kinetic isotope effects show that C-H bond cleavage is the first irreversible step in catalysis (*65*). Therefore, the ^{15}N kinetic isotope effects can be used to determine the relative timing of changes in the nitrogen bond order and C-H bond cleavage, and thereby distinguish between the mechanisms of Schemes 3.2-3.4.

EXPERIMENTAL PROCEDURES

Materials. Sarcosine (*N*-methylglycine) was purchased from Sigma Chemical Company (St. Louis, MO) or ACROS Organics (Morris Plains, NJ). MTOX was purified on a HiTrap Chelating HP column as previously described (*65*).

Sample Preparation. Sarcosine consumption reactions were run over a pH range of 7.5 to 9.7. Starting conditions were typically 0.2 M sarcosine and 100 μg mL^{-1} catalase in 10 mL. Samples were buffered using potassium phosphate (pH 7.5), potassium pyrophosphate (pH 8-9) or sarcosine (pH > 9). A decrease in the sample pH was observed as the reaction progressed. Therefore, the pH was frequently monitored and adjusted with potassium hydroxide as necessary. With few exceptions, the reaction samples were kept within 0.1 pH units of the desired value. Additional MTOX was added periodically to keep the reaction progressing. Reactions were stirred in the dark at 25 ºC with wet 100% oxygen blowing over the surface. Reaction progress was

monitored using a Waters Delta 600 HPLC with a model 2487 Dual λ Absorbance Detector. A 100 µL sample was withdrawn and mixed with 500 µL of 50 mM monobasic potassium phosphate in 50 % MeCN. Protein was removed by either filtering the sample through a 0.20 µm nylon filter or by centrifugation for 20 min at 21000 x G. The sample was then loaded onto a Waters µBondapak-NH_2 column (3.9 x 300 mm) with a 100 µL loop and eluted isocratically with 5 mM potassium phosphate, in 77 % MeCN, pH* 7.2, at 3 mL min^{-1}. Sarcosine, glycine, and formaldehyde were detected by monitoring the absorbance at 210 nm. The fractional consumption of sarcosine was determined by comparing the peak areas of sarcosine and glycine to standard curves prepared using commercially available compounds.

After 30-50 % of the sarcosine had been oxidized, reactions were quenched by the addition of hydrochloric acid to yield a pH below 1. Protein was removed by centrifugation. Samples were dried using a rotary evaporator and resuspended in 4 to 5 mL of water. Acetonitrile was added to yield 40 to 50%, and the pH was adjusted to pH* 7. Samples (1 mL) were loaded onto a preparative Waters µBondapak-NH_2 column (7.8 x 300 mm) and eluted at 4 mL min^{-1} with 2.5 mM potassium phosphate, in 77% MeCN pH* 7.2, while collecting 8 mL fractions. The sarcosine and glycine fractions were separately pooled, dried on a rotary evaporator, resuspended in water, lyophilized, and submitted for isotope ratio mass spectrometry (IRMS) analysis.

IRMS Analysis. IRMS analysis was conducted by Dr. Mark A. Anderson[2] (U. Wisconsin) as follows. Quartz tubes (0.9 cm o.d. x 0.7 cm i.d. x 24 cm long) were charged with 100 mg of diatomaceous earth, 3-4 g of cupric oxide, 500 mg elemental copper, and either 8-10 mg of sarcosine or 6-8 mg of glycine. The tubes were placed under vacuum, flame-sealed, and combusted at 850 ºC. The nitrogen gas produced was distilled on a high vacuum line through two -78 °C traps and one -196 °C trap, and then trapped on molecular sieves at -196 ºC. The isotopic composition of the gas was determined using a Finnegan delta E isotope ratio mass spectrometer.

Data Analysis. The observed ^{15}N isotope effects were calculated from equations 3.1 and 3.2 (*87*), where *f* is the final fractional consumption of sarcosine, and R_S/R_0 and R_P/R_0 are the $^{15}N/^{14}N$ ratios for the sarcosine and enzymatically formed glycine, respectively, at *f* fraction conversion, divided by the isotope ratio of the sarcosine at 0 fraction conversion. The pH dependencies of the observed ^{15}N effects were fit to equation 3.3 using KaleidaGraph (Synergy Software, Reading, PA). Here, the pK_a is for the sarcosine amine, $^{15}K_{eq}$ is the equilibrium isotope effect for amine deprotonation, and ^{15}k is the pH-independent isotope effect obtained after correcting for the protonation state of the free substrate.

---

[2]Dr. Anderson is a member of Dr. W. Cleland's lab in the Institute for Enzyme Research and the Department of Biochemistry at the University of Wisconsin, Madison, WI.

$$^{15}(k_{cat}/K_m) = \frac{\log(1-f)}{\log[(1-f)(R_S/R_0)]} \quad (3.1)$$

$$^{15}(k_{cat}/K_m) = \frac{\log(1-f)}{\log(1-fR_P/R_0)} \quad (3.2)$$

$$^{15}(k_{cat}/K_m)_{obs} = {}^{15}k * [1+(^{15}K_{eq}-1)/(1+10^{pH-pKa})] \quad (3.3)$$

RESULTS AND DISCUSSION

Despite a great deal of study, the chemical mechanism of amine oxidation by flavin-dependent enzymes is still debated. Commonly proposed mechanisms utilize either a hydride transfer from the substrate carbon to N5 of the flavin cofactor (Scheme 3.2), a nucleophilic attack of the substrate nitrogen on the flavin cofactor to form a covalent adduct intermediate (Scheme 3.3), or a single electron transfer from the substrate nitrogen to the flavin, forming a flavin semiquinone intermediate (Scheme 3.4). ^{15}N kinetic isotope effects can be used to determine the relative timing of changes in the nitrogen bond order and C-H bond cleavage, and thereby allow for the discrimination between these three proposed mechanisms.

To determine ^{15}N isotope effects for MTOX, sarcosine solutions were oxidized by the enzyme to 30-50 % conversion, yielding a mixture of sarcosine, glycine, and formaldehyde. The sarcosine and glycine were separated by HPLC and analyzed for their $^{15}N/^{14}N$ content using IRMS. The observed ^{15}N isotope effects were calculated using equations 3.1 and 3.2, as described in *EXPERIMENTAL PROCEDURES*.

Calculation of the isotope effects using equations 3.1 and 3.2 requires an accurate determination of the final percent of sarcosine consumed (f). The relative error in f has less impact on the calculated isotope effect as f increases. Given the slow nature of both the enzymatic reaction and the rate of diffusion of oxygen into a solution, two to three days were typically required to achieve a usable percent consumption for sarcosine. This problem was exacerbated by a time-dependent loss of activity during turnover, which prevented reactions above pH 10 from reaching a usable percent consumption.

The observed isotope effects are pH-dependent (Figure 3.1), starting at a value of approximately 1.017 and decreasing with increasing pH. For each reaction, independent $^{15}(k_{cat}/K_m)_{obs}$ values were calculated from the remaining sarcosine (Figure 3.1A) and from the glycine product (Figure 3.1B); a comparison of the two values serves as an internal control for any artifactual ^{15}N fractionation that may result during sample preparation. The isotope effect calculated from the residual sarcosine was always slightly higher than that calculated from the product glycine. The first reaction at pH 8.5 showed the largest difference in $^{15}(k_{cat}/K_m)_{obs}$ values (0.0023). Therefore, a second reaction was run at the same pH which yielded a much smaller difference in $^{15}(k_{cat}/K_m)_{obs}$ values (0.0004). The averages of the isotope effects determined from substrate and product were nearly identical for both reactions (1.0168 and 1.0169). These observations are not consistent with random ^{15}N fractionation, which would affect the two determinations of $^{15}(k_{cat}/K_m)_{obs}$ independently and therefore alter the measured average isotope effects. Random fractionation is also unlikely to result in a consistent

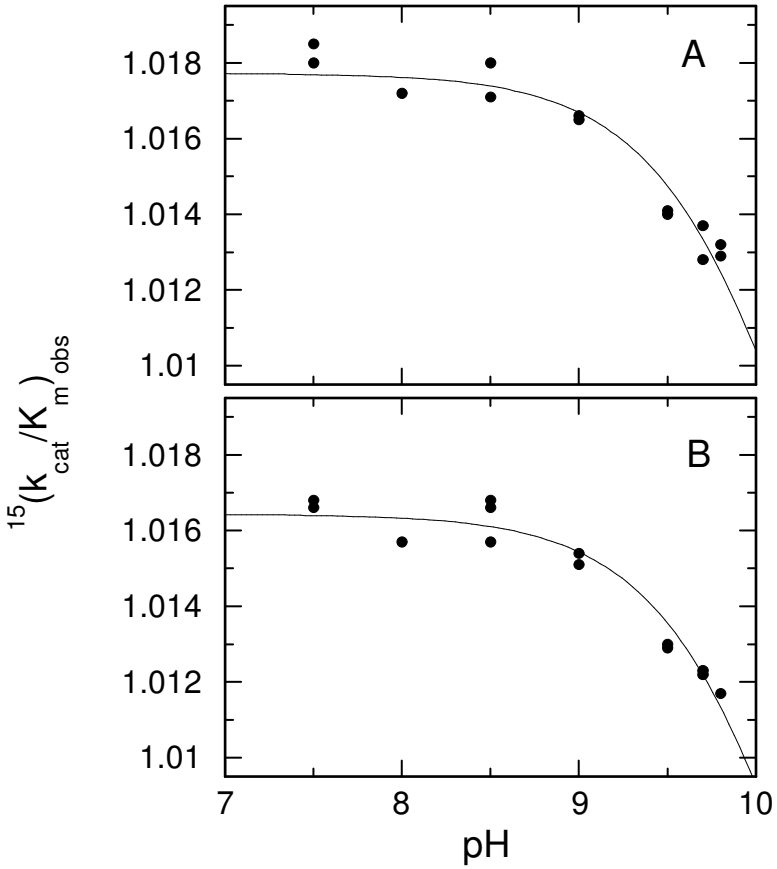

Figure 3.1. The observed ^{15}N kinetic isotope effects for sarcosine oxidation by MTOX. The values were determined from the isotopic content of sarcosine (A) and glycine (B) as described in EXPERIMENTAL PROCEDURES. The lines are from fits of the data to equation 3.3 using a $^{15}K_{eq}$ value of 1.0226.

increase of one value relative to the other. The above observations are instead consistent with a small systematic error in the determination of the percent conversion. Importantly, the same mechanistic conclusions are afforded whether one is using values derived from the sarcosine data, values derived from the glycine data, or values derived from simultaneous analysis of both data sets, as discussed below.

The pH dependence of the observed ^{15}N isotope effects is not due to changes in either the rate-limiting step or the transition state structure, as the observed deuterium kinetic isotope effect is pH-independent over the same pH range (*65*). The pH dependence can therefore be attributed to the ^{15}N equilibrium isotope effect ($^{15}K_{eq}$) on sarcosine deprotonation. Regardless of the mechanism of oxidation, a proton must be removed from the sarcosine nitrogen to form the Schiff-base product. Substitution of ^{14}N with ^{15}N increases the pK_a of an amine, making deprotonation less favorable; the $^{15}K_{eq}$ value is greater than one. As described by equation 3.3, the contribution of the sarcosine $^{15}K_{eq}$ value on the observed isotope effect is dependent upon the protonation state of the sarcosine in solution. When all the sarcosine in solution is deprotonated, the observed isotope effect is equal to ^{15}k. When all the sarcosine is protonated, the observed isotope effect is the product of ^{15}k and $^{15}K_{eq}$. A comparison of the observed isotope effects at pH values well above and well below the sarcosine pK_a would therefore allow for the determination of both contributing isotope effects. However, enzymatic instability during turnover limited the accessible pH range to conditions below pH 9.8, as discussed above.

Although the $^{15}K_{eq}$ value for sarcosine deprotonation could not be determined in

this study, a $^{15}K_{eq}$ value for glycine deprotonation of 1.0226 has been measured by two independent groups using ^{13}C NMR (*88, 89*). An identical value for the deprotonation of dimethylamine has been calculated using density functional theory[3]. This value is therefore a reasonable estimate for the $^{15}K_{eq}$ value for sarcosine deprotonation, and was used for all subsequent analysis.

Fitting the observed isotope effects for sarcosine oxidation to equations 3.3 and 3.4 yields ^{15}k values of 0.9953 ± 0.0003 and 0.9938 ± 0.0002, respectively, with an average value of 0.9946 ± 0.0010. (The variance between these numbers is discussed above.) A ^{15}k value of 0.9971 ± 0.0005 was previously calculated for oxidation of phenylalanine to the corresponding Schiff-base (*15*). A similar value of 0.9963 ± 0.0016 was observed for oxidation of D-serine by D-amino acid oxidase (*13*), which is generally accepted to utilize a hydride transfer mechanism (*8*). The agreement between these three values is consistent with C-H bond cleavage and rehybridization of the sarcosine nitrogen from sp^3 to sp^2 being concerted during MTOX oxidation of sarcosine. These results therefore strongly support a hydride transfer mechanism.

---

[3]Jennifer S. Hirschi and Daniel A. Singleton (TAMU), personal communication.

One alternative to a hydride transfer mechanism, shown in Scheme 3.3, involves as an intermediate a flavin-substrate adduct. This mechanism was originally proposed in 1970 (*23*) and later revised by Miller and Edmondson for monoamine oxidase (*27*) to involve a C-H bond cleavage that is concerted with formation of the adduct, thereby accounting for the observed deuterium kinetic isotope effects and the lack of a detectable flavin intermediate. As the original and revised mechanisms would have significantly different ^{15}N kinetic isotope effects, it is useful to review the arguments presented by Miller and Edmondson (*27*) as they apply to the flavin-dependent demethylation of sarcosine.

In the original mechanism, nucleophilic attack of the substrate on the flavin cofactor formed a covalent adduct in which the substrate C-H bond remained intact (*23*). For MTOX, the reactive methyl proton would then be removed by an undetermined active site base, resulting in productive decay of the adduct, as shown in Scheme 3.5. The magnitude of the observed isotope effect on this C-H bond cleavage is consistent with a symmetrical transition state, suggesting that the pK_a of the base abstracting the methyl proton is approximately equal to the pK_a of the methyl group itself (*90*). However, the pK_a of the methyl group is expected to be approximately 35 (compared to *N*-dimethylamine (*91*)), well above the values expected for amino acid side chains. It therefore seems unlikely that any amino acid residue is the catalytic base required by the mechanism of Scheme 3.5.

Scheme 3.5

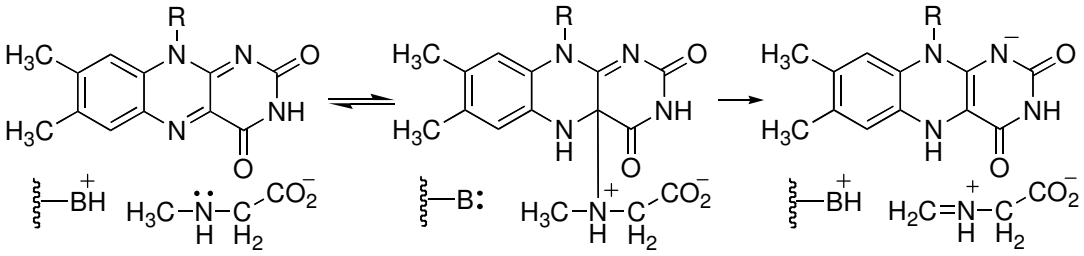

Alternatively, Miller and Edmondson (*27*) noted that as the substrate nitrogen attacks the flavin cofactor, the electron density increases at flavin N5, forming a strong base with a pK_a value that is expected to be in the range of anilines, i.e., approximately 30. The high pK_a value enables the flavin to abstract the substrate methyl proton; the agreement between the two pK_a values is consistent with a symmetrical transition state. As formation of the adduct results in formation of the strong base, this step is proposed to be concerted with C-H bond cleavage (Scheme 3.3). The mechanism of 3.3 is also consistent with the lack of a detectable flavin intermediate, as formation of the intermediate is rate-limiting.

Although the mechanism of Scheme 3.3 is consistent with the observed deuterium kinetic isotope effects (*65*), it is not consistent with the observed ^{15}N kinetic isotope effects for sarcosine turnover by MTOX. As indicated by the primary deuterium kinetic isotope effects (*65*), adduct formation is irreversible, indicating that subsequent steps are not part of k_{cat}/K_m and do not contribute to the observed ^{15}N isotope effects; ^{15}k for this mechanism is the isotope effect for formation of the sarcosine-flavin adduct. Adduct formation produces a fourth bond for the sarcosine nitrogen, but does not change

the nitrogen's hybridization. This step is therefore analogous to protonating the sarcosine amine, with an isotope effect equal to the reciprocal of the isotope effect for sarcosine deprotonation. As discussed above, the observed isotope effects approach a value equal to the product of ^{15}k and $^{15}K_{eq}$ at values below the sarcosine pK_a. As one value is the reciprocal of the other value, the product of these two isotope effects must equal 1.00, regardless of the magnitude of $^{15}K_{eq}$. As shown in Figure 3.1, the observed isotope effects at pH 7.5 are greater than 1.016 for both the glycine and sarcosine data, indicating that MTOX does not utilize a nuclephilic attack mechanism.

Radical mechanisms similar to Scheme 3.4 are frequently proposed for flavin-dependent amine oxidations (reviewed in (*9*)). These mechanisms start with the formation of an anionic flavin semiquinone and a substrate aminium radical, which can then be resolved through a step-wise electron and proton transfer (Scheme 3.4), or through abstraction of a hydrogen atom (Scheme 3.6). Support for radical-based mechanisms comes primarily from oxidation studies of cyclopropyl or cyclobutyl compounds with monoamine oxidase ((*9*), and references therein). These compounds undergo one electron oxidations of the amine followed by a rapid ring-opening, as predicted by the mechanism of Scheme 3.4; the ring-opened product then labels and inhibits the enzyme (*9, 68, 85*). Although the evidence supports a radical mechanism of inactivation by these inhibitors, the mechanism of Scheme 3.4 is inconsistent with the observed ^{15}N kinetic isotope effects. In the mechanism of Scheme 3.4, C-H bond cleavage is concerted with rehybridization of the aminum radical to an sp^3 hybridization for the nitrogen. After correcting for the sarcosine protonation state, the ^{15}N isotope

effects report on the formation of the carbon radical from free sarcosine. As these two species have nearly identical bonding orders for the sarcosine nitrogen, the ^{15}k value for this mechanism is not expected to differ significantly from unity. The limiting observed value at low pH should therefore equal $^{15}K_{eq}$. The observed limiting isotope effects at low pH and the calculated ^{15}k value of 0.9946 ± 0.0010 are inconsistent with this mechanism.

Scheme 3.6

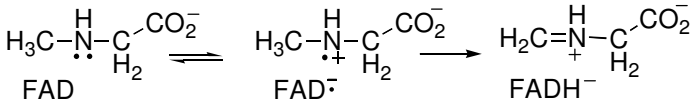

An alternative radical mechanism is presented in Scheme 3.6, where C-H bond cleavage is concerted with Schiff-base formation. The ^{15}N isotope effects for this mechanism report on the same net reaction as for a hydride transfer mechanism. This mechanism is therefore consistent with the observed $^{15}(k_{cat}/K_m)$ values. Although the mechanism of Scheme 3.6 cannot be ruled out by the present kinetic isotope effects, the lack of a detectable flavin intermediate during flavin reduction is not consistent with the involvement of a flavin radical (*65*). Furthermore, such a mechanism would be energetically unfavorable. Although reliable determinations of one electron reduction potentials for amines and their corresponding aminium radicals are complicated by radical instability (*92*), the one electron reduction potentials for dimethyl and diethylsulfate have been measured at 1.66 and 1.60 V vs. SHE, respectively (*93*).

Replacing sulfur with the more electronegative nitrogen would likely increase this reduction potential further. Therefore, 1.6 V vs. SHE can be used as a conservative lower limit for the reduction potential of sarcosine. In contrast, the reduction potentials for flavoenzymes are typically below 200 mV vs. SHE; the one electron reduction potential for monomeric sarcosine oxidase is approximately 80 mV vs. SHE (*72*). The approximately 1.5 V difference in reduction potentials allows for the calculation of an equilibrium constant of 10^{-26} for the reversible formation of the flavin-substrate radical pair.

Similarly unfavorable equilibrium constants have been used to argue against the oxidation of primary amines via a radical mechanism by monoamine oxidase (*27*). Proponents of a radical mechanism for monoamine oxidase have proposed that a large energetic barrier to radical formation may not prevent the reaction in an enzyme active site if substrate binding significantly alters the redox properties of the substrate, the flavin, or both, or if radical formation is followed by a thermodynamically favorable event (*94*). Although the available data cannot explicitly rule out these possibilities, the difference in the substrate and flavin reduction potentials would have to be decreased by

greater than 700 mV to be consistent with the observed rates of catalysis.[4] Such a dramatic change in reduction potentials upon substrate binding is unprecedented. Furthermore, such a slow formation of an unstable radical followed by a rapid hydrogen atom abstraction is effectively indistinguishable from a hydride transfer.

In summary, the ^{15}N kinetic isotope effects, combined with the previously determined deuterium kinetic isotope effects, and the lack of a detectable flavin intermediate (*65*), are all best explained by a hydride transfer mechanism of sarcosine oxidation by MTOX. These results add to the growing body of evidence for hydride transfer mechanisms in flavoenzymes that oxidize amines, alcohols, α-amino acids, and α-hydroxy acids.

---

[4]As C-H bond cleavage is completely rate-limiting for sarcosine oxidation by MTOX (*65*), k_{cat} for the mechanism of Scheme 3.6 can be defined as the product of the rate constant for C-H bond cleavage, and the equilibrium constant for radical formation. The rate constant for C-H bond cleavage cannot be greater than 10^{14} s^{-1}, as this is the rate of a C-H bond vibration (*95*). Therefore, to account for the observed k_{cat} values, which approach 10^{1} s^{-1} at high pH (*65*), the equilibrium constant for radical formation must be greater than 10^{-13}. To achieve this equilibrium constant, the difference in the flavin and substrate reduction potentials must be reduced by greater than 700 mV.

CHAPTER IV

pH AND KINETIC ISOTOPE EFFECTS ON ALANINE OXIDATION BY TRYPTOPHAN 2-MONOOXYGENASE

The flavoenzyme tryptophan 2-monooxygenase (TMO) from *Pseudomonas savastoni* catalyzes the oxidative decarboxylation of L-tryptophan (Scheme 4.1) in the first step of a two-step biosynthetic pathway for the plant hormone indoleacetic acid (*39-41, 96*). The kinetic mechanism of TMO has been determined with its fastest substrate L-tryptophan (*42*), and can be divided into two half-reactions (Scheme 4.2). The reductive half-reaction involves cleavage of the α-C-H bond of the amino acid (AA) and transfer of a hydride equivalent to the FAD. In the oxidative half-reaction, the reduced cofactor reacts with oxygen to produce hydrogen peroxide (*43*). Decarboxylation of the imino acid is thought to occur through the reaction of hydrogen peroxide with the imino acid (pathway a), analogously to the mechanism proposed by Lockridge et al. (*44*) for the decarboxylation of pyruvate by lactate oxidase. Although indoleacetamide is the only product of tryptophan turnover by wild-type TMO, amine oxidation can be uncoupled from decarboxylation to yield a keto acid by using variant enzymes (pathway b) (*45, 46*)

or anaerobic conditions (*42*). Therefore, TMO can function not only as a monooxygenase, but also as a flavin-dependent amine oxidase.

Scheme 4.1

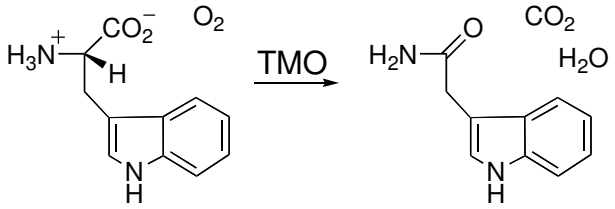

Scheme 4.2

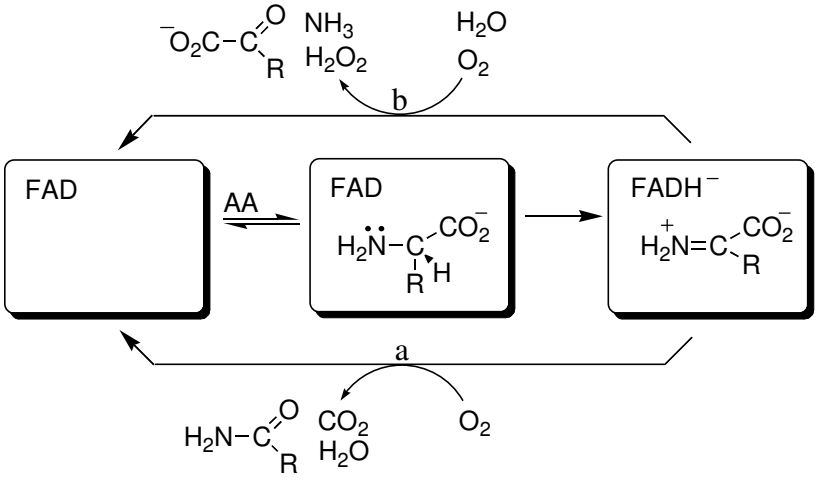

Despite their ubiquity and functional diversity, all flavin-dependent amine oxidases have thus far fallen into two structural families. One family includes D-amino acid oxidase (*12*), monomeric sarcosine oxidase (*28*) and glycine oxidase (*4*), while monoamine oxidase B (*17*), polyamine oxidase (*29*), and L-amino acid oxidase (*30*)

represent a separate family. Although structural information for TMO is unavailable, this enzyme was proposed by Sobrado and Fitzpatrick (*47*) to be in the second family of enzymes with monoamine oxidase and L-amino acid oxidase. Subsequent studies have supported this assignment (*45, 46*).

Despite a number of biochemical and kinetic studies, the mechanism of amine oxidation by flavoenzymes is still heavily debated. The commonly proposed mechanisms for the oxidation of primary amines (for recent reviews see (*9*) and (*8*)) are represented in Schemes 4.3-4.5, with alanine as a substrate. The simplest mechanism for amine oxidation, shown in Scheme 4.3, involves a direct hydride transfer from the substrate α-C to the flavin. The mechanism of Scheme 4.4 involves a nucleophilic attack of the substrate nitrogen on the flavin cofactor, resulting in a covalent flavin-alanine intermediate. Scheme 4.5 involves the formation of a flavin-substrate radical pair, which could then be resolved through either separate proton and electron transfers as shown, or through a hydrogen atom transfer from the substrate α-carbon.

Scheme 4.3

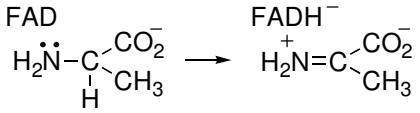

Scheme 4.4

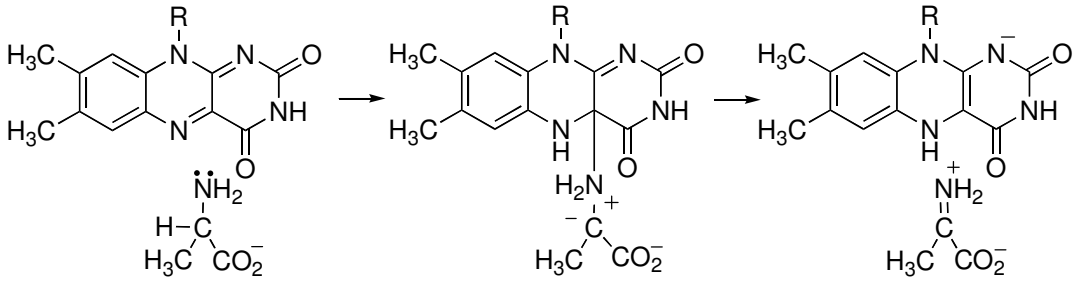

Scheme 4.5

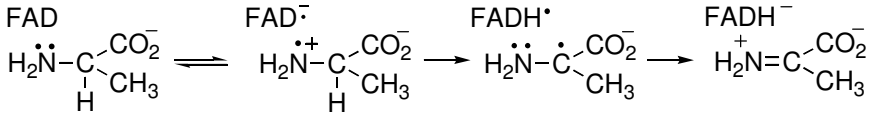

With the exception of a direct hydride transfer, each of the postulated mechanisms utilizes an intermediate flavin species between fully oxidized and fully reduced flavin. To date, there is no spectroscopic evidence for an intermediate flavin species in TMO. However, C-H bond cleavage is not fully rate-limiting in any of the well characterized substrates. It is therefore not unreasonable that formation of an intermediate flavin species may occur during or subsequent to a rate-limiting step, thereby preventing its detection. In the present study we characterize TMO turnover of L-alanine. pH studies and primary deuterium and ^{15}N kinetic isotope effects were used to identify the rate-limiting step and to evaluate the chemical mechanism. The results suggest that TMO utilizes a hydride transfer mechanism.

EXPERIMENTAL PROCEDURES

Materials. DL-α^2H-Alanine was purchased from Cambride Isotope Laboratories, Inc. (Andover, MA), and from MSD Isotopes (Montreal, Canada). The HiPrep DEAE column was from Amersham Pharmacia Biotech (Uppsala, Sweden).

Protein Expression and Purification. TMO was expressed in M15 *E. coli* (pREP4) using a pQE51-based plasmid as previously described (*45*). Methods for enzyme purification were based on those previously described for TMO (*97*), with several modifications. Cells harvested from 9 L of culture were resuspended in 100 mL of 0.1 M Tris, 12 mM β-mecaptoethanol, 50 μM indoleacetamide, 1 mM EDTA, 1 mM phenylmethylsulfonyl fluoride, 100 μg mL^{-1} lysozyme, pH 8.3, and lysed with a Branson Sonifier 450 for three 6 minute intervals at 30% output. The clarified lysate was prepared by centrifugation and treated with polyethyleneimine as previously described (*97*). The resulting supernatent was made 20 % saturated in ammonium sulfate, precipitated via centrifugation, and the precipitate discarded. The supernatant was made 60 % saturated in ammonium sulfate and precipitated as before. The resulting pellet was resuspended in 10-15 mL of 0.1 M Tris, 50 μM indoleacetamide, 1 mM EDTA, 1 mM dithiothreitol, pH 8.3, and dialyzed overnight against two changes of 50 to 100 volumes of the same buffer. Denatured protein was removed by centrifugation. The protein sample was purified in two portions using a 20 mL HiPrep 16/10 DEAE Fast Flow column. The column was equilibrated with 0.1 M Tris, 50 μM indoleacetamide, pH 8.3, loaded with a protein sample, and subsequently washed with 20 mL of equilibration buffer. Protein was eluted with a 400 mL linear gradient of 0-125 mM potassium

chloride in 0.1 M Tris, 50 μM indoleacetamide, pH 8.3. To regenerate the column, it was washed with 20 mL of 2 M sodium chloride, 10 mL of 1 M sodium hydroxide, and 50 mL of water, and then re-equilibrated with the starting buffer. The eluted fractions were analyzed for protein and flavin content, based on absorbance values at 280 and 466 nm, respectively. Fractions with the greatest flavin to protein ratio were pooled and precipitated with 60 % saturated ammonium sulfate. The purified enzyme was resuspended to a final concentration of 300-500 μM in 10 mM potassium pyrophosphate, 10 % glycerol, pH 8.3.

Removal of Bound 3-Indoleacetamide. Bound indoleacetamide was removed as previously described (*97*), with the modification that EDTA was omitted from dialysis buffers and 10 mM potassium pyrophosphate was used in place of 0.1 M Tris-HCl to avoid nitrogen-containing buffers.

Enzyme Assays. Enzyme concentrations were calculated from the absorbance at 466 nm using the previously determined extinction coefficient of 11.4 mM^{-1} cm^{-1} (*97*). The rate of oxygen consumption was measured using a Hansatech oxygen-monitoring system (Norfolk, U.K.) with a computer-interfaced graphical mode or a Yellow Springs Instrument model 5300 oxygen electrode (Yellow Springs, OH). Steady-state kinetic parameters were routinely determined at 25 ºC under atmospheric oxygen concentrations. When necessary, the oxygen concentration was varied by bubbling the desired oxygen/argon mixture through a reaction sample in the oxygen electrode cuvette until a constant oxygen concentration was observed. The reaction was then started by the addition of enzyme. Flavin reduction was monitored using a Hewlett Packard 8452A

photodiode array spectrophotometer. Substrates were prepared in 50 mM Tris, 5 mM D-glucose, pH 8.3, and made anaerobic by bubbling argon through 1 mL of solution for 15 minutes, prior to the addition of glucose oxidase (20 μg). A small volume of enzyme (50 μL) was placed in an anaerobic cuvette sealed with a rubber septum. The cuvette was made anaerobic by cycling between vacuum and argon. The reaction was started by injecting the substrate solution through the rubber septum.

^{15}N Kinetic Isotope Effects. ^{15}N Kinetic isotope effects were determined competitively using the natural abundance of ^{15}N and ^{14}N in L-alanine. Conditions were typically 0.3 M L-alanine, 0.3 M hydroxylamine, 20 mM potassium pyrophosphate, 100 μg mL^{-1} catalase, 10% glycerol, pH 8.0, in 3-5 mL. The sample pH slowly decreased as the reaction progressed. Therefore, the pH was frequently monitored and adjusted with potassium hydroxide as necessary to keep the reaction samples within 0.1 pH units of the desired value. Additional TMO was added periodically to keep the reaction progressing. Reactions were stirred in the dark at 25 ºC with wet 100% oxygen blowing over the surface. Reaction progress was monitored using a Waters Delta 600 HPLC with a model 2487 Dual λ Absorbance Detector. A 100 μL sample was withdrawn and mixed with 500 μL of 2.5 mM potassium phosphate in 70 % MeCN, pH* 8.0. Protein was removed by either filtering the sample through a 0.20 μm nylon filter or by centrifugation for 20 min at 21000 x G. The sample was then loaded onto a Waters μBondapak-NH_2 column (3.9 x 300 mm) with a 100 μL loop and eluted isocratically with 2.5 mM potassium phosphate in 80 % MeCN, pH* 8.0, at 3 mL min^{-1}. Alanine and pyruvate were detected by monitoring the absorbance at 210 nm and 250 nm, respectively. The fractional

conversion of alanine to pyruvate was determined by comparing the peak areas of alanine and pyruvate to standard curves prepared using commercially available compounds.

After 25-45 % of the alanine had been oxidized, reactions were quenched by the addition of 0.1 volume of concentrated hydrochloric acid. Protein was then removed by centrifugation. To remove free FAD, the sample was diluted to approximately 10 mg mL^{-1} alanine using 5 mM ammonium acetate and adjusted to pH 4 using potassium hydroxide; aliquots (1 mL) were loaded onto a Waters NovaPak C_{18} column (3.9 x 150 mm). The alanine and pyruvate eluted together within 10 minutes with 5 mM aqueous ammonium acetate as the mobile phase at 1 mL min^{-1}. The FAD was then eluted with a 10 mL gradient of 5 mM ammonium acetate in 0-50 % methanol. The eluate containing alanine and pyruvate was collected, pooled, and dried on a rotoevaporator. The dried sample was resuspended in 10 mL of approximately 1.3 mM potassium hydroxide and redried; this process was repeated three times to drive off ammonia.

Alanine and pyruvate were separated using a preparative Waters μBondapak-NH_2 column (7.8 x 300 mm). Dried samples were resuspended in water and acetonitrile to yield approximately 10 mg mL^{-1} alanine in 40 to 50% acetonitrile. The pH was adjusted to pH* 7. Samples (1 mL) were loaded onto the column and eluted at 4 mL min^{-1} with 80 % MeCN, 2.5 mM potassium phosphate, pH* 7.5, while collecting 8 mL fractions. Alanine elutes around 25 minutes. The alanine fractions were pooled, dried on a rotary evaporator, resuspended in water, and lyophilized.

For isotope ratio mass spectrometry (IRMS) analysis, the alanine samples were

combusted to produce nitrogen gas. Quartz tubes (0.9 cm o.d. x 0.7 cm i.d. x 24 cm long) were charged with 8-10 mg of alanine, 100 mg of diatomaceous earth, 3-4 g of cupric oxide, and 500 mg of elemental copper. The tubes were placed under vacuum, flame- sealed, and combusted at 850 ºC. The nitrogen gas produced was distilled on a high vacuum line through two -78 °C traps and one -196 °C trap, and then trapped on molecular sieves at -196 ºC. The isotopic composition of the gas was determined using a Finnegan delta E isotope ratio mass spectrometer.

Data Analysis. The kinetic data were analyzed using the programs KaleidaGraph (Synergy Software, Reading, PA), Igor (Wavemetrics, Lake Oswego, OR), and SPECFIT (Spectrum Software Associates, Marlborough, MA). When the concentration of only one substrate was varied, the initial rates of oxygen consumption were fit to the Michaelis-Menton equation. When the concentrations of both alanine and oxygen were varied, the initial rates of oxygen consumption (ν) were fit to equation 4.1, which describes a ping-pong reaction. The k_{cat} and k_{cat}/K_{ala} values determined at different pH were fit to equations 4.2 and 4.3, respectively. Equation 4.2 describes a profile in which deprotonation of a single ionizable group with pK_1 increases catalytic activity from a value of C_L to a value of C_H. Equation 4.3 describes a profile in which deprotonation of one ionizable group with pK_2 is essential for activity, deprotonation of a second group with pK_1 increases the activity, and deprotonation of a third group with pK_3 results in a loss of activity. This profile has two plateau regions defined by the term C_I and the sum of C_I and C_H. In both equation 4.2 and equation 4.3, H is the concentration of the hydronium ion. Deuterium kinetic isotope effects were obtained from fits of the data to

equation 4.4, which describes equal isotope effects on k_{cat} and k_{cat}/K_{ala}; ν is the initial rate of oxygen consumption, F_i is the fraction of the heavy atom, and E_{KIE} is the isotope effect. The rates of flavin reduction under anaerobic conditions were determined from fits of the data to equation 4.5, which describes a monophasic exponential decay; *k* is the first-order rate constant, A_t is the absorbance at time *t*, and A_∞ is the final absorbance. The observed ^{15}N kinetic isotope effect (E_{obs}) was calculated using equation 4.6 (*87*), where *f* is the final fraction of alanine oxidized, and R_S/R_0 is the $^{15}N/^{14}N$ ratio of the alanine remaining after enzymatic oxidation divided by the $^{15}N/^{14}N$ ratio of the alanine prior to oxidation. The observed isotope effect was corrected for the protonation state of the free substrate using equation 4.7, where $^{15}k_{chem}$ is the pH-independent isotope effect on k_{cat}/K_m, $^{15}K_{eq}$ is the equilibrium effect for alanine deprotonation, and 9.87 is the pK_a value of the alanine amine (*82*).

$$v = \frac{k_{cat}AB}{K_A B + K_B A + AB} \tag{4.1}$$

$$\log(k_{cat}) = \log\left[C_L + \frac{C_H - C_L}{1 + H/K_1}\right] \tag{4.2}$$

$$\log\left(\frac{k_{cat}}{K_m}\right) = \log\left[\frac{C_I + C_H/\left(1 + H/K_1\right)}{1 + H/K_2 + K_3/H}\right] \tag{4.3}$$

$$v = \frac{k_{cat}A}{(K_m + A)(1 - F_i + E_{KIE}F_i)} \tag{4.4}$$

$$A_{\text{total}} = A_t e^{-kt} + A_\infty \tag{4.5}$$

$$R_S / R_0 = (1 - f)^{\left(1/E_{obs}\right)-1} \tag{4.6}$$

$$^{15}k_{chem} = \frac{E_{obs}}{1 + [(^{15}K_{eq} - 1)/(1 + 10^{pH-9.87})]} \tag{4.7}$$

RESULTS

Steady-State Kinetics. The use of slow substrates is often beneficial in the study of enzyme mechanisms, as it increases the chances that chemical steps rather than substrate binding or product release will be rate-limiting. This allows for the direct measurement of intrinsic rate constants and isotope effects under steady-state conditions (*74*). L-Alanine was previously identified as a slow substrate for TMO (*42*). Consequently, alanine was further characterized as a substrate for TMO.

To determine the oxygen dependence of alanine turnover, initial rates of oxygen consumption were measured at 0.1 and 1.0 M L-alanine while varying the oxygen concentration from 50 to 425 μM. All assays were done at 25 ºC in 50 mM Tris, pH 8.3, varying the potassium chloride concentration to maintain a constant ionic strength of approximately 1 M. As shown in Figure 4.1, the rates of oxygen consumption at high and low alanine concentrations appear to be independent of the oxygen concentration, consistent with a K_{O2} value of less than 25 μM. The low K_{O2} value allows for the determination of k_{cat} and k_{cat}/K_{ala} under ambient oxygen concentrations. The lack of a

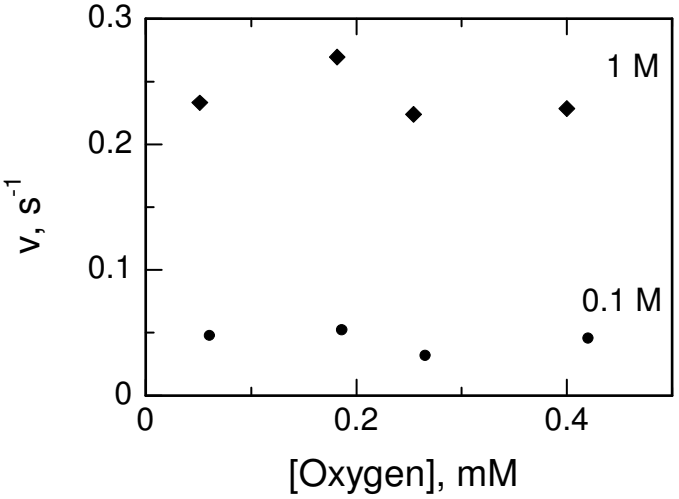

Figure 4.1. Initial rates of oxygen consumption by TMO measured at various oxygen concentrations in 50 mM Tris, pH 8.3, 25 ºC. No dependence on the oxygen concentration was observed over the measured range using either 1 M (diamonds) or 0.1 M (circles) L-alanine.

visible enzyme-product complex during flavin reduction (see below) is consistent a rapid release of the imino-acid product from the reduced enzyme-product complex prior to reoxidation of the flavin cofactor. This would result in the formation of pyruvate and hydrogen peroxide rather than acetamide and carbon dioxide. Rates of oxygen consumption were therefore determined in the presence or absence of 170 μg mL^{-1} catalase. The presence of catalase slowed the reaction by a factor of 2.2 ± 0.1[5], consistent with a stoichiometric amount of hydrogen peroxide being released per oxygen consumed.

pH Effects. The k_{cat} and k_{cat}/K_{ala} values were determined over the pH range 6.4 to 10.1 (Figure 4.2) using a constant ionic strength buffer. Potassium chloride and L-alanine concentrations were varied to maintain a constant ionic strength of 1.1 M. The k_{cat} pH profile (Figure 4.2A) could be fit to a linear dependence on the proton concentration (dotted line) and to equation 4.2 (solid line). Equation 4.2 was used to fit the pH profile of all three previously characterized amino acid substrates (*98*). It describes a pH dependence with catalytic activity at low pH that increases upon deprotonation of a single ionizable group, with an apparent pK_a of 8.4 ± 0.3. The increase in K_m values at high pH precluded the determination of k_{cat} values above pH 9.5. The k_{cat}/K_m pH dependence (Figure 4.2B) is similar to the pH dependence

---

[5]The reported value is the ratio of the averages from three determinations each in the presence or absence of catalase.

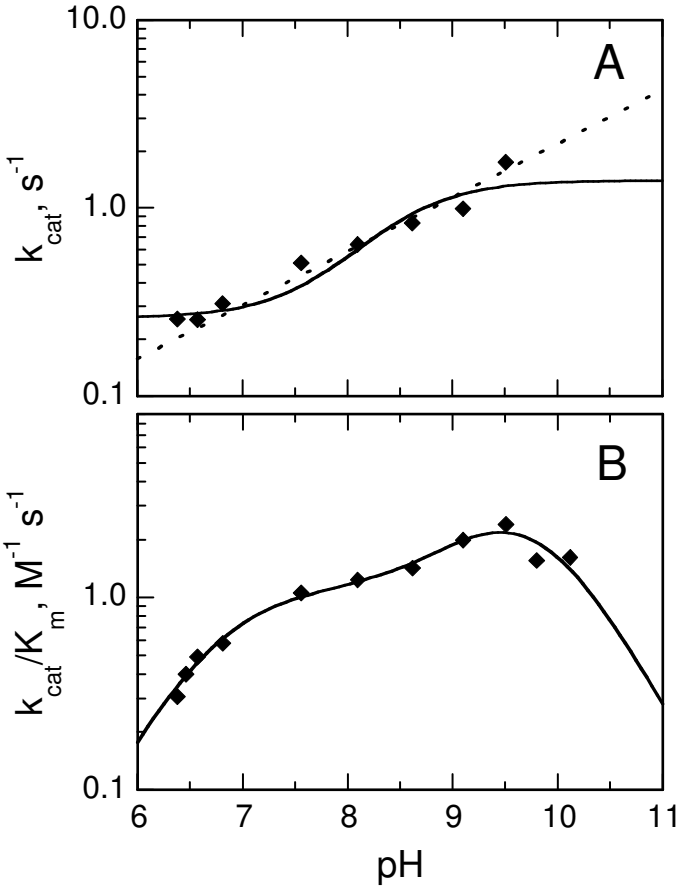

Figure 4.2. pH profiles for alanine oxidation by TMO. k_{cat} values (A) were fit to a linear dependence on the proton concentration (dotted line) and to equation 4.2 (solid line). k_{cat}/K_m values (B) were fit to equations 4.2 and 4.3, respectively. Assays were done in 0.1 M ACES, 52 mM Tris, 52 mM ethanolamine-HCl, while varying potassium chloride and alanine concentrations to maintain a constant 1.1 M ionic strength at 25 ºC. The average error in the data for each profile is indicated by the size of the markers.

previously seen for TMO oxidation of L-methionine (*98*). This pH profile was therefore fit to equation 4.3, which describes a pH dependence with three dissociation constants and plateau regions at intermediate and high pH. The best fit was obtained by using identical dissociation constants for K_1 and K_3; the resulting pK_a value of 9.6 ± 0.1 represents the average of pK_1 and pK_3. Deprotonation of an additional ionizable group with a pK_a value of 6.8 ± 0.1 (pK_2) was required for activity.

Deuterium Kinetic Isotope Effects. Deuterium kinetic isotope effects were determined by comparing the rates of oxygen consumption using α-protiated and α-deuterated DL-alanine at the pH extremes, 6.5 and 10, and at the intermediate pH region 8.0. The data at pH 6.5 and 8.0 fit best to equation 4.4, consistent with an equal isotope effect on k_{cat} and k_{cat}/K_m[6]. As shown in Table 4.1, theisotope effects are pH-independent with an average value of 6.0 ± 0.5. This value is in reasonable agreement with previous studies that showed a $^{D}(k_{cat}/K_m)$ value of 5.3 ± 0.5 at pH 8.3 (*98*). The pH-independence of the isotope effect and its equal expression in k_{cat} and k_{cat}/K_m are consistent with irreversible C-H bond cleavage and with the observed isotope effect being equal to the intrinsic isotope effect.

---

[6]Due to the high alanine concentrations necessary to saturate the enzyme, a $^{D}k_{cat}$ value was not determined at pH 10.0.

Table 4.1. Deuterium kinetic isotope effects on alanine oxidation by TMO.

pH	kinetic isotope effect
6.5[a,b]	5.4 ± 0.7
8.0[a,c]	6.6 ± 0.6
10.0[a,c]	6.0 ± 0.3
8.3[d]	6.3 ± 0.9

[a]Determined from steady-state kinetic analysis at 25 ºC in air-saturated buffers. [b] 0.1 M ACES, 52 mM Tris, 52 mM ethanolamine-HCl with varied potassium chloride at 1.1 M ionic strength. [c] 0.1 M potassium pyrophosphate. [d] Determined from the rate constants for TMO flavin reduction using 1 M DL-alanine in 50 mM Tris, 5 mM D-glucose, pH 8.3.

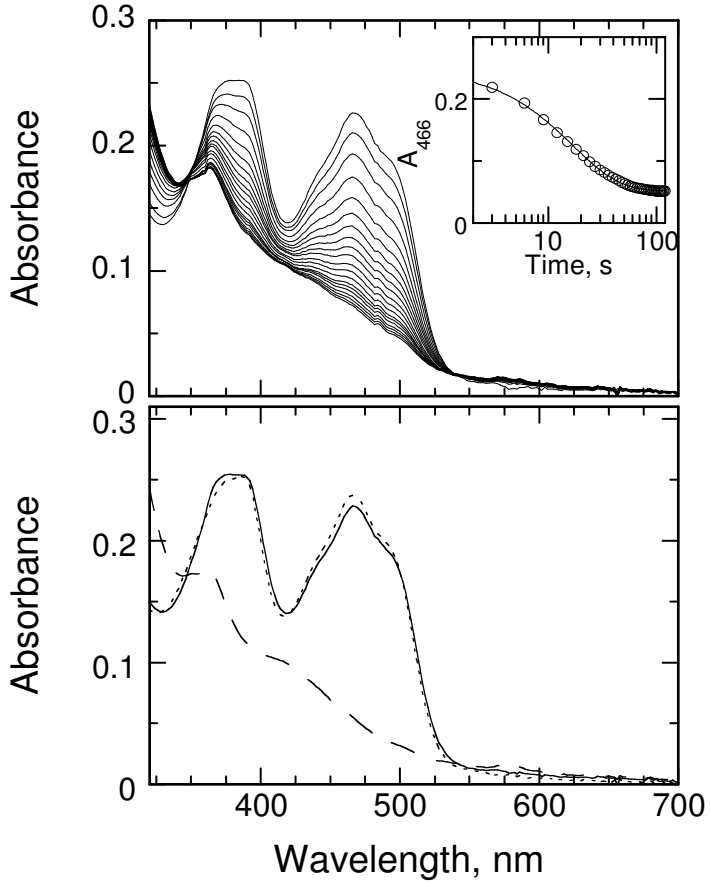

Figure 4.3. Changes in the TMO flavin absorbance spectrum during anaerobic reduction with 1 M L-alanine, pH 8.3. Conditions were as described in EXPERIMENTAL PROCEDURES. (A) The spectra were recorded at 2 second intervals for 40 seconds. The inset shows the corrected absorbance at 466 nm, measured at 1 second intervals. Every third data point is shown for clarity. The line shows the fit of the data to equation 4.5, which describes a single exponential decay. (B) Calculated starting (solid line) and final spectra (dashed line) from a global analysis of the data are compared to the spectrum of free enzyme (dotted line).

Reductive Half-Reaction Kinetics. The reduction of the flavin in TMO by L-alanine was monitored under anaerobic conditions. As shown in Figure 4.3A, mixing 1 M protiated L-alanine with enzyme resulted in an isosbestic conversion of fully oxidized to fully reduced flavin. A global analysis of the data from 320 to 800 nm fit nicely to a single exponential decay with a rate constant of 0.062 ± 0.001 s^{-1}. Figure 4.3B shows the starting and final spectra calculated from the global analysis. These spectra are consistent with fully oxidized and reduced flavin, respectively. The similarities between the calculated starting spectrum and the spectrum of free TMO indicates that very little flavin chemistry occurred during the mixing time of the experiment. The absence of any obvious charge transfer complex in the calculated final spectrum is consistent with a rapid release of product from the reduced enzyme-product complex. As the postulated intermediate flavin species in Schemes 4.4 and 4.5 occur prior to C-H bond cleavage, reducing flavin with α-deuterated alanine should cause a larger accumulation of the intermediate species, thereby increasing any associated absorbance changes. The reduction of the TMO flavin by 1 M α-^{2}H-DL-alanine was monitored under anaerobic conditions. As with the protiated substrate, the absorbance changes fit best to a single exponential decay with no indication of an intermediate flavin species. A comparison of the rate constants from the global analyses of flavin reduction using protiated and deuterated alanine gave an isotope effect of 6.3 ± 0.9. This value is in reasonable agreement with the kinetic isotope effects determined under steady-state conditions.

Nitrogen Kinetic Isotope Effects. To determine the ^{15}N kinetic isotope effect on alanine oxidation, L-alanine solutions were oxidized by TMO, yielding a mixture of

alanine, pyruvate, and ammonia[7]. As shown by equation 4.6, calculation of the isotope effect requires an accurate determination of the final percent of alanine consumed (f). The relative error in f has less impact on the calculated isotope effect as f increases. Given the slow nature of both the enzymatic reaction and the rate of diffusion of oxygen into a solution, several days were typically required to achieve a usable percent consumption for alanine. This problem was greatly exacerbated by a time-dependent loss of enzyme activity during turnover. At pH 8.0 and 8.3, it was possible to obtain approximately 25-45 % consumption. At higher pH values, the rapid loss of enzymatic activity prevented reactions from reaching a useable percent consumption for alanine. This observation is consistent with a previous analysis of enzyme stability, which shows that TMO is most stable around pH 8 (*97*). After reaching a useable percent consumption, reactions were quenched with acid, and the remaining alanine was isolated and analyzed for its nitrogen isotopic composition. The resulting R_S/R_0 values were analyzed as a function of the percent consumption using equation 4.6 (Figure 4.4). The data fit to an observed ^{15}N kinetic isotope effect of 1.0145 ± 0.0007.

---

[7]HPLC traces were consistent with pyruvate being the product of alanine oxidation; no evidence of acetamide formation was found

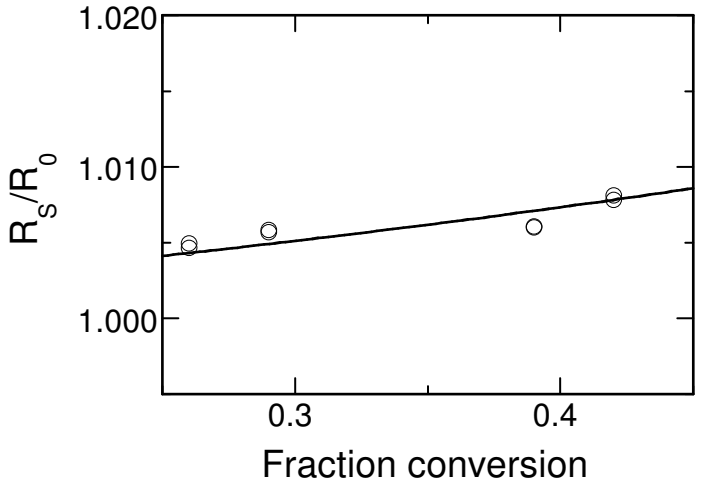

Figure 4.4. Nitrogen isotopic composition of alanine consumption reactions. Samples were analyzed to determine the change in isotopic composition upon oxidation of alanine (R_S/R_0) as described in the EXPERIMENTAL PROCEDURES. The line is from the fit of the data to equation 4.6.

DISCUSSION

Tryptophan 2-monooxygenase is the best-studied member of a small class of poorly characterized flavoproteins that catalyze the oxidative decarboxylation of amino acids (*99, 100*). For TMO, turnover has been shown to proceed through oxidation of the substrate C-N bond, yielding an imino acid intermediate (*42*). Consequently, TMO can be classified as a flavin-dependent amine oxidase. Like most members of this larger class of enzymes, the chemical mechanism of substrate oxidation by TMO is still controversial.

A preliminary characterization of L-alanine oxidation by TMO suggested that C-H bond cleavage was rate-limiting for this substrate (*98*). All of the kinetic data presented here are consistent with this conclusion. Therefore, a more thorough characterization of L-alanine oxidation by TMO allows for the determination of intrinsic isotope effects and pK_a values, and provides insight into the chemical mechanism of amine oxidation.

The kinetic mechanism of TMO was previously determined with the three best substrates, tryptophan, phenylalanine, and methionine (*42*). These substrates have K_{O2} values of 90 μM or higher, indicating that observed k_{cat} values may be lower than the intrinsic values when determinations are made using air-saturated oxygen concentrations. In the present study, the K_{O2} value for alanine turnover was determined to be less than 25 μM, allowing for the determination of intrinsic k_{cat} values using air saturated oxygen concentrations.

A log plot of the k_{cat} pH dependence fits well to a straight line with a slope of

0.25 ± 0.02. A linear dependence is seen for specific acid or specific base catalyzed reactions (*101*). However, the pH dependencies for these types of reactions have a positive or negative slope of unity (*101*). As the pH dependence in question has a slope well below unity, the significance of such a fit is uncertain. Alternatively, the k_{cat} pH profiles for TMO oxidation of tryptophan, phenylalanine, and methionine, all fit to equation 4.2 (*98*), which describes an increase in activity upon deprotonation of a single ionizable group. A similar pH dependence is seen in the k_{cat} profile for D-alanine oxidation by D-amino acid oxidase (*102*). The k_{cat} pH profile for alanine oxidation by TMO was therefore fit to equation 4.2 with a poorly defined pK_a of 8.4 ± 0.3. For both the DAO and the previously observed TMO pH profiles, the observed pK_a was previously attributed to a conformational change in the enzyme-product complex, as product release is rate-limiting with the faster substrates (*98, 102*). However, for TMO turnover of L-alanine, the observed primary deuterium kinetic isotope effects indicate that C-H bond cleavage is fully rate-limiting for both k_{cat} and k_{cat}/K_m. The observed pK_a value of 8.4 may instead be attributed to the alanine amine in the enzyme-substrate complex. Free alanine has a pK_a value of 9.87 (*82*), consistent with an approximately 1.5 pH units shift upon binding the enzyme. Similar changes for substrate pK_a values have been proposed for other flavin-dependent amine oxidases, including trimethylamine dehydrogenase (*103*), monomeric sarcosine oxidase (*104*), and D-amino acid oxidase (*105*). Therefore, although other interpretations of the k_{cat} profile for alanine oxidation by TMO are possible, the above interpretation appears to be the simplest explanation of the available data.

The pH dependence of k_{cat}/K_m shows an ionizable group with a pK_a of 6.8 ± 0.1 that must be deprotonated for activity. A pK_a value of approximately 6.2 was previously measured for the pH dependence of TMO inhibition by competitive inhibitors; the pK_a was attributed to the deprotonation of a histidinyl residue (*98*). As competitive inhibitors do not participate in catalysis, this pK_a value represents the intrinsic pK_a for the ionizable group involved in binding substrates and inhibitors (*74*). This value is in reasonable agreement to the value of 6.8 observed for alanine oxidation, again consistent with a lack of a forward commitment to catalysis for alanine turnover. The difference in the observed pK_a values can be attributed to an increased stabilization of the positively charged histidinyl residue under the higher ionic strength conditions used for the current study (1.1 vs. 0.1 M).

Above pH 7, the k_{cat}/K_m values appear to increase in activity upon deprotonation of a second ionizable group and decrease in activity upon deprotonation of a third ionizable group. A similar k_{cat}/K_m pH profile was previously described for TMO oxidation of methionine (*98*). With methionine, deprotonation of a group with a reported pK_a of 9.4 increases activity, while deprotonation of a group with a reported pK_a of 9.8 results in a loss of activity. These values are in excellent agreement with the observed average pK_a value of 9.6 ± 0.1 for alanine oxidation. The lower pK_a value was attributed to deprotonation of free methionine (*98*), while the higher value was later attributed to deprotonation of an active site tyrosyl residue (*46*). The pK_a for free alanine is greater than that for free methionine (9.9 vs. 9.3) (*82*), while the observed pK_a for the tyrosyl residue should be lower in the present study due to both the increased ionic strength and

loss of forward commitment to catalysis. The observed average pK_a value of 9.6 ± 0.1 is consistent with these predictions. The observed primary deuterium kinetic isotope effects are pH-independent, with equal values on k_{cat} and k_{cat}/K_m, consistent with the observed value of 6.0 ± 0.5 being the intrinsic value. This value is in excellent agreement with the previously observed value of 5.3 ± 0.5 for L-alanine oxidation at pH 8.3 (*98*). This value is also in agreement with the intrinsic deuterium kinetic isotope effect of 5.7 for D-amino acid oxidase with D-alanine as substrate (*14*), suggestive of similar transition states for alanine oxidation by these two enzymes.

The culmination of several decades of study has led to the general consensus that D-amino acid oxidase utilizes a hydride transfer mechanism for substrate oxidation (see (*8*) for a recent review). However, the mechanism for other flavin-dependent amine oxidases is still debated. The same chemical mechanisms can be proposed for members of both the D-amino acid oxidase structural family and members of the L-amino acid oxidase family such as TMO (*47*). With the exception of a hydride transfer, the proposed mechanisms, represented by Schemes 4.4 and 4.5, require an intermediate flavin species between fully oxidized and fully reduced flavin for which there is no spectroscopic evidence. For TMO oxidation of L-alanine, the observed deuterium kinetic isotope effects rule out the rate-limiting formation of an intermediate in which the C-H bond is intact. Furthermore, as C-H bond cleavage occurs approximately 6-fold slower with α-deuterated alanine than with the protiated substrate, reduction with this slower substrate should result in a comparable increase in the accumulation of any preceding intermediates. No such intermediate is seen. Although this observation is insufficient to

rule out the above proposed mechanisms[8], the simplest explanation for the lack of a detectable intermediate flavin species is a mechanism which does not form any intermediate flavin species, i.e, a hydride transfer mechanism.

Heavy atom isotope effects can be used to further address this and other mechanistic possibilities for TMO. The ^{15}N kinetic isotope effects on k_{cat}/K_m report on changes in the alanine nitrogen's bonding order that occur prior to or during the first irreversible step in oxidation. The observed deuterium kinetic isotope effects are consistent with an irreversible C-H bond cleavage. Therefore, the ^{15}N kinetic isotope effects also report on the relative timing of changes in the nitrogen bond order and C-H bond cleavage.

Regardless of the mechanism of amino acid oxidation, a proton must be removed from the substrate nitrogen to form the imino acid product. Therefore the observed ^{15}N isotope effect is a product of the pH-dependent equilibrium isotope effect on alanine deprotonation ($^{15}K_{eq}$) and the pH-independent isotope effect on nitrogen rehybridization ($^{15}k_{chem}$). Equilibrium isotope effects for deprotonation of an amino acid have been

---

[8]Although the lack of an observed intermediate is insufficient to rule out its formation, this observation does provide an upper limit for the amount of enzyme flavin that may accumulate in any postulated intermediate form. As previously argued for the flavoenzyme N-methyltryptophan oxidase (*65*), if one assumes that any flavin intermediate that accumulates to 35% would be detected, the lack of a detectable intermediate during flavin reduction with the deuterated substrate places an upper limit of 6% on the amount of enzyme that accumulates in this form prior to C-H bond cleavage.

measured for phenylalanine (*106*) and for glycine (*88, 89*) with values of 1.0167 and 1.0226, respectively. Although no value has been directly measured for alanine deprotonation, the value is expected to be intermediate between these two measured values, as the alanine side chain is intermediate in size between those of phenylalanine and glycine. A value of 1.0033 has been proposed as a correction factor to use when estimating ^{15}N kinetic isotope effects if a proton on the carbon next to the nitrogen of the control system is replaced with a methyl group in the experimental system (*15*). Applying this correction to the $^{15}K_{eq}$ value for glycine deprotonation yields a value of 1.019 for alanine deprotonation.

Correction of the observed ^{15}N kinetic isotope effect value using equation 4.7 with $^{15}K_{eq}$ and pK_a values of 1.019 and 9.87, respectively, yields a pH-independent $^{15}k_{chem}$ value of 0.9958 ± 0.0007[9]. Importantly, an inverse isotope effect is calculated regardless of which of the above $^{15}K_{eq}$ values is used, with values ranging from 0.9981 to 0.9924. A $^{15}k_{chem}$ value of 0.9971 ± 0.0005 was previously calculated for conversion of an unprotonated primary amino acid to a protonated imine based on experimentally

---

[9]The reported value does not account for one of the four alanine consumption reactions being run at pH 8.3 instead of pH 8.0. This difference can be accounted for by combining equations 4.6 and 4.7 and fitting the observed R_S/R_0 values simultaneously as a function of both *f* and pH. This analysis yields a value of 0.9959 ± 0.0006. As the two values are indistinguishable, the simpler analysis was used.

determined equilibrium isotope effects (*15*). A similar value of 0.9963 ± 0.0007 was observed for D-serine oxidation by D-amino acid oxidase (*13*). These values are in excellent agreement with the observed value for TMO oxidation of L-alanine, consistent with both TMO and D-amino acid oxidase utilizing a hydride transfer mechanism.

As one alternative to a hydride transfer mechanism for oxidation of amines by flavoenzymes, Miller and Edmondson have proposed the involvement of a covalent substrate-flavin adduct for monoamine oxidase (*27*). This mechanism, shown in Scheme 4.4 for TMO oxidation of alanine, involves a nucleophilic attack of the alanine nitrogen on the flavin cofactor. As the alanine attacks the flavin C4a, the increase in electron density at N5 results in the formation of a strong base with a pK_a value of approximately 30 (*27*), equivalent to that of an amino acid α-carbon (*107*). Thus, formation of the adduct is concerted with cleavage of the alanine C-H bond. This mechanism is consistent with the lack of detectable flavin intermediates for TMO oxidation of alanine, as the postulated intermediate is formed during the rate-limiting step. However, it is not consistent with the observed ^{15}N kinetic isotope effects. As previously mentioned, $^{15}(k_{cat}/K_m)$ values report on changes that occur prior to or during the first irreversible step. For the mechanism of Scheme 4.4, formation of the flavin adduct is concerted with C-H bond cleavage and therefore irreversible; subsequent steps do not contribute to the observed $^{15}(k_{cat}/K_m)$ values. Adduct formation involves formation of a fourth bond to the deprotonated alanine nitrogen without changing the nitrogen's hybridization. This reaction is analogous to protonating the amine. The equilibrium kinetic isotope effect for protonation of the amine is simply the reciprocal of the equilibrium effect for

deprotonation of the amine. Therefore, the observed isotope effect should equal 1.00 at pH 8 and have a $^{15}k_{chem}$ value between 0.984 and 0.978, depending on which $^{15}K_{eq}$ value is used. Alternatively, formation of the covalent adduct can be compared to the nucleophilic attack of phenylalanine on the enzyme cofactor in phenylalanine ammonia-lyase (Scheme 4.6), for which a pH-independent ^{15}N kinetic isotope effect of approximately 0.98 was previously measured (*106*). These estimated ^{15}N isotope effects are well outside the range of the observed value. The observed results suggest that TMO does not use the proposed nucleophilic attack mechanism.

Scheme 4.6

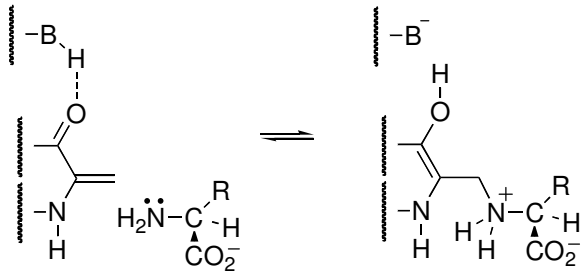

In addition to the mechanisms of Schemes 4.3 and 4.4, mechanisms involving single electron transfers are often proposed for flavin-dependent amine oxidations (*9*). These mechanisms start with the formation of an anionic flavin semiquinone and a substrate aminium radical, which can then be resolved through a step-wise proton and electron transfer (Scheme 4.5) or through the direct transfer of a hydrogen atom (Scheme 4.7). For the mechanism of Scheme 4.5, C-H bond cleavage is concerted with rehybridization of the substrate aminium radical to an sp^3 hybridization for the nitrogen.

As this is the first irreversible step, the $^{15}(k_{cat}/K_m)$ values for this mechanism report on the formation of the alanine α-carbon radical from free alanine. The nitrogen bonding order is essentially identical for this radical and the unprotonated free alanine. The $^{15}k_{chem}$ value for this mechanism is not expected to differ significantly from unity, while the observed isotope effect at pH 8.0 would be greater than 1.016. This mechanism is therefore inconsistent with the observed ^{15}N kinetic isotope effects.

Scheme 4.7

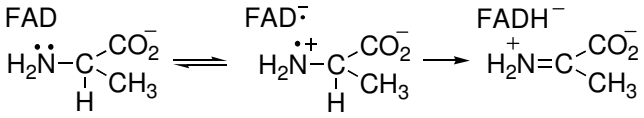

In Scheme 4.7, C-H bond cleavage is concerted with rehybridization of the aminium radical to form the Schiff base product. The $^{15}(k_{cat}/K_m)$ values for this mechanism report on the same net reaction as for a hydride transfer mechanism. This mechanism is therefore consistent with the observed ^{15}N isotope effects. However, as discussed above, this mechanism is not supported by the lack of a detectable flavin intermediate during flavin reduction.

Although the mechanism of Scheme 4.7 cannot be ruled out by the present kinetic isotope effects, energetic arguments have previously been raised against formation of the initial radical pair. Walker and Edmondson (*108*) argue that flavoenzymes, whose reduction potentials are typically less than 0.2 V vs SHE[10], are unlikely to catalyze the one electron oxidation of primary amines, which have estimated reduction potentials well above 1 V vs SHE[11]. In light of these arguments, the simplest conclusion is that TMO does not utilize any of the currently proposed single electron transfer mechanisms.

The reported value does not account for one of the four alanine consumption reactions being run at pH 8.3 instead of pH 8.0. This difference can be accounted for by combining equations 4.6 and 4.7 and fitting the observed R_S/R_0 values simultaneously as a function of both f and pH. This analysis yields a value of 0.9959 ± 0.0006. As the two values are indistinguishable, the simpler analysis was used.

---

[10]Values as large as 230 and approximately 300 mV have been reported for trimethylamine dehydrogenase (*109*) and monoamine oxidase (*110*), respectively. However, the conclusion of the presented argument remains unchanged even with these more favorable reduction potentials.

[11]One electron reduction potentials for primary sulfyl compounds have been reported in the range of 1.4 V vs SHE (*93*). Replacing sulfur with the more electronegative nitrogen would likely raise this potential.

The lack of visible flavin intermediates during anaerobic flavin reduction, the fully expressed deuterium and nitrogen kinetic isotope effects, and the predicted symmetrical transition state are all consistent with a hydride transfer mechanism for amine oxidation by tryptophan 2-monooxygenase. Currently, D-amino acid oxidase is the only other flavin-dependent amine oxidase for which deuterium and nitrogen kinetic isotope effect data are available (*8*). As discussed above, the similarity between the observed isotope effects is consistent with similar transition states for alanine oxidation by these two enzymes; D-amino acid oxidase is accepted to utilize a hydride transfer mechanism (*8*). D-Amino acid oxidase and tryptophan 2-monooxygenase represent the two different structural families of flavin-dependent amine oxidases. These results therefore add to the growing body of evidence that a hydride transfer mechanism is common among all flavin-dependent amine oxidases.

CHAPTER V

CHARACTERIZATION OF METAL LIGAND VARIANT PROTEINS OF TYROSINE HYDROXYLASE*

Tyrosine hydroxylase (TyrH) is a tetrahydropterin-dependent monooxygenase that catalyzes the hydroxylation of L-tyrosine, yielding L-dihydroxyphenylalanine (DOPA) in the rate-determining step for the biosynthesis of catecholamines (Scheme 5.1) (*111*). The two other tetrahydropterin-dependent aromatic amino acid hydroxylases, phenylalanine hydroxylase and tryptophan hydroxylase, have catalytic domains that are homologous to that of TyrH (*111, 112*). All three enzymes contain one iron atom per monomer, which is essential for hydroxylation of the amino acid substrate (*113-115*). The protein ligands to the iron in both tyrosine hydroxylase and phenylalanine hydroxylase have been identified by site-directed mutagenesis and direct structure determination as two histidines and a glutamate (*49, 63, 64, 116*). This motif has been found in a number of other enzymes and has been termed a 2-His-1-carboxylate facial triad by Que (*57*).

---

*Reproduced with permission from Fitzpatrick, P.F., Ralph, E.C., Ellis, H.R., Willmon, O.J., and Daubner, S.C. (2003) *Biochemistry 42*, 2081-2088 (*117*). Copyright 2003 American Chemical Society.

Scheme 5.1.

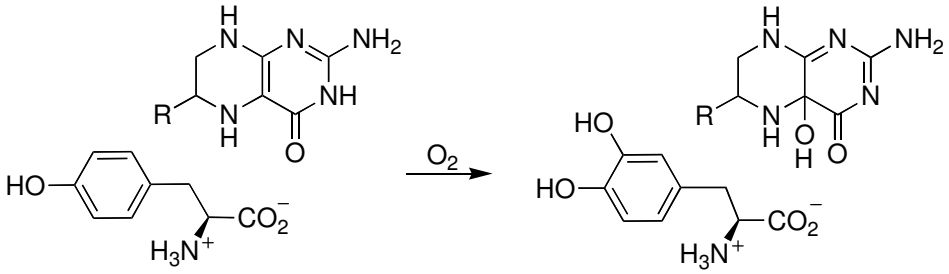

The increasing number of enzymes which contain the 2-His-1-carboxylate triad suggests that this arrangement of metal ligands provides unique advantages to iron-dependent oxidases. Complete understanding of the specific properties of this set of ligands which contribute to its differential reactivities will require a combination of biochemical and biomimetic studies of the different enzyme classes. The present study describes the effects of amino acid substitutions of the iron ligands in TyrH on catalysis, iron binding, and binding of substrates and inhibitors. The results should provide a reference point for further structural studies of the pterin-dependent enzymes and for similar studies of other enzymes sharing this iron-binding motif.

EXPERIMENTAL PROCEDURES

Materials. Custom oligonucleotides were purchased from the Gene Technology Laboratory of Texas A&M University. Restriction endonucleases were from New England Biolabs Inc. Pfu DNA polymerase was obtained from Stratagene USA. Plasmids were purified using kits from Qiagen Inc. 6-Methyltetrahydropterin was purchased from Schircks Laboratories. Leupeptin, pepstatin, and catalase were from

Boehringer Mannheim Corp. Sheep dihydropteridine reductase, L-tyrosine, dopamine, NADH, and cytochrome c were from Sigma Chemical Co. Heparin-Sepharose was from Pharmacia Biotech Inc. *o*-Pthaldehyde and 3-mercaptopropionic acid were from Aldrich Chemical Co. Superoxide dismutase was from Worthington Biochem. Co.

Vectors for Enzyme Expression. The preparation of pETYHH331A, pETYHE331Q, pETYHE336A, and pETYHH336Q has been previously described (*63*). Construction of the pETYHH331E, pETYHH336E, pETYHE376H, and pETYHE376Q plasmids was done by Dr. S. Collete Daubner[12], or under her direct guidance, using the Stratagene QuikChange Kit using *Pfu* DNA polymerase and plasmid pETYH8 as the template (*118*). pETYHE376H was similarly used as a template for construction of pETYHH331E/E376H and pETYHH336E/E376H. Mutated plasmids were detected by electrophoretic analysis of restriction digests. In all cases, the entire coding region was sequenced to confirm the desired mutation.

Bacterial Cell Growth and Protein Purification. Bacterial cells expressing wild-type rat TyrH were grown as previously described (*119*). Variant proteins were obtained by introducing the appropriate plasmids into competent *E.coli* BL21(DE3) cells. Cell growth and protein purification were as previously described for other TyrH variant

---

[12]Dr. Daubner is a member of the Fitzpatrick lab at Texas A&M University.

proteins (*120*) with the following modifications. After induction with IPTG, cells were grown at 20 °C for 14-18 hours. Nucleic acid precipitation was done with 2% (w/v) streptomycin sulfate. The H331Q and the H336E/E376H variant proteins could not be expressed, even at low termperatures. Consequently, these proteins were not characterized. Purified proteins were stored in 50 mM HEPES, 10% glycerol, and 100 mM KCl, pH 7, at -80 ºC.

Assays. Initial characterization of the H336Q and H376Q tyrosine hydroxylase enzymes was done by Dr. Holly E. Ellis[13]. Opal J. Willmon[13] assisted in further characterization of the H336Q and H336E enzymes. The iron contents of all enzymes were determined by atomic absorbance spectroscopy as previously described (*121*), except that all samples and standards were prepared in a final concentration of 0.25 M nitric acid. Enzyme concentrations were determined from their absorbance at 280 nm (*55*). Two assays were used to measure the rate of DOPA formation from tyrosine. In the case of enzymes with moderate activity (>5% wild type), a colorimetric end point assay was used as previously described (*118*). Standard assay conditions were 170 μg mL^{-1} catalase, 1.7 mM dithiothreitol, 250 μM tyrosine, 130 μM ferrous ammonium sulfate, and 70 mM HEPES/NaOH, pH 7, 25 °C. For enzymes with lower activity, an HPLC

---

[13]Dr. Ellis and Opal Willmon are former members of the Fitzpatrick lab at Texas A&M University.

assay was used. The assay conditions were the same as for the colorimetric assay. Reactions were run 2-5 minutes and quenched by the addition of concentrated sodium borate, pH 9.5, to give 73 mM final concentration. The amount of DOPA produced was measured by HPLC analysis of the *o*-phthaldehyde derivative; the conditions for this reaction were as described previously (*122*). The HPLC elution conditions were 3 minutes of 100% 12.5 mM sodium phosphate, 0.5% tetrahydrofluoric acid, pH 7.0 (solvent A), a 3 minute linear increase to 20% acetonitrile, 80% A, and a final 19 minute linear increase to 40% acetonitrile, 60% A at 0.2 mL min^{-1}, using a 2 x 150 mm Waters NovaPak C18 column. The modified amino acids were detected using a Waters Model 470 fluorescence detector, with an excitation wavelength of 344 nm and an emission wavelength of 450 nm. Under these conditions, the elution time for DOPA is 21.5 minutes. The rate of tetrahydropterin oxidation was determined under similar assay conditions, coupling dihydropterin formation to NADH consumption with dihydropteridine reductase and measuring the decrease in absorbance at 340 nm, as previously described (*123*). Standard assay conditions were 0.2-0.4 units mL^{-1} sheep dihydropteridine reductase, 40 μM 6-methyltetrahydropterin, 60 μg mL^{-1} catalase, 60 μM tyrosine, 100 μM NADH, 200 μM ferrous ammonium sulfate, 100 mM HEPES/NaOH, pH 7, 25 °C. When the concentration of either the metal or a substrate were varied, steady state kinetic data were fit directly to the Michaelis-Menten equation using the program KaleidaGraph (Adelbeck Software, Reading, PA).

To obtain the enzyme-dopamine complex, proteins (200 μM) were incubated with a 2-10 fold stoichiometric excess of dopamine for a minimum of 10 minutes in 50

mM HEPES/NaOH, 10-30%glycerol, pH 7, at 20 °C. For those proteins that showed a substoichiometric amount of iron (H336Q, H336E, E376Q, and H331E/E376H), ferrous ammonium sulfate was added in 10 μM aliquots to yield a stoichiometric equivalent of iron. Catalase was also added in the cases of the E376H and E376Q enzymes. After the addition of dopamine, the absorption spectra were monitored from 250-800 nm until no further changes were seen.

RESULTS

Iron Content of Variant Proteins. The three protein ligands to the iron in TyrH are His331, His336, and Glu376. When either histidine residue is substiuted by alanine or glutamine, the resultant protein is essentially iron free and lacks significant activity in a standard tyrosine hydroxylase assay (*63*); this result previously allowed identification of these residues as iron ligands prior to the availability of a three-dimensional structure. As a more extensive probe of the plasticity of the 2-histidine-1-carboxylate triad in this enzyme, each of the three residues was individually replaced with glutamate, glutamine, or histidine; all but the H331Q enzyme were successfully expressed and purified. In addition, the expression constructs for both the His331E/E376H and His336E/ E376H enzymes were made, but only the former enzyme could be expressed successfully.

The effects of the amino acid substitutions on the iron contents of the individual proteins are shown in Table 5.1. The iron content is not significantly altered by the substitution of Glu376 by histidine or glutamine or by the substitution of His331 by glutamate. In contrast, substitution of His336 decreases the iron content, with the H336Q

Table 5.1. Iron content and relative catalytic activities of tyrosine hydroxylase variant enzymes

Enzyme	Fe:Protein	Pterin oxidation[a]	Tyrosine hydroxylation[b]
H331E	1.2 ± 0.2	2.4 ± 0.4	< 0.002
H336Q	0.050 ± 0.003	11.9 ± 1.3	3.7 ± 0.5
H336E	0.51 ± 0.13	6.3 ± 1.5	0.78 ± 0.17
E376Q	0.83 ± 0.13	0.4 ± 0.1	0.39 ± 0.07
E376H	1.2 ± 0.3	< 0.4	0.0027 ± 0.0011
H331E/E376H	0.21 ± 0.08	< 0.4	< 0.002

[a]Percentage of wild-type value of 2.5 s^{-1} (*118*). Conditions were 0.2-0.4 units mL^{-1} sheep dihydropteridine reductase, 100 μM 6-methyltetrahydropterin, 170 μg mL^{-1} catalse, 250 μM tyrosine, 100 μM NADH, 130 μM ferrous ammonium sulfate, 70 mM HEPES/ NaOH, pH 7, 25 ºC. [b]Percentage of wild-type value. Conditions were 170 μg mL^{-1} catalase, 1.7 mM dithiothreitol, 400 μM 6-methyltetrahydropterin, 250 μM tyrosine, 130 μM ferrous ammonium sulfate, and 70 mM HEPES/NaOH, pH 7, 25 ºC. Rates were determined by HPLC analysis, with the exception of H336Q, which was assayed using a colorimetric assay as described in EXPERIMENTAL PROCEDURES.

enzyme being effectively iron-free. Although both the H331E and the E376H enzymes have normal levels of iron, the double variant H331E/E376H contains significantly less iron.

Catalytic Activity. None of the recombinant enzymes had significant activity in a standard tyrosine hydroxylation assay (results not shown). However, the low iron contents of some of the variant proteins raised the possibility that the lack of activity was due to a lack of iron. Consequently, the abilities of the variant enzymes to catalyze tyrosine hydroxylation were determined in the presence of 130 μM Fe(II). To extend the sensitivity of our measurements, an HPLC-based assay was used for enzymes having less than 5% residual activity in tyrosine hydroxylation. The ability of these enzymes to catalyze tetrahydropterin oxidation was also measured, since a number of active site substitutions of TyrH have been described in which the effect on the ability to catalyze tyrosine hydroxylation is much greater than the effect on the ability to catalyze tetrahydropterin oxidation (*55, 118, 120*). The results of these assays are given in Table 5.1. Both enzymes in which His336 had been substituted had substantial activity as tyrosine-dependent tetrahydropterin oxidases in the presence of high concentrations of iron. The H336Q enzyme also was able to hydroxylate tyrosine at a substantial rate, although less than the rate of pterin oxidation. Thus, one effect of this substitution is to partially uncouple tetrahydropterin oxidation from tyrosine hydroxylation, so that a fraction of reducing equivalents is consumed unproductively. Replacement of His336 with glutamate has a more drastic effect on the coupling of pterin oxidation and amino acid hydroxylation than does replacement with glutamine. Replacement of His331 with

glutamate results in an enzyme with some ability to oxidize pterin and a decrease in the ability to hydroxylate tyrosine of at least 50 000-fold. Thus, this substitution partially and probably completely uncouples pterin oxidation and tyrosine hydroxylation. Both substitutions of Glu376 greatly decrease the catalytic activity. In the case of the E376Q enzyme, there is low but detectable activity in the pterin oxidation assay. This activity is identical to the activity found in the tyrosine hydroxylation assay, so that these two reactions do not appear to be uncoupled by this substitution. It is not possible to ascertain the relative stoichiometry of tetrahydropterin oxidation and tyrosine hydroxylation for the E376H enzyme, since the pterin oxidation activity is below our detection limits. However, the ability to hydroxylate tyrosine is down 37,000-fold and is very close to the limit of our ability to detect such activity; this is consistent with our inability to detect catalysis of pterin oxidation. The double variant H331E/E376H was also analyzed to determine if either single substitution could be rescued by a complementary change in another ligand; no activity could be detected in either assay. As noted above, the other such double variant, H331E/E376H, could not be expressed.

Iron Dependence. As a more quantitative measure of the effects of the amino acid substitutions on the iron affinities, the dependence on iron concentration of the activities was determined for the three enzymes with significant activity, H336E, H336Q, and H331E. The results are illustrated in Figure 5.1. The concentrations of Fe(II) in assays at which half-maximal activity is found, the K_{Fe} value, for these enzymes are given in Table 5.2. The values are consistent with the iron contents of the

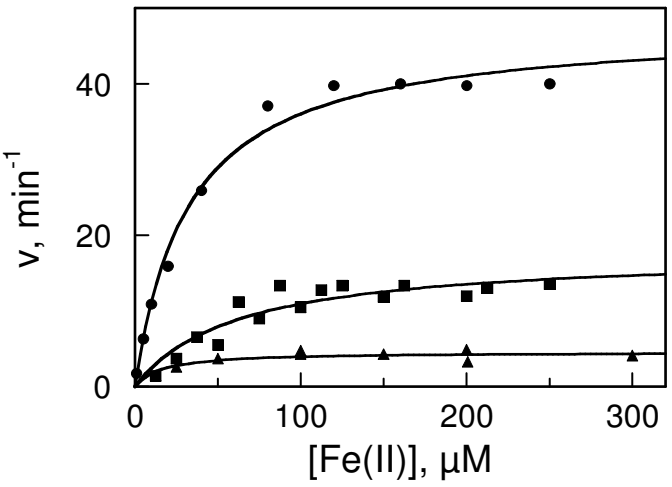

Figure 5.1. Iron dependence of H336Q (circles), H336E (squares), and H331E (triangles) tyrosine hydroxylase. The lines were obtained by fitting the data to the Michaelis-Menten equation. For the H336Q enzyme, rates of tyrosine hydroxylation were measured using the colorimetric assay described in EXPERIMENTAL PROCEDURES. For the H336E and H331E enzymes, the rate of pterin oxidation was measured as described in EXPERIMENTAL PROCEDURES.

Table 5.2. Steady state kinetic parameters of tyrosine hydroxylase variant proteins[a]

kinetic parameter	wild-type[b]	H336Q[c]	H336E[d]	H331E
k_{cat} (min^{-1})	180 ± 9	61 ± 4[e]	1.33 ± 0.03	18 ± 3[g]
K_{tyr} (μM)	51 ± 6	310 ± 40	330 ± 20	NA
K_{MPH4} (μM)	51 ± 16	409 ± 50	190 ± 110	340 ± 100[g]
K_{Fe} (μM)	0.15[f]	135 ± 18	62 ± 20	16 ± 7[g]

[a]Conditions: 125 μg mL^{-1} catalase, 1 mM dithiothreitol, 50 mM HEPES/NaOH, pH 7.1 at 25 ºC. [b]The concentrations of the nonvaried substrates were 250 μM tyrosine, 1 mM 6-$MePH_4$, and 10 μM ferrous ammonium sulfate. [c]The concentrations of the nonvaried substrates were 600 μM tyrosine, 1 mM 6-$MePH_4$, and 300 μM ferrous ammonium sulfate. [d]The concentrations of the nonvaried substrates were 1 mM tyrosine, 1 mM 6-$MePH_4$, and 300 μM ferrous ammonium sulfate. [e]At saturating concentrations of Fe(II), from the data of Figure 5.1. [f]From reference (*114*). [g]Determined from the rate of 6-$MePH_4$ oxidation.

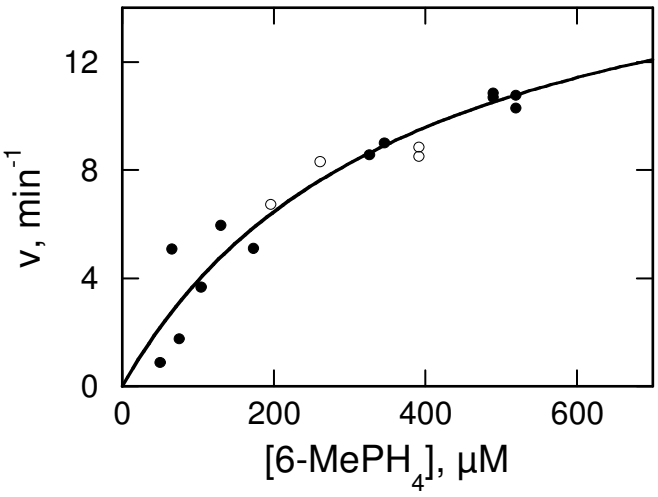

Figure 5.2. Effect of 6-methyltetrahydropterin and tyrosine on the rate of pterin oxidation by H331E tyrosine hydroxylase. The rate of oxidatino of 6-$MePH_4$ was measured in the presence (filled circles) and absence (empty circles) of 250 µM tyrosine with 0.2-0.4 units mL-1 sheep dihydropterinidine reductase, 170 µg mL-1 catalase, 100 µM NADH, 130 µM ferrous ammonium sulfate, 70 mM HEPES/NaOH, pH 7, at 25 °C. The line is a fit of the data to the Michaelis-Menten equation.

purified enzymes (Table 5.1). The apparent affinity of the H336Q enzyme for iron is down 1000-fold from the wild-type value. The H336E substitution has a slightly less drastic effect on iron binding, while the K_{Fe} value for the H331E enzyme is increased about 100-fold.

Steady-State Kinetics. The effects of both His336 substitutions on steady-state kinetic parameters were determined using the tyrosine hydroxylation assay. The results are given in Table 5.2. With both variant proteins, the K_m values for both tyrosine and 6-$MePH_4$ increase severalfold. The k_{cat} value for the H336Q enzyme is down only 3-fold from the wild-type value. Since the rate of pterin oxidation by this enzyme is more than twice the rate of tyrosine hydroxylation, the replacement of His336 with glutamine has only a small effect on the ability of the protein to catalyze pterin oxidation. The H331E enzyme lacks any detectable activity at tyrosine hydroxylation, so the steady-state kinetic parameters of this enzyme were determined using the pterin oxidation assay. Varying the concentration of 6-$MePH_4$ gives typical Michaelis Menten kinetics (Figure 5.2), with a k_{cat} value for pterin oxidation of 18 ± 3 min^{-1}. Remarkably, the rate of oxidation of 6-$MePH_4$ was independent of the concentration or even the presence of tyrosine (Figure 5.2). Thus, the H331E substitution converts TyrH into a tetrahydropterin oxidase.

Dopamine Binding. The ferric form of wild-type TyrH will bind dopamine with a K_d value of about 5 nM, resulting in a ligand-to-metal charge-transfer band at about 700 nm (*56, 124*). Model studies have shown the λ_{max} of this band is sensitive to the charge and orientation of the metal ligands (*125*). Therefore, the position of this band was used

as a probe of the metal ligands in the variant enzymes. The complex obtained with the H331E protein has a λ_{max} at about 660 nm (Figure 5.3). This is blue shifted from the wild-type absorbance band, consistent with the expected reduction in the Lewis acidity of the iron upon replacement of an imidazole ligand with a carboxylate. The H336Q enzyme has a maximum absorbance at about 680 nm (Figure 5.3), intermediate between the wild-type enzyme and H331E TyrH. Ligation of the glutamine amide moiety is expected to involve the amide oxygen (*126*). The blue shift of the dopamine complex is consistent with some anionic character to this oxygen. In studies of biomimetic models for nonheme iron proteins, Mandal and Que (*127*) previously found that an amide ligated to Fe(III) behaves more like a carboxylate than a neutral amide, consistent with the absorbance maximum of the H336Q enzyme. No long-wavelength absorbing species was seen in the visible absorbance spectra of the H336E and H331E/E376H proteins in the presence of dopamine concentrations up to 500 μM. Instead, a species with maximal absorbance at 580 nm was formed. An identical species formed when dopamine was added to a solution of ferrous ammonium sulfate in the absence of enzyme, suggesting that this is an iron-catecholate complex rather than an enzyme bound species.

Incubation of the E376H or E376Q enzyme with dopamine, rather than leading to formation of a stable complex, resulted in a time-dependent accumulation of a new species with a λ_{max} at 435 nm at pH 7 (Figure 5.4). The formation of this yellow species was much slower than the formation of the blue complex seen with the wild-type enzyme. The colored compound could be separated from the enzyme by passage down a

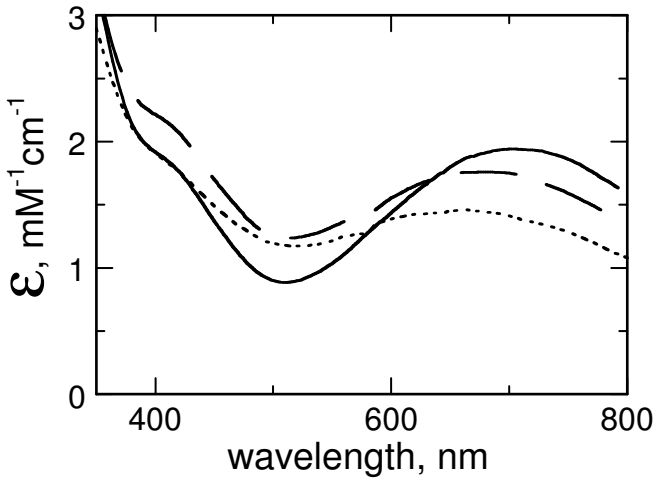

Figure 5.3. Absorbance spectra of complexes of dopamine-bound wild-type (solid line), H336Q (broken line), and H331E (dotted line) tyrosine hydroxylase.

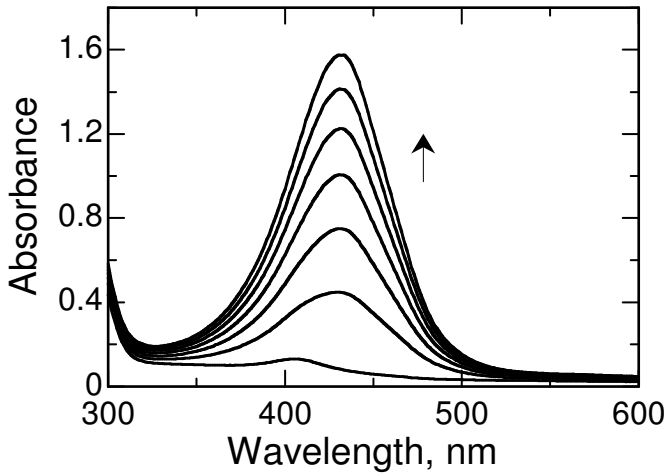

Figure 5.4. Dopamine oxidation by E376H tyrosine hydroxylase. Enzyme was incubated with 290 μM dopamine in 50 mM HEPES/NaOH, 100 mM KCl, 0.125 mg per mL catalase, 25% glycerol, pH 7, at 20 C. Spectra were taken at 2 minute intervals.

gel filtration column, demonstrating that it is not bound tightly to the enzyme. When the pH was decreased to below 6, the λ_{max} value shifted to 350 nm, with a decrease in the extinction coefficient, consistent with a pK_a value between 5 and 6. When the experiment was done under anaerobic conditions, no formation of the yellow compound was seen, suggesting that the reaction requires oxygen (data not shown). No increase in visible absorbance was seen upon the addition of dopamine if 370 μM 6-methyltetrahydropterin was added first. Addition of a tetrahydropterin to the ferric enzyme reduces the iron to the ferrous form *(121)*; thus, the reaction appears to require Fe(III). Both the rate of the reaction and magnitude of the final absorbance at 435 nm increased in the presence of 0.125 mg mL^{-1} catalase and decreased in the presence of superoxide dismutase or cytochrome c. These results suggest that the yellow compound is formed in a redox reaction involving an initial reaction between the Fe(III) in the TyrH active site and dopamine. While it proved possible to separate the chromophore from the enzyme, all efforts to isolate a pure compound for further analysis were unsuccessful.

DISCUSSION

The 2-histidine-1-carboxylate triad has been found in an increasing number of iron enzymes in the last several years, suggesting that this arrangement of metal ligands is especially effective or especially versatile. There are several different families of such enzymes (*57*): the pterin-dependent aromatic amino acid hydroxylases phenylalanine hydroxylase (PheH), TyrH, and tryptophan hydroxylase; several enzymes in β-lactam biosynthesis, including isopenicillin N synthase and the α-ketoglutarate-dependent

dioxygenases, clavaminic acid synthase and taurine dioxygenase; the extradiol cleaving catechol dioxygenases; and the aromatic dioxygenases such as naphthalene and toluene dioxygenase. The three-dimensional structures of these enzymes are quite distinct but all share a common metal-binding motif with two histidines and one carboxylic amino acid. In all cases that have been described to date, replacement of a ligand to the metal with alanine results in inactive enzyme (*58-62*), similar to the case with TyrH (*63*) and PheH (*64*). To our knowledge, the only previous report of residual activity upon amino acid substitution of any of the residues is the report by Khaleei et al. (*59*) that the H145Q and H280Q clavaminate synthase enzymes have low (<3%) residual activity. While no further characterization of these proteins has been described, the similarities between the reported results and the current study suggest that the results we have found with TyrH may be relevant to other families of enzymes with this arrangement of metal ligands.

Heme-dependent enzymes are another family of enzymes that utilize a high valence ferryl-oxo intermediate. Peroxidases contain histidine as the axial ligand, and it has proved possible to replace that ligand in cytochrome *c* peroxidase with other amino acids. Substitution of His175 of cytochrome *c* peroxidase by glutamine has no significant effect on the k_{cat} value of the enzyme and increases the K_m value for H_2O_2 by an order of magnitude (*128*). The structure of the variant enzyme is the same as that of the wild-type, with the His175 N3 replaced by the amide oxygen of the glutamine (*128*). The H175E enzyme also has the same structure as the wild-type enzyme, with a severalfold greater k_{cat} value (*129*). Critically, in both the H175E and H175Q enzymes, the rate of formation of compound I, the Fe(IV)=O/porphyrin cation radical, is

comparable to that of the wild-type enzyme, but its rate of decay is much greater (*129*). These results provide some precedent for retention of activity upon replacement of the histidine distal to the oxygen site with a glutamine.

The results described here with the H336Q enzyme are similar to those of the cytochrome *c* peroxidase H175Q enzyme. This TyrH enzyme retains substantial ability to catalyze tyrosine hydroxylation and an almost complete ability to catalyze tetrahydropterin oxidation. The major defects are decreased affinity for substrates and iron and some uncoupling of pterin oxidation and amino acid hydroxylation. The hydroxylating intermediate in TyrH is probably an Fe(IV)=O species (*120*) with properties similar to that of the hydroxylating intermediate in cytochrome P450 (*130*), an Fe(IV)=O/porphyrin radical cation similar to compound I of peroxidases (*131, 132*). The rate-limiting step in the TyrH reaction occurs in the formation of this hydroxylating intermediate (*133*). The retention of pterin oxidase activity in the H336Q enzyme suggests that early events in the catalytic pathway are relatively unaffected by the substitution, but instead the substitution destabilizes the hydroxylating intermediate.

The site on the iron at which oxygen binds TyrH is not established. In the enzyme-pterin-amino acid Fe(II) complex of PheH, the iron is in a distorted square pyramidal geometry (*134*) with His285 (homologous to TyrH His331), a bidentate glutamate, and a water molecule as the equatorial ligands (*135*). On the basis of modeling of oxygen into the active site, Andersen et al. (*135*) have suggested that oxygen binds in place of the water molecule. This would place the oxygen molecule between the iron atom and the C4a position of the pterin, with His290 approximately

opposite the oxygen on the other side of the iron atom. Such an arrangement would make His336 in TyrH most analogous to the axial histidine in cyt_c peroxidase, consistent with the comparable effects of the histidine to glutamine variations in the two enzymes.

The effect of replacing His331 on the activity of TyrH is much greater than is the case for His336. The His331Q enzyme expresses very poorly (*63*), suggesting that it is unstable, while the H331E enzyme has no detectable tyrosine hydroxylation ability. This enzyme does have some activity as a tetrahydropterin oxidase. More remarkably, this activity does not require the presence of tyrosine. The PheH pterin-amino acid Fe(II) structure shows that this histidine forms part of the binding site for the amino acid substrate, with the aromatic ring of the substrate stacking against the imidazole ring of the histidine. Thus, the His331Q substitution has removed much of the binding site for the amino acid substrate. In the case of the wild-type enzyme, binding of the amino acid substrate to the enzyme-pterin complex causes a significant conformational change (*134, 135*). This conformational change is required before oxygen will react with the bound tetrahydropterin to initiate the catalytic cycle (*133*). The tyrosine-independent tetrahydropterin oxidase activity of H331E TyrH suggests that this conformational change may occur even in the absence of the amino acid substrate in the variant enzyme.

Substitution of Glu376 has the greatest effect on catalysis, in that both variant enzymes have essentially no detectable activity at either tyrosine hydroxylation or tetrahydropterin oxidation. While the carboxylate of this residue in both TyrH and PheH binds the iron in monodentate fashion in the free enzyme and in the binary complex with tetrahydrobiopterin (*136, 137*), the interaction becomes bidentate in the ternary complex

(*135*). Such an interaction is clearly not possible with an imidazole, so that the lack of activity in the E376H enzyme is consistent with the structural data. In contrast, the E376Q enzyme has measurable, if very low, activity. The amide is clearly less likely to coordinate in the bidentate fashion seen in the structure of the PheH ternary complex. If the amide remains monodentate throughout the catalytic cycle, presumably with a water molecule remaining bound, the residual activity provides an approximation of the gain in activity upon bidentate coordination. Alternatively, a very small fraction of the protein may have the amide coordinating the iron through both the deprotonated nitrogen and the oxygen.

The properties of the dopamine complexes of the variant proteins provide further insights into the effects of the substitutions. While the Fe(III)-catecholamine complex is not an intermediate in catalysis, it is critical for the regulatory properties of TyrH (*56*). No structure is available of TyrH with dopamine bound, but structures are available of the catalytic domain of PheH with different catecholamines bound (*138*). In each of the structures, the catechol oxygens bind the metal in bidentate fashion, consistent with the conclusions drawn from spectroscopic studies of both enzymes (*125, 139*). In the PheH structures, the catechol oxygens replace the water molecules opposite the two histidines; given the homology of PheH and TyrH, it is likely that an identical arrangement is found in TyrH. Despite this apparent similarity of the roles of the two histidines in such a complex, the effects of replacing His331 and His336 on catecholamine binding are distinctly different. In the case of His336, replacement of histidine with glutamine results in an enzyme that still binds dopamine with the characteristic charge transfer

absorbance band. In this case the absorbance band is shifted to slightly higher energies. While replacement of an imidazole with an amide formally results in the replacement of one neutral ligand with another (*127*), in Fe(III) complexes there is some anionic character to the amide oxygen (*127*). Since the position of the absorbance band is sensitive to the identity of the ligands, with replacement of a neutral nitrogen with a partially negative oxygen shifting the band to higher energies (*125*), the absorbance maximum of the dopamine complex of the H336Q enzyme is fully consistent with replacement of a histidine with a glutamine. It was also possible to form a dopamine complex of the H331E enzyme. The charge-transfer band of this complex absorbs at higher energy than that of either the wild-type enzyme or the H336Q enzyme, consistent with the explicit negative charge on the carboxylate.

In contrast to the stability of the dopamine complex of the H331E and H336Q enzymes, addition of dopamine to the H336E enzyme resulted in the loss of the metal. Catechols bind to the iron in both TyrH and PheH as dianions (*138, 139*). In structures of PheH with catechols bound, the oxygen at C4 of the catechol is opposite His285 (His331 in TyrH); this histidine is within hydrogen bonding distance of the phenolic oxygen of Tyr325 (Tyr371 in TyrH) and a carboxylate oxygen of the metal ligand Glu330 (Glu376) (*138*). These interactions could compensate in part for the increased negative charge on the metal ligand upon introduction of a negative glutamate in place of the neutral histidine. In contrast, no amino acid residue is within hydrogen bonding distance of the catechol C3 oxygen to ameliorate the increased negative charge density required to form

the catechol complex. As a result, binding of dopamine to the H336E enzyme results in loss of the iron.

The two Glu376 substituted enzymes also stand out in their reactions with dopamine. In both cases a stable complex is not formed. Instead, there is the formation of a new chromophore. While the product of this reaction has not been identified, the results are most consistent with it being an oxidized form of dopamine. The reaction requires Fe(III) and oxygen, is inhibited by superoxide dismutase and cytochrome *c*, and is potentiated by catalase. This is consistent with initial formation of a dopamine-iron chelate in the active site, as occurs with the wild-type enzyme and the H336Q and H331E enzymes. In the case of the Glu376 variants, this species is not stable but undergoes one-electron transfer from dopamine to Fe(III) to form Fe(II) and dopamine semiquinone. Such a reaction has been shown to occur readily with free iron (*140*), with the neurotoxin 6-hydroxydopamine quinone as one of the products (*141*). Release of the semiquinone from the enzyme would then be followed by its reaction with oxygen or disproportionation to form the final product(s). Thus, the effect of replacing Glu376 is to destabilize the enzyme-dopamine complex. This is consistent with an increased redox potential at the iron due to the loss of the carboxylate ligand. The 430 nm species is not dopamine quinone, the two electron oxidized product, since this has an absorbance maximum at 390 nm (*142*), or the further oxidation product dopaminochrome, which absorbs at 480 nm. Dopamine oxidation products produced in neurons containing TyrH have been implicated in neurodegenerative diseases such as Parkinson's disease (*143, 144*). It is likely that the structure of TyrH has evolved to minimize redox reactions of

the active site iron with catecholamines. On the basis of the results of the amino acid substitutions described here, Glu376 plays a major role in modulating this reactivity.

In several cases, substitition of a metal ligand dramatically decreases the affinity of TyrH for iron. On the basis of the ability to reconstitute the enzyme with iron, replacement of His336 has the most drastic effect. Replacement of this residue also dramatically reduces the affinity for Fe(II), on the basis of the concentration dependence of the activity shown in Figure 5.1. The concentration of Fe(II) required for half-maximal activity increases by 3 orders of magnitude with both the H336Q and H336E enzymes. This is a far larger effect on catalytic activity than is seen with the H336Q enzyme.

The present understanding of the catalytic mechanism of TyrH and the other pterin-dependent hydroxylases is shown in Scheme 5.2 (*48*). This mechanism has no explicit role for the iron in the initial reaction between tetrahydropterin and oxygen. If the iron is truly not involved in this partial reaction, there is the possibility that proteins lacking iron would still be able to catalyze tetrahydropterin oxidation. The decreased affinities of the H331E, H336E, and H336Q enzymes for iron obviates a common problem in demonstrating a metal requirement for enzymatic activity, the presence of contaminating metal at concentrations comparable to the concentrations of enzyme used in assays, ~0.1 μM. With all three variant proteins, the ability to catalyze tetrahydropterin oxidation was dependent upon Fe(II). The dependence of both pterin oxidation and tyrosine hydroxylation activities on the presence of ferrous iron is consistent with a requirement for the metal for both partial reactions.

Scheme 5.2

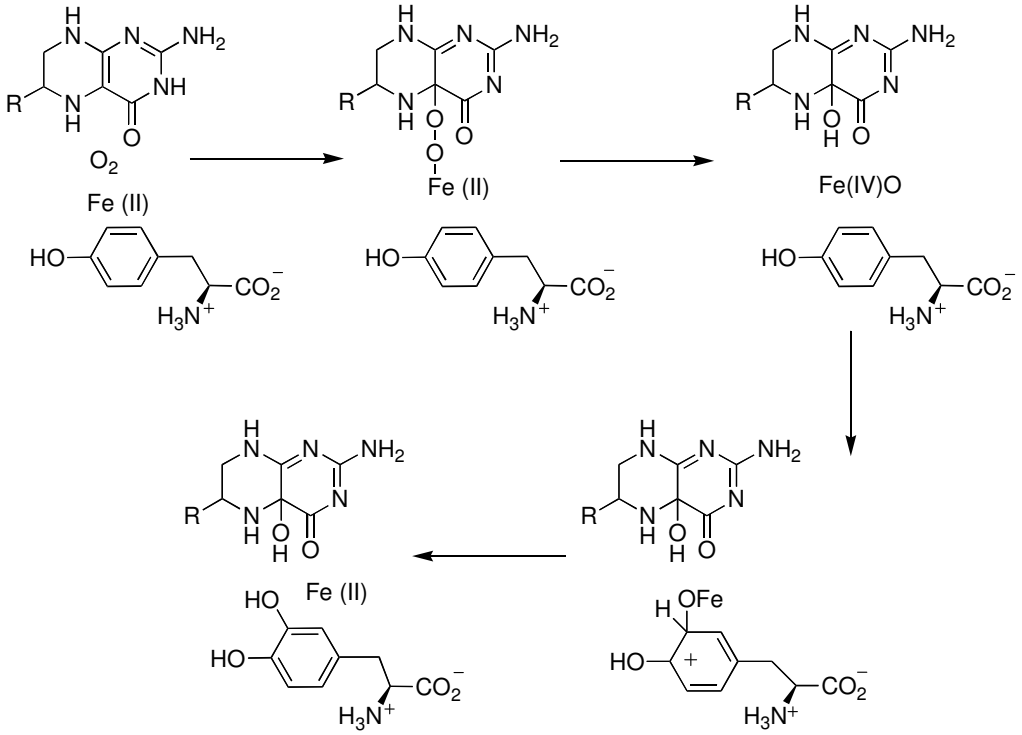

The results presented here provide insight into the properties of the 2-histidine-1-carboxylate triad which are critical for catalysis by the pterin-dependent aromatic amino acid hydroxylases. Most straightforward is the optimization of iron affinity with these three ligands. However, other arrangements of ligands are found in enzymes which bind iron at least as tightly. The requirement for a glutamate residue can be attributed in part to the need for a ligand capable of both mono and bidentate binding. The imidazoles provided by the two histidines cannot be replaced by more electronegative amides or carboxylates without destabilizing the hydroxylating intermediate. Whether these results are general for other iron enzymes which also utilize the 2-histidine-1-carboxylate triad

will require that similar analyses be carried out with those enzymes. Comparison of those results with the results of the present studies should result in a much better understanding of the molecular basis for the ubiquity of this motif and the factors responsible for its properties in individual systems.

CHAPTER VI

SUMMARY

Chapters II-IV focused on the chemical mechanism of amine oxidation by two flavoenzymes, *N*-methyltryptophan oxidase and tryptophan 2-monooxygenase. The proposed chemical mechanisms for these enzymes involve either the formation of a flavin semiquinone, formation of a substrate-flavin adduct, or a concerted two-electron and proton transfer in the form of a hydride.

In chapter II, pH and primary deuterium kinetic isotope effects were utilized to probe the mechanism of sarcosine oxidation by *N*-methyltryptophan oxidase (MTOX). The results were consistent with a fully rate-limiting irreversible step involving C-H bond cleavage. No intermediate flavin species was detected when stopped-flow spectroscopy was used to monitor enzyme reduction by either protiated or deuterated substrate. These results are most consistent with a hydride transfer mechanism of sarcosine oxidation, but cannot explicitly rule out other proposed mechanisms. The mechanistic possibilities were further addressed in Chapter III using ^{15}N kinetic isotope effects. The results are consistent with a mechanism in which C-H bond cleavage is concerted with rehybridization of the nitrogen orbitals from the substrate sp^3 configuration to the sp^2 configuration of the Schiff-base product. Taken together the evidence presented in Chapters II and III very strongly supports a hydride transfer mechanism for MTOX oxidation of sarcosine.

In Chapter IV, pH and primary deuterium and ^{15}N kinetic isotope effects were

utilized to study the chemical mechanism of a second flavoenzyme, tryptophan 2-monooxygenase (TMO). As was the case for sarcosine oxidation by MTOX, the observed isotope effects for L-alanine oxidation by TMO are consistent with a chemical mechanism in which changes in the nitrogen bonding order are concerted with a fully rate-limiting and irreversible C-H bond cleavage. Monitoring flavin reduction by either the protiated or deuterated substrate again revealed no intermediate flavin species. Therefore, the evidence presented in Chapter IV strongly supports a hydride transfer mechanism for L-alanine oxidation by TMO. As TMO and MTOX represent the two separate structural families of flavin-dependent amine oxidases, these results suggest that all members of this class of enzymes may utilize a similar hydride transfer mechanism for catalysis.

Chapter V addressed the plasticity of the iron-ligating motif of tyrosine hydroxylase. For this enzyme, the active-site iron is ligated by two conserved histidine residues and a conserved glutamate. Each of the iron-ligating amino acids in this enzyme was substituted with either histidine, glutamate, or glutamine. The resulting variant proteins were characterized with regards to catalytic activity, iron affinity, and changes in the absorbance spectra of the enzyme-dopamine complex, relative to wild-type tyrosine hydroxylase. In general, enzyme resulting from substitutions of the H336 residue retained more catalytic activity than the E376 variant enzymes, although the iron affinity of these enzymes was greatly reduced. E376 variant enzymes catalyze dopamine oxidation, a phenomenon previously undocumented in the wild-type enzyme. Surprisingly, the H331E enzyme is able to oxidize pterin in a tyrosine-independent

manner. Although many non-heme iron-dependent enzymes have now been found to contain a two-His-one-carboxylate arrangement of iron ligands similar to that found in tyrosine hydroxylase, this study represents the first detailed analysis of the plasticity of this motif. This study can therefore serve as a reference point for similar studies on other enzymes in which this motif is found.

REFERENCES

1. Massey, V. (2000) The chemical and biological versatility of riboflavin, *Biochem. Soc. Trans. 28*, 283-296.

2. Garrett, R., and Grisham, C. M. (1999) *Biochemistry*, 2nd ed., Saunders College, Fort Worth, TX.

3. Massey, V., and Palmer, G. (1966) On the existence of spectrally distinct classes of flavoprotein semiquinones. A new method for the quantitative production of flavoprotein semiquinones, *Biochemistry 5*, 3181-3189.

4. Settembre, E. C., Dorrestein, P. C., Park, J., Augustine, A. M., Begley, T. P., and Ealick, S. E. (2003) Structural and mechanistic studies on *thiO*, a glycine oxidase essential for thiamin biosynthesis in Bacillus subtilis, *Biochemistry 42*, 2971-2981.

5. Shi, Y., Lan, F., Matson, C., Mulligan, P., Whetstine, J. R., Cole, P. A., and Casero, R. A. (2004) Histone demethylation mediated by the nuclear amine oxidase homolog LSD1, *Cell 119*, 941-953.

6. Molla, G., Sacchi, S., Bernasconi, M., Pilone, M. S., Fukui, K., and Polegioni, L. (2006) Characterization of human D-amino acid oxidase, *FEBS Lett. 580*, 2358-2364.

7. Fitzpatrick, P. F. (2001) Substrate dehydrogenation by flavoproteins, *Acc. Chem. Res. 34*, 299-307.

8. Fitzpatrick, P. F. (2004) Carbanion versus hydride transfer mechanisms in flavoprotein-catalyzed dehydrogenations, *Bioorg. Chem. 32*, 125-139.

9. Scrutton, N. S. (2004) Chemical aspects of amine oxidation by flavoprotein enzymes, *Nat. Prod. Rep. 21*, 722-730.

10. Krebs, H. A. (1932) The metabolism of amino acids in the animal body, *Klinische Wochenschrift 11*, 1744-1748.

11. Mizutani, H., Miyahara, I., Hirotsu, K., Nishina, Y., Shiga, K., Setoyama, C., and Miura, R. (1996) Three-dimensional structure of porcine kidney D-amino acid oxidase at 3.0 Å resolution, *J. Biochem. 120*, 14-17.

12. Mattevi, A., Vanoni, M. A., Todone, F., Rizzi, M., Teplyakov, A., Coda, A., Bolognesi, M., and Curti, B. (1996) Crystal structure of D-amino acid oxidase: A case of active site mirror-image convergent evolution with flavocytochrome b_2, *Proc. Natl. Acad. Sci. U.S.A. 93*, 7496-7501.

13. Kurtz, K. A., Rishavy, M. A., Cleland, W. W., and Fitzpatrick, P. F. (2000) Nitrogen isotope effects as probes of the mechanism of D-amino acid oxidase, *J. Am. Chem. Soc. 122*, 12896-12897.

14. Denu, J. M., and Fitzpatrick, P. F. (1994) Intrinsic primary, secondary, and solvent kinetic isotope effects on the reductive half-reaction of D-amino acid oxidase: Evidence against a concerted mechanism, *Biochemistry 33*, 4001-4007.

15. Rishavy, M. A., and Cleland, W. W. (1999) ^{13}C, ^{15}N, and ^{18}O equilibrium isotope effects and fractionation factors, *Can. J. Chem. 77*, 967-977.

16. Silverman, R. B. (1995) Radical ideas about monoamine oxidase, *Acc. Chem. Res. 28*, 335-342.

17. Binda, C., Newton-Vinson, P., Hubalek, F., Edmondson, D. E., and Mattevi, A. (2002) Structure of human monoamine oxidase B, a drug target for the treatment of neurological disorders, *Nat. Struct. Biol. 9*, 22-26.

18. Sherry, B., and Abeles, R. H. (1985) Mechanism of action of methanol oxidase, reconstitution of methanol oxidase with 5-deazaflavin, and inactivation of methanol oxidase by cyclopropanol, *Biochemistry 24*, 2594-2605.

19. McCann, A. E., and Sampson, N. S. (2000) A C6 - flavin adduct is the major product of irreversible inactivation of cholesterol oxidase by 2a,3a-cyclopropano-5a-cholestan-3b-ol, *J. Am. Chem. Soc. 122*, 35-39.

20. Cavener, D. R. (1992) GMC oxidoreductases a newly defined family of homologous proteins with diverse catalytic activities, *J. Mol. Biol. 223*, 811-814.

21. Menon, V., Hsieh, C. T., and Fitzpatrick, P. F. (1995) Substituted alcohols as mechanistic probes of alcohol oxidase, *Bioorg. Chem. 23*, 42-53.

22. Lario, P. I., Sampson, N., and Vrielink, A. (2003) Sub-atomic resolution crystal structure of cholesterol oxidase: what atomic resolution crystallography reveals about enzyme mechanism and the role of the FAD cofactor in redox activity, *J. Mol. Bio. 326*, 1635-1650.

23. Brown, L. E., and Hamilton, G. A. (1970) Some model reactions and a general mechanism for flavoenzyme-catalyzed dehydrogenations, *J. Am. Chem. Soc. 92*, 7225-7227.

24. Kim, J. M., Cho, I. S., and Mariano, P. S. (1991) Amine-flavin electron transfer photochemistry. Potential models for monoamine oxidase catalysis and inhibition, *J. Org. Chem. 56*, 4943-4955.

25. Kim, J. M., Bogdan, M. A., and Mariano, P. S. (1993) Mechanistic analysis of the 3-methyllumiflavin-promoted oxidative deamination of benzylamine. A potential model for monoamine oxidase catalysis, *J. Am. Chem. Soc. 115*, 10591-10595.

26. Kim, J. M., Hoegy, S. E., and Mariano, P. S. (1995) Flavin chemical models for monoamine oxidase inactivation by cyclopropylamines, a-silylamines, and hydrazines, *J. Am. Chem. Soc. 117*, 100-105.

27. Miller, J. R., and Edmondson, D. E. (1999) Structure-activity relationships in the oxidation of para-substituted benzylamine analogues by recombinant human liver monoamine oxidase A, *Biochemistry 38*, 13670-13683.

28. Trickey, P., Wagner, M. A., Jorns, M. S., and Mathews, F. S. (1999) Monomeric sarcosine oxidase: structure of a covalently flavinylated amine oxidizing enzyme, *Structure 7*, 331-345.

29. Binda, C., Coda, A., Angelini, R., Federico, R., Ascenzi, P., and Mattevi, A. (1999) A 30 Å long U-shaped catalytic tunnel in the crystal structure of polyamine oxidase, *Structure 7*, 265-276.

30. Pawelek, P. D., Cheah, J., Coulombe, R., Macheroux, P., Ghisla, S., and Vrielink, A. (2000) The structure of L-amino acid oxidase reveals the substrate trajectory into an enantiomerically conserved active site, *EMBO J. 19*, 4204-4215.

31. Fraaije, M. W., and Mattevi, A. (2000) Flavoenzymes: diverse catalysts with recurrent features, *TIBS 25*, 126-132.

32. Yoshida, T., and Fukuyama, S. (1944) Metabolic changes in nitrogen-substituted amino acids. VIII. Demethylase. 2. Distribution, *J. Biochem. (Tokyo) 36*, 349-353.

33. Moritani, M. (1952) Demethylase. IV. Kinetics and reaction mechanism, *Hukuoka Acta. Med. 43*, 651-658.

34. Magaki, I. (1955) Abrine demethylase of *Escherichia coli*, *Osaka Daigaku Igaku Zasshi 7*, 359-367.

35. Wang, S. P. (1957) Demethylase of bacteria, *Taiwan Yixuehui Zazhi 56*, 362-369.

36. Ting, S. M., and Tung, T. (1966) Some properties of the particulate and soluble oxidative de-methylases from rabbit kidney, *Taiwan Yixuehui Zazhi 65*, 169-177.

37. Koyama, Y., and Ohmori, H. (1996) Nucleotide sequence of the *Escherichia coli solA* gene encoding a sarcosine oxidase-like protein and characterization of its product., *Gene 181*, 179-183.

38. Wagner, M. A., Khanna, P., and Jorns, M. S. (1999) Structure of the flavocoenzyme of two homologous amine oxidases: Monomeric sarcosine oxidase and N-methyltryptophan oxidase, *Biochemistry 38*, 5588-5595.

39. Comai, L., and Kosuge, T. (1980) Involvement of plasmid deoxyribonucleic acid in indoleacetic acid synthesis in Pseudomonas savastanoi, *J. Bacteriol. 143*, 950-957.

40. Comai, L., and Kosuge, T. (1982) Cloning and characterization of iaaM, a virulence determinant of Pseudomonas savastanoi, *J. Bacteriol. 149*, 40-46.

41. Klee, H., Montoya, A., Horodyski, F., Lichtenstein, C., Garfinkel, D., Fuller, S., Flores, C., Peschon, J., Nester, E., and Gordon, M. (1984) Nucleotide sequence of the tms genes of the pTiA6NC octopine Ti plasmid: Two gene products involved in plant tumorigenesis (Agrobacterium tumefaciens), *Proc. Natl. Acad. Sci. U.S.A. 81*, 1728-1732.

42. Emanuele, J. J., Jr., and Fitzpatrick, P. F. (1995) Mechanistic studies of the flavoprotein tryptophan 2-monooxygenase. 1. Kinetic mechanism, *Biochemistry 34*, 3710-3715.

43. Eberlein, G., and Bruice, T. C. (1983) The chemistry of a 1,5-diblocked flavin. 2. Proton and electron transfer steps in the reaction of dihydroflavins with oxygen, *J. Am. Chem. Soc. 105*, 6685-6697.

44. Lockridge, O., Massey, V., and Sullivan, P. A. (1972) Mechanism of action of the flavoenzyme lactate oxidase, *J. Biol. Chem. 247*, 8097-8106.

45. Sobrado, P., and Fitzpatrick, P. F. (2003) Analysis of the role of the active site residue Arg98 in the flavoprotein tryptophan 2-monooxygenase, a member of the L-amino oxidase family, *Biochemistry 42*, 13826-13832.

46. Sobrado, P., and Fitzpatrick, P. F. (2003) Identification of Tyr413 as an active site residue in the flavoprotein tryptophan 2-monooxygenase and analysis of its contribution to catalysis, *Biochemistry 42*, 13833-13838.

47. Sobrado, P., and Fitzpatrick, P. F. (2002) Analysis of the roles of amino acid residues in the flavoprotein tryptophan 2-monooxygenase modified by 2-oxo-3-pentynoate: characterization of His338, Cys339, and Cys511 mutant enzymes, *Arch. Biochem. Biophys. 402*, 24-30.

48. Fitzpatrick, P. F. (2000) The aromatic amino acid hydroxylases, in *Advances in Enzymology and Related Areas of Molecular Biology* (D. L. Purich, Ed.), pp 235-294, John Wiley & Sons, Inc.

49. Goodwill, K. E., Sabatier, C., Marks, C., Raag, R., Fitzpatrick, P. F., and Stevens, R. C. (1997) Crystal structure of tyrosine hydroxylase at 2.3 Å and its implications for inherited diseases, *Nat. Struct. Biol. 4*, 578-585.

50. Wang, L., Erlandsen, H., Haavik, J., Knappskog, P. M., and Stevens, R. C. (2002) Three-dimensional structure of human tryptophan hydroxylase and its implications for the biosynthesis of the neurotransmitters serotonin and melatonin, *Biochemistry 41*, 12569-12574.

51. Andersen, O. A., Stokka, A. J., Flatmark, T., and Hough, E. (2003) 2.0 Å Resolution crystal structures of the ternary complexes of human phenylalanine hydroxylase catalytic domain with tetrahydrobiopterin and 3-(2-thienyl)-L-alanine or L-norleucine: substrate specificity and molecular motions related to substrate binding, *J. Mol. Biol. 333*, 747-757.

52. Pavon, J. A., and Fitzpatrick, P. F. (2005) Intrinsic isotope effects on benzylic hydroxylation by the aromatic amino acid hydroxylases: evidence for hydrogen

tunneling, coupled motion, and similar reactivities, *J. Am. Chem. Soc. 127*, 16414-16415.

53. Frantom, P. A., Ragsdale, S. W., and Fitzpatrick, P. F. (2006) Reduction and oxidation of the active site iron in yyrosine hydroxylase: Kinetics and specificity, *Biochemistry 45*, 2372-2379.

54. Ramsey, A. J., and Fitzpatrick, P. F. (2000) Effects of phosphorylation on binding of catecholamines to tyrosine hydroxylase: specificity and thermodynamics, *Biochemistry 39*, 773-778.

55. Daubner, S. C., Lauriano, C., Haycock, J. W., and Fitzpatrick, P. F. (1992) Site-directed mutagenesis of Ser40 of rat tyrosine hydroxylase. Effects of dopamine and cAMP-dependent phosphorylation on enzyme activity, *J. Biol. Chem. 267*, 12639-12646.

56. Ramsey, A. J., and Fitzpatrick, P. F. (1998) Effects of phosphorylation of serine 40 of tyrosine hydroxylase on binding of catecholamines: Evidence for a novel regulatory mechanism, *Biochemistry 37*, 8980-8986.

57. Que Jr., L. (2000) One motif-many different reactions, *Nat. Struct. Biol. 7*, 182-184.

58. Hogan, D. A., Smith, S. R., Saari, E. A., McCracken, J., and Hausinger, R. P. (2000) Site-directed mutagenesis of 2,4-dichlorophenoxyacetic acid/α-keto-glutarate dioxygenase, *J. Biol. Chem. 275*, 12400-12409.

59. Khaleeli, N., Busby, R. W., and Townsend, C. A. (2000) Site-directed mutagenesis and biochemical analysis of the endogenous ligands in the ferrous active site of clavaminate synthase. The his-3 variant of the 2-his-1-carboxylate model. *Biochemistry 39*, 8666-8673.

60. Jiang, H., Parales, R. E., Lynch, N. A., and Gibson, D. T. (1996) Site-directed mutagenesis of conserved amino acids in the alpha subunit of toluene dioxygenase: potential mononuclear non-heme iron coordination sites, *J. Bacteriol. 178*, 3133-3139.

61. Borovok, I., Landman, O., Kreisberg-Zakarin, R., Aharonowitz, Y., and Cohen, G. (1996) Ferrous active site of isopenicillin N synthase: genetic and sequence analysis of the endogenous ligands, *Biochemistry 35*, 1981-1987.

62. Doan, L. X., Hassan, A., Lipscomb, S. J., Dhanda, A., Zhang, Z., and Schofield, C. J. (2000) Mutagenesis studies on the iron binding ligands of clavaminic acid synthase, *Biochem. Biophys. Res. Commun. 279*, 240-244.

63. Ramsey, A. J., Daubner, S. C., Ehrlich, J. I., and Fitzpatrick, P. F. (1995) Identification of iron ligands in tyrosine hydroxylase by mutagenesis of conserved histidinyl residues, *Prot. Sci. 4*, 2082-2086.

64. Balasubramanian, S., Carr, R. T., Bender, C. J., Peisach, J., and Benkovic, S. J. (1994) Identification of metal ligands in Cu(II)-inhibited *Chromobacterium violaceum* phenylalanine hydroxylase by electron spin echo envelope modulation analysis of histidine to serine mutations, *Biochemistry 33*, 8532-8537.

65. Ralph, E. C., and Fitzpatrick, P. F. (2005) pH and kinetic isotope effects on sarcosine oxidation by N-methyltryptophan oxidase, *Biochemistry 44*, 3074-3081.

66. Naoi, M., and Yagi, K. (1976) Oxidation of sarcosine and N-alkyl derivatives of glycine by D-amino-acid oxidase, *Biochim. Biophys. Acta 438*, 61-70.

67. Zhao, G., and Jorns, M. S. (2002) Monomeric sarcosine oxidase: evidence for an ionizable group in the E·S complex, *Biochemistry 41*, 9747-9750.

68. Zhao, G., Qu, J., Davis, F. A., and Jorns, M. S. (2000) Inactivation of monomeric sarcosine oxidase by reaction with N-(cyclopropyl)glycine, *Biochemistry 39*, 14341-14347.

69. Harris, R. J., Meskys, R., Sutcliffe, M. J., and Scrutton, N. S. (2000) Kinetic studies of the mechanism of carbon-hydrogen bond breakage by the heterotetrameric sarcosine oxidase of *Arthrobacter sp*. 1-IN, *Biochemistry 39*, 1189-1198.

70. Khanna, P., and Jorns, M. S. (2001) N-Methyltryptophan oxidase from *Escherichia coli*: reaction kinetics with N-methyl amino acid and carbinolamine substrates, *Biochemistry 40*, 1451-1459.

71. Wagner, M. A., and Jorns, M. S. (2000) Monomeric sarcosine oxidase: 2. Kinetic studies with sarcosine, alternate substrates, and a substrate analogue, *Biochemistry 39*, 8825-8829.

72. Zhao, G., Song, H., Chen, Z., Mathews, S., and Jorns, M. S. (2002) Monomeric

sarcosine oxidase: role of histidine 269 in catalysis, *Biochemistry 41*, 9751-9764.

73. Ellis, K. J., and Morrison, J. F. (1982) Buffers of constant ionic strength for studying pH-dependent processes, *Methods Enzymol. 87*, 405-426.

74. Cleland, W. W. (1986) Enzyme kinetics as a tool for determination of enzyme mechanisms, in *Investigation of Rates and Mechanism,* 4th ed., Vol. 6, Part I (C. F. Bernasconi, Ed.), pp 791-870, John Wiley & Sons, New York.

75. Fisher, H. F., and Saha, S. K. (1996) Interpretation of transient-state kinetic isotope effects, *Biochemistry 35*, 83-88.

76. Maniscalco, S. J., Tally, J. F., and Fisher, H. F. (2004) The interpretation of multiple-step transient-state kinetic isotope effects, *Arch. Biochem. Biophys. 425*, 165-172.

77. Yagi, K., Lange, R., and Douzou, P. (1980) Spectroscopic demonstration of an initial stage of the complex of D-amino acid oxidase and its substrate D-α-aminobutyric acid, *Biochem. Biophys. Res. Commun. 97*, 370-374.

78. Khanna, P., and Schuman Jorns, M. (2001) Characterization of the FAD-containing N-methyltryptophan oxidase from *Escherichia coli*, *Biochemistry 40*, 1441-1450.

79. Bright, H. J., and Porter, D. J. T. (1975) Flavoprotein oxidases, in *The Enzymes,* 3rd ed., Vol. XII (P. Boyer, Ed.), pp 421-505, Academic Press, New York.

80. Palmer, G., and Massey, V. (1968) Mechanisms of flavoprotein catalysis, in *Biological Oxidations* (T. P. Singer, Ed.), pp 263-300, John Wiley and Sons, New York.

81. Cook, P. F., and Cleland, W. W. (1981) pH variation of isotope effects in enzyme-catalyzed reactions. 1. Isotope- and pH-dependent steps the same, *Biochemistry 20*, 1797-1805.

82. Dawson, R. M. C., Elliott, D. C., Elliott, W. H., and Jones, K. M. (1986) *Data for Biochemical Research,* 3rd ed., Clarendon Press, Oxford.

83. Wagner, M. A., Trickey, P., Chen, Z. W., Mathews, F. S., and Jorns, M. S. (2000) Monomeric sarcosine oxidase: 1. Flavin reactivity and active site binding

determinants, *Biochemistry 39*, 8813-8824.

84. Ghisla, S., Massey, V., and Choong, Y. S. (1979) Covalent adducts of lactate oxidase. Photochemical formation and structure identification, *J. Biol. Chem. 254*, 10662-10669.

85. Chen, Z. W., Zhao, G., Martinovic, S., Jorns, M. S., and Mathews, F. S. (2005) Structure of the sodium borohydride-reduced N-(cyclopropyl)glycine adduct of the flavoenzyme monomeric sarcosine oxidase, *Biochemistry 44*, 15444-15450.

86. Bannister, A. J., Schneider, R., and Kouzarides, T. (2002) Histone methylation: dynamic or static? *Cell 109*, 801-806.

87. Cleland, W. W. (2005) The use of isotope effects to determine enzyme mechanisms, *Arch. Bioch. Biophys. 433*, 2-12.

88. Rabenstein, D. L., and Mariappan, S. V. S. (1993) Determination of ^{15}N isotope effects on the acid-base equilibria of amino groups in amino acids by ^{13}C NMR, *J. Org. Chem. 58*, 4487-4489.

89. Pehk, T., Kiirend, E., Lippmaa, E., Ragnarsson, U., and Grehn, L. (1997) Determination of isotope effects on acid-base equilibria by ^{13}C NMR spectroscopy., *J. Chem. Soc. Perkin Trans. 2*, 445-450.

90. Bell, R. P. (1973) Kinetic isotope effects in proton-transfer reactions, in *The Proton in Chemistry,* 2nd ed., pp 250-296, Cornell University Press, Ithaca, NY.

91. Reutov, O. A. (1978) *CH-Acids: A Guide to All Existing Problems of CH-Acidity with New Experimental Methods and Data, Including Indirect Electrochemical, Kinetic and Thermodynamic Studies.*, Vol. 1, Pergamon Press, Oxford.

92. Alfassi, Z. (1998) *N-Centered Radicals*, Wiley, New York.

93. Alfassi, Z. (1999) *S-Centered Radicals*, Wiley, New York.

94. Rigby, S. E., Hynson, R. M., Ramsay, R. R., Munro, A. W., and Scrutton, N. S. (2005) A stable tyrosyl radical in monoamine oxidase A, *J. Biol. Chem. 280*, 4627-4631.

95. McMurry, J. (1995) *Organic Chemistry*, 4th ed., Brooks/Cole Pub., Pacific

Grove, CA.

96. Ralph, E. C., Anderson, M., Cleland, W. W., and Fitzpatrick, P. F. (2006) pH and kinetic isotope effects on alanine oxidation by tryptophan 2-monooxygenase *Manuscript in preparation*.

97. Emanuele, J. J., Jr., Heasley, C. J., and Fitzpatrick, P. F. (1995) Purification and characterization of the flavoprotein tryptophan 2-monooxygenase expressed at high levels in E. coli, *Arch. Biochem. Biophys. 316*, 241-248.

98. Emanuele, J. J., Jr., and Fitzpatrick, P. F. (1995) Mechanistic studies of the flavoprotein tryptophan 2-monooxygenase. 2. pH and kinetic isotope effects, *Biochemistry 34*, 3716-3723.

99. Flashner, M. I. S., and Massey, V. (1974) Purification and properties of L-lysine monooxygenase from Pseudomonas fluorescens, *J. Biol. Chem. 249*, 2579-2586.

100. Koyama, H. (1982) Purification and characterization of a novel L-phenylalanine oxidase (deaminating and decarboxylating) from Pseudomonas sp. P-501, *J. Biochem. 92*, 1235-1240.

101. Carey, F. A., and Sundberg, R. J. (2000) *Advanced Organic Chemistry*, 4th ed., Springer, New York.

102. Denu, J. M., and Fitzpatrick, P. F. (1994) pH and kinetic isotope effects on the oxidative half-reaction of D-amino-acid oxidase, *J. Biol. Chem. 269*, 15054-15059.

103. Basran, J., Sutcliffe, M. J., and Scrutton, N. S. (2001) Optimizing the Michaelis complex of trimethylamine dehydrogenase: identification of interactions that perturb the ionization of substrate and facilitate catalysis with trimethylamine base, *J. Biol. Chem. 276*, 42887-42892.

104. Zhao, G., and Jorns, M. S. (2005) Ionization of zwitterionic amine substrates bound to monomeric sarcosine oxidase, *Biochemistry 44*, 16866-16874.

105. Harris, C. M., Pollegioni, L., and Ghisla, S. (2001) pH and kinetic isotope effects in D-amino acid oxidase catalysis: Evidence for a concerted mechanism in substrate dehydrogenation via hydride transfer, *Eur. J. Bioch. 268*, 5504-5520.

106. Hermes, J. D., Weiss, P. M., and Cleland, W. W. (1985) Use of nitrogen-15 and deuterium isotope effects to determine the chemical mechanism of phenylalanine ammonia-lyase, *Biochemistry 24*, 2959-2967.

107. Rios, A., Amyes, T., and Richard, J. (2000) Formation and stability of organic zwitterions in aqueous solution: Enolates of the amino acid glycine and its derivatives, *J. Am. Chem. Soc. 122*, 9373-9385.

108. Walker, M. C., and Edmondson, D. E. (1994) Structure-activity relationships in the oxidation of benzylamine analogues by bovine liver mitochondrial monoamine oxidase B, *Biochemistry 33*, 7088-7098.

109. Pace, C. P., and Stankovich, M. T. (1991) Oxidation-reduction properties of trimethylamine dehydrogenase: effect of inhibitor binding, *Arch. Biochem. Biophys. 287*, 97-104.

110. Sablin, S. O., and Ramsay, R. R.-. (2001) Substrates but not inhibitors alter the redox potentials of monoamine oxidases, *Antioxid. Redox Signal 3*, 723-729.

111. Fitzpatrick, P. F. (1999) The tetrahydropterin-dependent amino acid hydroxylases, *Ann. Rev. Biochem. 68*, 355-381.

112. Hufton, S. E., Jennings, I. G., and Cotton, R. G. H. (1995) Structure and function of the aromatic amino acid hydroxylases, *Biochem. J. 311*, 353-366.

113. Gottschall, D. W., Dietrich, R. F., and Benkovic, S. J. (1982) Phenylalanine hydroxylase. Correlation of the iron content with activity and the preparation and reconstitution of the apoenzyme, *J. Biol. Chem. 257*, 845-849.

114. Fitzpatrick, P. F. (1989) The metal requirement of rat tyrosine hydroxylase, *Biochem. Biophys. Res. Commun. 161*, 211-215.

115. Moran, G. R., Daubner, S. C., and Fitzpatrick, P. F. (1998) Expression and characterization of the catalytic core of tryptophan hydroxylase, *J. Biol. Chem. 273*, 12259-12266.

116. Erlandsen, H., Fusetti, F., Martinez, A., Hough, E., Flatmark, T., and Stevens, R. C. (1997) Crystal structure of the catalytic domain of human phenylalanine hydroxylase reveals the structural basis for phenylketonuria, *Nat. Struct. Biol. 4*, 995-1000.

117. Fitzpatrick, P. F., Ralph, E. C., Ellis, H. R., Willmon, O. J., and Daubner, S. C. (2003) Characterization of metal ligand mutants of tyrosine hydroxylase: insights into the plasticity of a 2-histidine-1-carboxylate triad, *Biochemistry 42*, 2081-2088.

118. Daubner, S. C., Hillas, P. J., and Fitzpatrick, P. F. (1997) Characterization of chimeric pterin dependent hydroxylases: Contributions of the regulatory domains of tyrosine and phenylalanine hydroxylase to substrate specificity, *Biochemistry 36*, 11574-11582.

119. Daubner, S. C., and Fitzpatrick, P. F. (1998) Mutation to phenylalanine of tyrosine 371 in tyrosine hydroxylase increases the affinity for phenylalanine, *Biochemistry 37*, 16440-16444.

120. Ellis, H. R., Daubner, S. C., and Fitzpatrick, P. F. (2000) Mutation of serine 395 of tyrosine hydroxylase decouples oxygen-oxygen bond cleavage and tyrosine hydroxylation, *Biochemistry 39*, 4174-4181.

121. Ramsey, A. J., Hillas, P. J., and Fitzpatrick, P. F. (1996) Characterization of the active site iron in tyrosine hydroxylase: Redox states of the iron, *J. Biol. Chem. 271*, 24395-24400.

122. Hillas, P. J., and Fitzpatrick, P. F. (1996) A mechanism for hydroxylation by tyrosine hydroxylase based on partitioning of substituted phenylalanines, *Biochemistry 35*, 6969-6975.

123. Fitzpatrick, P. F. (1991) The steady state kinetic mechanism of rat tyrosine hydroxylase, *Biochemistry 30*, 3658-3662.

124. Andersson, K. K., Cox, D. D., Que, L., Jr., Flatmark, T., and Haavik, J. (1988) Resonance Raman studies on the blue-green-colored bovine adrenal tyrosine 3-monooxygenase (tyrosine hydroxylase). Evidence that the feedback inhibitors adrenaline and noradrenaline are coordinated to iron, *J. Biol. Chem. 263*, 18621-18626.

125. Cox, D. D., Benkovic, S. J., Bloom, L. M., Bradley, F. C., Nelson, M. J., Que, L., Jr., and Wallick, D. E. (1988) Catecholate LMCT bands as probes for the active sites of nonheme iron oxygenases, *J. Am. Chem. Soc. 110*, 2026-2032.

126. Sigel, H., and Martin, R. B. (1982) Coordinating properties of the amide bond. stability and structure of metal ion complexes of peptides and related ligands,

Chem. Rev. 82, 385-426.

127. Mandal, S. K., and Que Jr., L. (1997) Models for amide ligation in nonheme iron enzymes, *Inorg. Chem. 36*, 5424-5425.

128. Sundaramoorthy, M., Choudhury, K., Edwards, S. L., and Poulos, T. L. (1991) Crystal structure and preliminary functional analysis of the cytochrome c peroxidase his175gln proximal ligand mutant, *J. Am. Chem. Soc. 113*, 7755-7757.

129. Choudhury, K., Sundaramoorthy, M., Mauro, J. M., and Poulos, T. L. (1992) Conversion of the proximal histidine ligand to glutamine restores activity to an inactive mutant of cytochrome c peroxidase, *J. Biol. Chem. 267*, 25656-25659.

130. Frantom, P. A., Pongdee, R., Sulikowski, G. A., and Fitzpatrick, P. F. (2002) Intrinsic deuterium isotope effects on benzylic hydroxylation by tyrosine hydroxylase, *J. Am. Chem. Soc. 124*, 4202-4203.

131. Sono, M., Roach, M. P., Coulter, E. D., and Dawson, J. H. (1996) Heme-containing oxygenases, *Chem. Rev. 96*, 2841-2888.

132. Isaac, I. S., and Dawson, J. H. (1999) Haem iron-containing peroxidases, *Essays in Biochemistry 34*, 51-69.

133. Fitzpatrick, P. F. (1991) Studies of the rate-limiting step in the tyrosine hydroxylase reaction: Alternate substrates, solvent isotope effects, and transition state analogs, *Biochemistry 30*, 6386-6391.

134. Wasinger, E. C., Mitic, N., Hedman, B., Caradonna, J., Solomon, E. I., and Hodgson, K. O. (2002) X-ray absorption spectroscopic investigation of the resting ferrous and cosubstrate-bound active sites of phenylalanine hydroxylase, *Biochemistry 41*, 6211-6217.

135. Andersen, O. A., Flatmark, T., and Hough, E. (2002) Crystal structure of the ternary complex of the catalytic domain of human phenylalanine hydroxylase with tetrahydrobiopterin and 3-(2-thienyl)-L-alanine, and its implications for the mechanism of catalysis and substrate activation, *J. Mol. Biol. 320*, 1095-1108.

136. Andersen, O. A., Flatmark, T., and Hough, E. (2001) High resolution crystal structures of the catalytic domain of human phenylalanine hydroxylase in its catalytically active Fe(II) form and binary complex with tetrahydrobiopterin, *J.*

Mol. Biol. 314, 279-291.

137. Goodwill, K. E., Sabatier, C., and Stevens, R. C. (1998) Crystal structure of tyrosine hydroxylase with bound cofactor analogue and iron at 2.3 Å resolution: self-hydroxylation of phe300 and the pterin-binding site, *Biochemistry 37*, 13437-13445.

138. Erlandsen, H., Flatmark, T., Stevens, R. C., and Hough, E. (1998) Crystallographic analysis of the human phenylalanine hydroxylase catalytic domain with bound catechol inhibitors at 2.0 Å resolution, *Biochemistry 37*, 15638-15646.

139. Michaud-Soret, I., Andersson, K. K., Que, L., Jr., and Haavik, J. (1995) Resonance Raman studies of catecholate and phenolate complexes of recombinant human tyrosine hydroxylase, *Biochemistry 34*, 5504-5510.

140. El-Ayaan, U., Herlinger, E., Jameson, R. F., and Linert, W. (1997) Anaerobic oxidation of dopamine by iron(III), *J. Chem. Soc.*, 2813-2818.

141. Napolitano, A., Pezzella, A., and Prota, G. (1999) New reaction pathways of dopamine under oxidative stress conditions: nonenzymatic iron-assisted conversion to norepinephrine and the neurotoxins 6-hydroxydopamine and 6,7-dihydroxytetrahydroisoquinoline, *Chem. Res. Toxicol. 12*, 1090-1097.

142. Jimenez, M., Garcia-Carmona, F., Garcia-Canovas, F., Iborra, J. L., Lozano, J. A., and Martinez, F. (1984) Chemical intermediates in dopamine oxidation by tyrosinase, and kinetic studies of the process, *Arch. Biochem. Biophys. 235*, 438-448.

143. Hastings, T. G., Lewis, D. A., and Zigmond, M. J. (1996) Role of oxidation in the neurotoxic effects of intrastriatal dopamine injections, *Proc. Natl. Acad. Sci. U.S.A. 93*, 1956-1961.

144. Linert, W., Herlinger, E., Jameson, R. F., Kienzl, E., Jellinger, K., and Youdim, M. B. H. (1996) Dopamine, 6-hydroxydopamine, iron, and dioxygen-their mutual interactions and possible implication in the development of Parkinson's disease, *Biochim. Biophys. Acta 1316*, 160-168.

APPENDIX

The derivation of equation 4.6 is shown below, where E_{obs} is the observed ^{15}N isotope effect on k_{cat}/K_m, f is the final fraction of alanine oxidized, and R_S/R_0 is the $^{14}N/^{15}N$ ratio of the alanine after oxidation divided by the isotope ratio of the alanine prior to any enzymatic oxidation.

$$E_{obs} = \log(1-f)/\log[(1-f)(R_S/R_0)]$$

$$\log[(1-f)*R_S/R_0] = [\log(1-f)]/E_{obs}$$

$$(1-f)*R_S/R_0 = (1-f)^{\left(1/E_{obs}\right)}$$

$$R_S/R_0 = (1-f)^{\left(1/E_{obs}\right)-1}$$

VITA

Name:	Erik C. Ralph
Address:	Department of Biochemistry Biophysics
	Texas A&M University
	College Station, TX, 77843
Email Address:	erikralph@tamu.edu
Education:	B.S., Biochemistry, Bucknell University, 2000
	Ph.D., Biochemistry, TexasA&M University, 2006